REALIZATION CALCULUS

Special Functions

Function families and their structure

Coupled growth, arithmetic depth and finite resolution

Komorebi P.

REALIZATION CALCULUS

Special Functions

Function families and their structure

Coupled growth, arithmetic depth and finite resolution

Komorebi P.

A mathematical monograph

Preface

Structure beyond a finite window

The theory of special functions begins with explicit definitions, but the information those definitions carry need not be visible in a small sample of values. A contraction in a differential equation can determine the growth of an entire function. A prime omitted from an arithmetic sum can change its exact parameter signature. A finite collection of positive moment matrices can conceal a negative mass in the underlying measure.

This volume studies these distinctions through five families. Scalar nonlinear feedback leads to entire functions with explicit growth laws. Arithmetic depth leads to positive kernels and an exact inverse problem. Prime sieves give a setting in which positivity and finite detection can be separated. Zero orbits provide spectral coordinates. Coupled contraction functions bring local coefficients, global growth and finite observation into one system.

The first seven chapters develop the constructions, their principal arguments and worked examples. Ten appendices supply the longer proofs and computational details. The evidence register, glossary and references follow at the back. Figures accompany the mathematics they explain, rather than forming a separate gallery.

Each result is read with its own hypotheses. Classical inputs are identified where they enter. Exact rational certificates, numerical illustrations and analytic proofs remain distinct, and unresolved questions retain their stated scope. A change of representation does not, by itself, establish historical priority.

The recurring question is precise: what can be recovered from finite information, and what additional resolution is needed to distinguish the underlying structure?

Contents

Preface ii

Reading map v

Part I Entire functions and their growth 1

1 Contracted nonlinear feedback 2

Part II Arithmetic depth and signed measures 10

2 Arithmetic at complex depth 11

3 Prime sieves and signed measures 17

Part III Orbit spectra and exact coordinates 24

4 Spectral functions of zero orbits 25

5 Sequences, trees and polyphase 30

Part IV Coupled systems and finite resolution 36

6 Coupled contraction functions 37

7 Limits of finite observation 46

Part V Proofs and mathematical evidence **52**

The proof architecture 53

A Growth and tap continuity 54

B Arithmetic inverse and character resolution 59

C Prime sieves and signed-atom detection 68

D Spectral continuation and regularization 75

E Sequence and polyphase laboratory 84

F Coupled growth and Perron type 91

G Reduction and intrinsic parameters 99

H Constant linear coordinates 102

I Finite-resolution certificates 106

J Exact laboratory and certified evaluation 115

Evidence and limitations 118

Notation and glossary 124

References 126

Reading map

Five families, one mathematical question

This monograph investigates structural invariants in five families of special functions. Feedback scales, arithmetic frequencies, signed prime masses, rotation orbits, and coupled channels provide distinct settings. Their connections are established through specific formulas, invariants, and obstructions, not assumed from a shared vocabulary.

The argument starts with entire functions defined by contracted nonlinear feedback. It then studies arithmetic generating functions and prime-sieve measures, before passing to orbit spectral zeta functions and exact coefficient laboratories. Coupled entire systems connect several of these ideas, while a resolution atlas measures the difference between finite observation and global mathematical structure.

The main chapters give defining formulas, stated hypotheses, mathematical consequences, and computational figures. Extended proofs follow as technical appendices. The final notes distinguish analytic proofs, finite checks, classical inputs, and questions that remain open.

Four starting constructions

The first four families lead to distinct results: an entire-growth law, an obstruction to finite differential equations, a positivity boundary, and a rotation-invariant spectral coordinate. A coupled fifth family is developed in Part IV.

Family	Structure worked out	Status of the construction
Asymmetric dilation	Entire solutions; exact growth balance; off-diagonal nonrescaling; intrinsic feedback banks	Candidate extension of a known one-dilation tangent analog
Complex arithmetic depth	Exact exponential type; coupled shift calculus; strict positive kernel; exact parameter recovery; no polynomial-coefficient linear ODE	Candidate extension of the project's integer arithmetic energy
Prime-sieve packets	Exact moment field; real Hankel singularities; positivity-margin collapse; multiple-prime geometry; arithmetic resolvent	Candidate arithmetic specialization of classical orthogonal-polynomial machinery
Orbit spectral zeta	Global meromorphic continuation; rational integer values; regularized product; multiplicity-aware orbit quotient	Worked specialization of known Mittag–Leffler seeds and spectral-zeta methods

An established diagonal antecedent

The equation $f_q'(z) = 1 + f_q(qz)^2$, $f_q(0) = 0$, is already present in Méndez [1, Example 2.4]. It remains an important baseline, but its definition is not a discovery of this project. The asymmetric extension keeps two separate contractions and permits a proved distinction from every amplitude/argument rescaling of that baseline.

How to read the evidence

Theorem statements below concern exact infinite objects under the displayed hypotheses. Plots and decimal roots illustrate them. Finite assertions check implementations within recorded ranges. None of these three forms of evidence establishes historical priority by itself.

The source archive preserves extended arguments, earlier review records, negative controls, and open questions. The evidence register distinguishes those records from the checks performed for this edition.

PART I

Entire functions and their growth

Contractions, coefficients and nonlinear feedback.

CHAPTER I

Contracted nonlinear feedback

1.1 Two scales inside the function

For real $0 < q, r < 1$, define the normalized odd solution

$$\boxed{T'_{q,r}(z) = 1 + T_{q,r}(qz)T_{q,r}(rz), \qquad T_{q,r}(0) = 0.}$$

The contractions are part of the defining feedback. The function is symmetric in q, r, but unequal scales retain left/right address information.

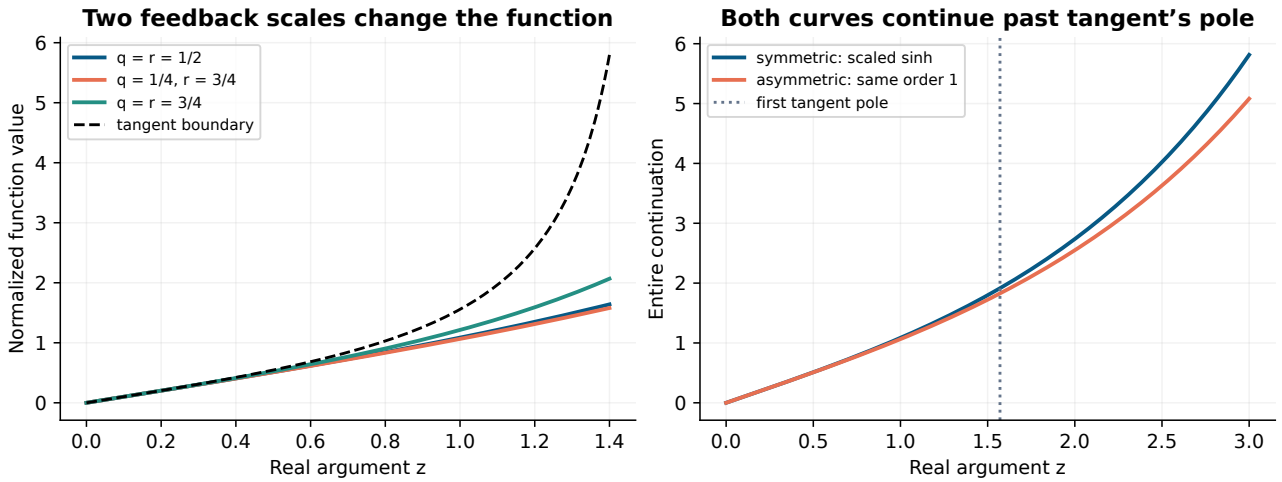


Figure 1.1. Computed Taylor curves. Each entire curve uses terms through z^{321}; positive-coefficient Cauchy estimates bound the omitted tail on each displayed interval. The black dashed curve is ordinary tangent.

For $T_{q,r}(z) = \sum_{n\geq 0} c_n z^{2n+1}$, $c_0 = 1$, coefficient matching gives

$$c_n = \frac{1}{2n+1} \sum_{i=0}^{n-1} q^{2i+1} r^{2(n-1-i)+1} c_i c_{n-1-i}, \qquad n \geq 1.$$

In particular,

$$T_{q,r}(z) = z + \frac{qr}{3} z^3 + \frac{q^2 r^2 (q^2 + r^2)}{15} z^5 + O(z^7).$$

The coefficients are positive and bounded by tangent coefficients, giving a convergent germ. If the solution is known on $|z| < R$, its integral equation extends it to $|z| < R/\max(q, r)$. Repetition proves that it is entire.

The parameters can be recovered, up to swapping, from c_1, c_2. Put $p = 3c_1$ and $u = 15c_2/p^2$. Then q, r are the roots of $x^2 - \sqrt{u + 2p}\, x + p = 0$.

1.2 A scale-balance atlas

$$\boxed{\rho(T_{q,r}) = \rho \quad \text{where} \quad q^\rho + r^\rho = 1.}$$

Here $M_f(R) = \max_{|z|=R} |f(z)|$ and $\rho(f) = \limsup_{R\to\infty} \log\log M_f(R)/\log R$ is the order of an entire function. Moreover $\log M_T(R) = O(R^\rho)$: the upper type is finite.

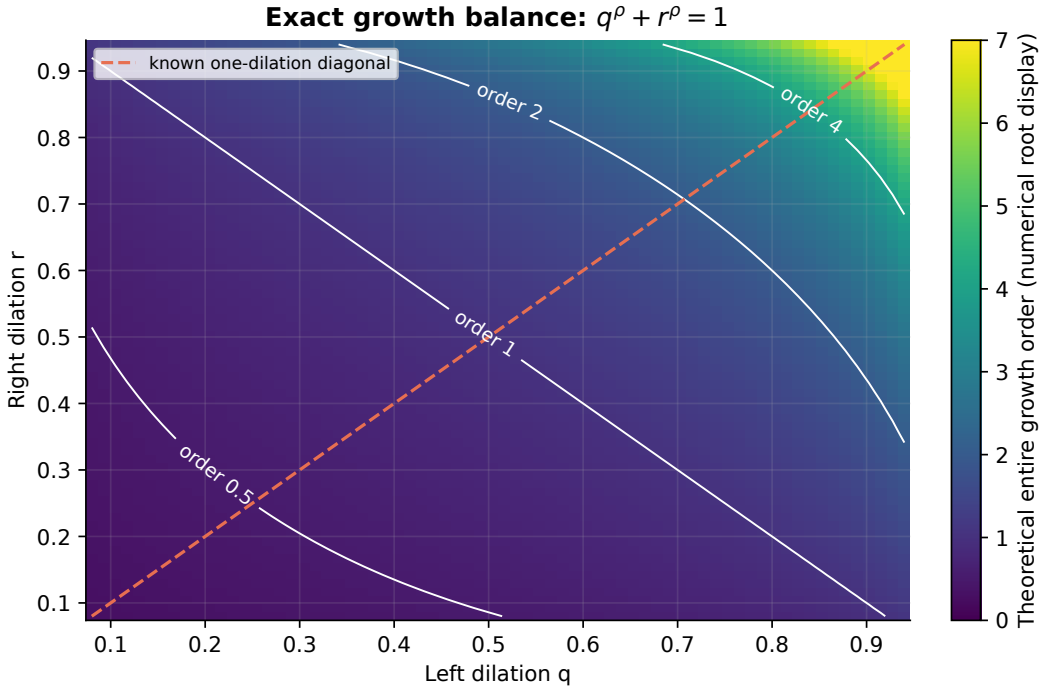


Figure 1.2. The displayed values numerically solve the proved characteristic equation. Colors saturate at order 7; the upper corner contains larger orders. The dashed diagonal is the previously known one-scale family.

Scales	Order	Interpretation
$q = r = 1/4$	$1/2$	Slow entire growth
$q + r = 1$	1	Many distinct functions at one order
$q = r = 1/\sqrt{2}$	2	Quadratic logarithmic growth scale
$q = r = 3/4$	$\log 2/\log(4/3)$	Approximately 2.4094208397

Why this equation appears

Nonnegative coefficients give $M(R) = T_{q,r}(R)$. The integral equation implies

$$M(R) \le R[1 + M(qR)M(rR)],$$

$$M(R) \ge (1-\alpha)RM(\alpha qR)M(\alpha rR), \quad 0 < \alpha < 1.$$

Taking logarithms turns product feedback into a sum over contracted scales. Comparison with CR^ρ proves the upper bound; comparison with cR^{ρ_α}, where $(\alpha q)^{\rho_\alpha} + (\alpha r)^{\rho_\alpha} = 1$, proves the lower bound. Letting $\alpha \uparrow 1$ gives the same order. The complete interval-induction proof is given in Appendix A.

1.3 The exact order has positive lower type

The single-channel result extends to finite positive feedback banks. Here a bank has weights $h_j > 0$ with $\sum_j h_j = 1$, contractions $0 < q_j, r_j < 1$, and normalized solution

$$F'(z) = 1 + \sum_j h_j F(q_j z)F(r_j z), \qquad F(0) = 0.$$

Write $M(R) = M_F(R)$ and let $q_j^{\rho_j} + r_j^{\rho_j} = 1$. Then, with $\rho = \max_j \rho_j$,

$$\boxed{0 < \liminf_{R\to\infty} \frac{\log M(R)}{R^\rho} \le \limsup_{R\to\infty} \frac{\log M(R)}{R^\rho} < \infty.}$$

Thus logarithmic growth is trapped between two positive multiples of R^ρ. In particular,

$$\lim_{R\to\infty} \frac{\log\log M(R)}{\log R} = \rho.$$

The theorem does not assert that $\log M(R)/R^\rho$ has a limit.

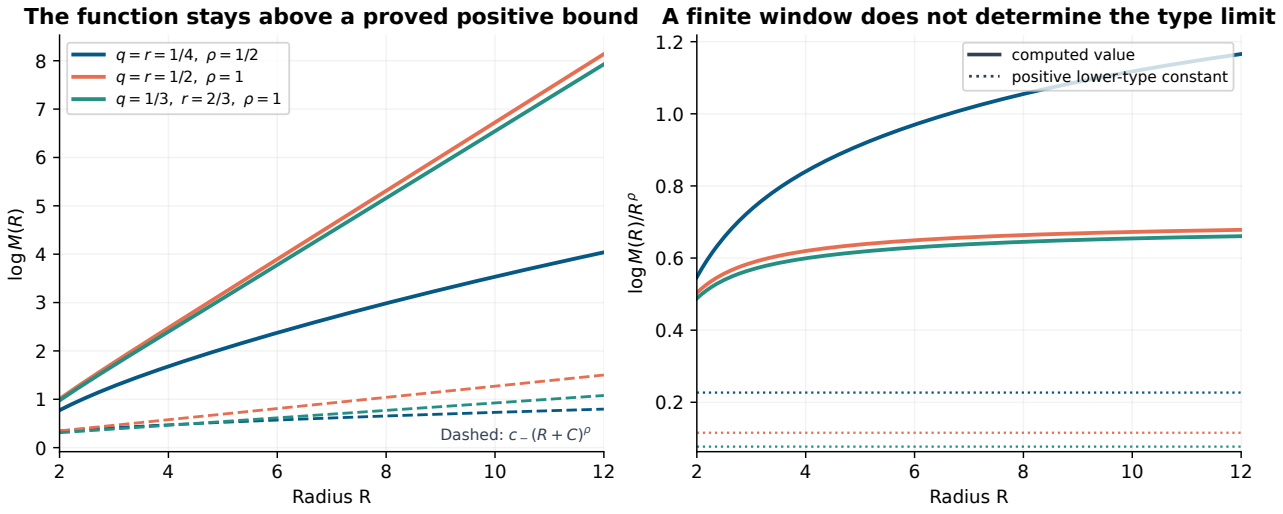


Figure 1.3. Finite-radius logarithmic growth and its proved lower comparison. The normalized curves illustrate scale dependence; the plot is not a proof of convergence to a type constant. Analytic truncation envelopes and ordinary high-precision rounding are recorded separately.

A lower bound at the exact exponent

Choose a maximizing channel (h, q, r) and integrate over a fixed-width terminal interval. Let

$$L = 1/h, \quad C = \max\left(\frac{qL}{1-q}, \frac{rL}{1-r}\right), \quad B = L + \frac{2}{\min(q,r)}, \quad c_- = \frac{\log 2}{(B+C)^\rho}.$$

The result is the explicit all-radius bound

$$\log M(R) \geq c_-(R+C)^\rho, \qquad R \geq 2.$$

Unlike a fixed fractional window, the terminal window loses only an additive radius. The shift C absorbs that loss without changing the exponent.

1.4 A translated power comparison

Write $H(R) = \log M(R)$. Positivity gives

$$M(R) \geq h \int_{R-L}^{R} M(qt)M(rt)\,dt \geq M(q(R-L))M(r(R-L)), \qquad R \geq B.$$

The choice of C ensures

$$q(R-L) + C \geq q(R+C), \qquad r(R-L) + C \geq r(R+C).$$

On the seed interval $[2, B]$, $H(R) \geq \log R \geq \log 2 \geq c_-(R+C)^\rho$. If this comparison holds at the two child radii, then

$$\begin{aligned} H(R) &\geq H(q(R-L)) + H(r(R-L)) \\ &\geq c_-\{[q(R-L)+C]^\rho + [r(R-L)+C]^\rho\} \\ &\geq c_-(q^\rho + r^\rho)(R+C)^\rho = c_-(R+C)^\rho. \end{aligned}$$

Let $Q_* = \max(q, r)$ and $d = (1-Q_*)B + Q_*L > 0$. Each child radius is at most $R - d$ and at least two. Induction on successive intervals of length d propagates the seed comparison to every $R \geq B$. The argument uses monotonicity of positive powers and works also when $\rho < 1$.

Explicit upper constants are available too

Set $Q = \max_j \max(q_j, r_j)$, $m = \min_j \min(q_j, r_j)$, $\Delta = \log(1/m)$, and $B_+ = \max_j \log(1/(q_j r_j)) + \log 2$. Choose an integer K with $Q^{-K} \geq 3/m$ and put

$$V_K = (2^{K+1} - 1)\log 2 + (2^{K+1} - K - 2)\log(1/Q),$$

$$c_+ = e^{-\rho}(V_K + 1 + \Delta + B_+).$$

Then $\log M(R) \leq c_+ R^\rho - \log R - B_+$ for $R \geq e$. The tangent majorant $M(1) < 2$, followed by the integral recurrence on radii Q^{-k}, bounds the initial seed by V_K. The logarithmic-radius comparison then supplies the displayed upper constant. The full induction is in Appendix A.

These constants are constructive and conservative. Their purpose is to establish two-sided growth, not to estimate the optimal type.

1.5 More than a rescaled one-scale seed

Nonrescaling theorem

If $q \neq r$, then $T_{q,r}$ cannot equal $Af_s(Bz)$ for nonzero constants A, B and any real $0 < s < 1$, where $f_s' = 1 + f_s(sz)^2$ is the known family.

Suppose such an equality held. Normalization gives $AB = 1$. Write $p = qr$, $u = q^2 + r^2$, and let ρ be the common order. The first two nontrivial coefficients and the growth law force

$$B^2 s^2 = p, \qquad s^2 = u/2, \qquad 2s^\rho = q^\rho + r^\rho = 1.$$

Consequently

$$2\left(\frac{q^2 + r^2}{2}\right)^{\rho/2} = q^\rho + r^\rho.$$

For $\rho \neq 2$, strict convexity or concavity of $x^{\rho/2}$ forces $q = r$. For the exceptional case $\rho = 2$, we have $u = 1$, $s^2 = 1/2$, $B^2 = 2p$. The two z^7 coefficients become

$$\frac{p^3(3 - p^2)}{315} \quad \text{and} \quad \frac{11p^3}{1260}.$$

Their equality forces $p = 1/2$ and again $(q - r)^2 = u - 2p = 0$. This completes the exceptional-order case.

A worked order-one member

$$T_{1/3,2/3}(z) = z + \frac{2}{27}z^3 + \frac{4}{2187}z^5 + \frac{232}{11160261}z^7 + O(z^9).$$

It has order one, and $T_{1/3,2/3}(1) \approx 1.0759239897408249$. The diagonal point $q = r = 1/2$ gives $f_{1/2}(z) = \sqrt{2}\sinh(z/\sqrt{2})$. Every off-diagonal member is separated from all rescaled diagonal members by the theorem above.

A combinatorial address formula

Sum over full ordered binary trees with n internal vertices. A vertex with i internal vertices in its left subtree and j in its right contributes

$$\frac{q^{2i+1}r^{2j+1}}{2(i + j + 1) + 1}.$$

Multiply these factors over internal vertices, then sum over trees. Root splitting reproduces the coefficient recurrence exactly. Unequal contractions therefore record left and right path lengths separately.

This is a precise separation result from one authenticated antecedent. It does not prove that no earlier author studied the asymmetric equation.

1.6 Feedback banks and weak-channel sensitivity

Choose finitely many channels $j = 1, \dots, J$, with $h_j > 0$, $\sum_j h_j = 1$, and $0 < q_j, r_j < 1$. Define

$$F'_\Theta(z) = 1 + \sum_j h_j F_\Theta(q_j z) F_\Theta(r_j z), \qquad F_\Theta(0) = 0.$$

These taps act inside the nonlinear definition. With $\mu_1 = \sum_j h_j q_j r_j$ and $\mu_2 = \sum_j h_j q_j r_j (q_j^2 + r_j^2)$,

$$F_\Theta(z) = z + \frac{\mu_1}{3} z^3 + \frac{\mu_1 \mu_2}{15} z^5 + O(z^7).$$

If $q_j^{\rho_j} + r_j^{\rho_j} = 1$, then

$$\boxed{\rho(F_\Theta) = \max_{j \text{ active}} \rho_j.}$$

The positive weights alter local coefficients. The most expansive active channel determines the asymptotic order. A zero-weight channel is removed before taking the maximum.

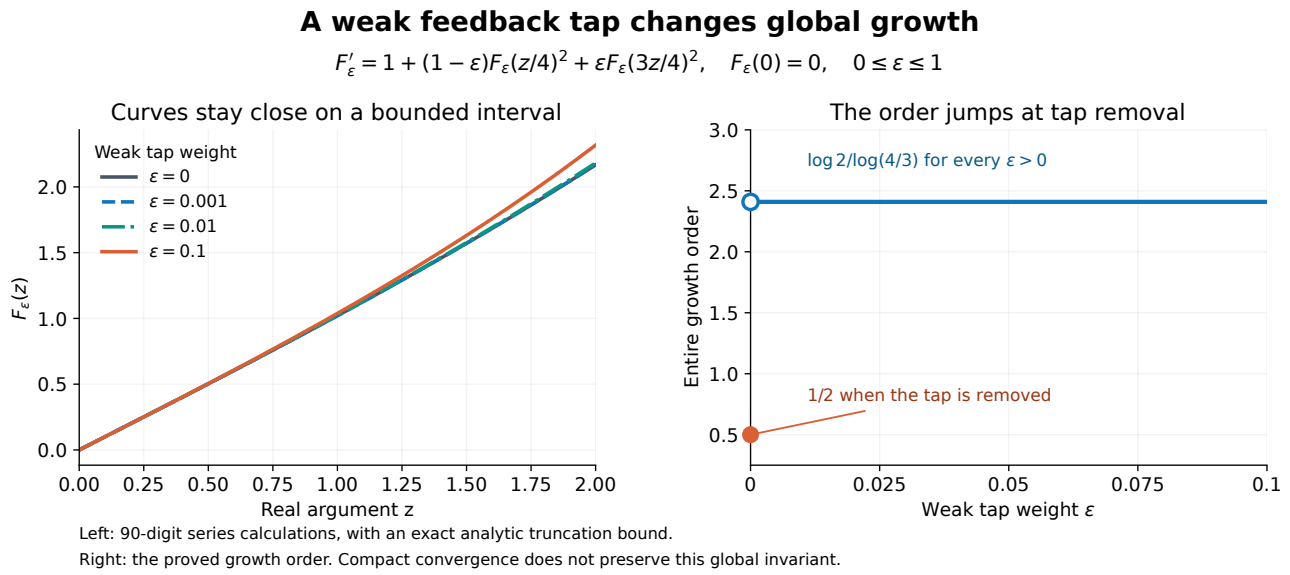


Figure 1.4. A two-channel example: scales $(1/4, 1/4)$ with weight $1 - \varepsilon$, and $(3/4, 3/4)$ with weight ε. The function varies continuously on every fixed compact set, while its growth order jumps when the second channel becomes active.

For $0 < \varepsilon \le 1$ the order is $\log 2 / \log(4/3)$; at $\varepsilon = 0$ it is $1/2$. Coefficients depend continuously on ε and are dominated by those of the entire $f_{3/4}$. Dominated convergence of the Taylor series therefore proves uniform convergence on compact sets as $\varepsilon \downarrow 0$.

This gives a useful design distinction: finite-window similarity does not control entire growth order. For a bank with weights $1/4, 3/4$ at these scales,

$$F(z) = z + \frac{7}{48} z^3 + \frac{427}{30720} z^5 + \frac{176681}{188743680} z^7 + O(z^9).$$

1.7 A quantitative compact-continuity law

Fix the contractions and let h, g be two normalized nonnegative tap vectors. Set $Q = \max_j \max(q_j, r_j) < 1$ and $d = \|h - g\|_1$. Then

$$\sup_{|z|\le R} |F_h(z) - F_g(z)| \le \frac{d}{4}\,[Rf_Q'(R) - f_Q(R)].$$

The right side is an explicitly defined entire majorant. It measures local sensitivity without asserting continuity of the asymptotic growth order.

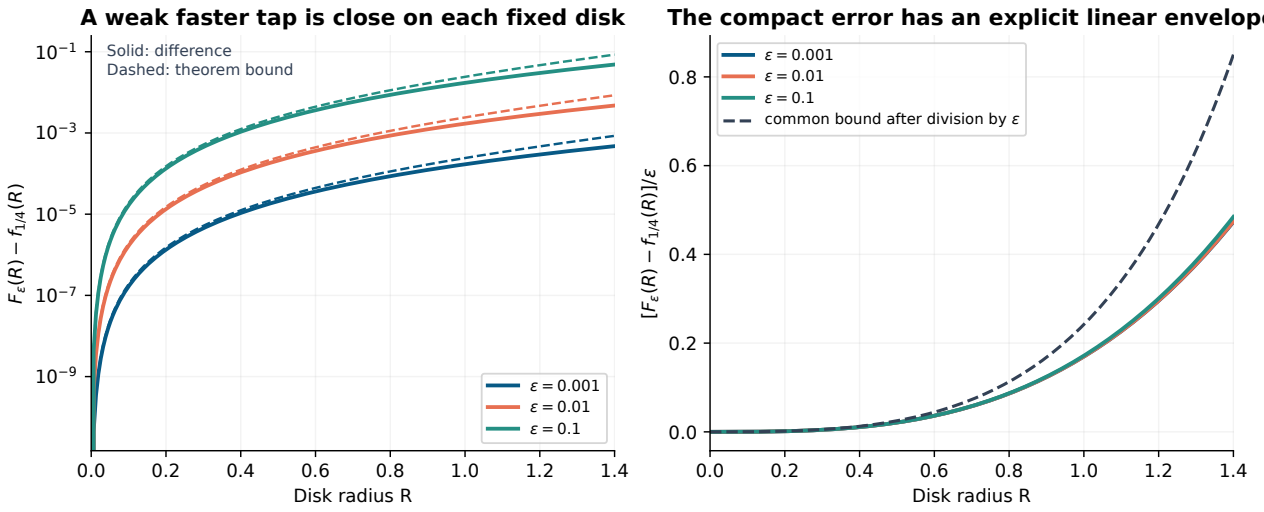


Figure 1.5. Computed weak-tap differences lie below the proved compact bound. For a slow/faster two-channel bank, $d = 2\varepsilon$, so the envelope is $\varepsilon[Rf_{3/4}'(R) - f_{3/4}(R)]/2$.

Each $c_n(h)$ is a positive polynomial homogeneous of degree n in the weights. Coefficientwise comparison gives $c_n(h) \le d_n(Q)(\sum_j h_j)^n$, where $f_Q = \sum_n d_n(Q) z^{2n+1}$. Every weight partial derivative on the simplex lies in $[0, nd_n(Q)]$. The positive and negative parts of $h - g$ each have mass $d/2$, giving $|c_n(h) - c_n(g)| \le (d/2)nd_n(Q)$. Summing this inequality uses $\sum_n nd_n(Q)R^{2n+1} = [Rf_Q'(R) - f_Q(R)]/2$.

1.8 An analytic family with a discontinuous invariant

For fixed finite J, allow complex h_j, q_j, r_j, with $|q_j|, |r_j| < 1$. The coefficient recurrence defines polynomials in all these parameters. On a compact parameter set choose $Q < 1$ and $W > 0$ such that $|q_j|, |r_j| \le Q$ and $\sum_j |h_j| \le W$. Then

$$|c_n(h, q, r)| \le W^n d_n(Q), \qquad \sum_n |c_n| R^{2n+1} \le W^{-1/2} f_Q(\sqrt{W}R).$$

Normal convergence proves joint holomorphic dependence on parameters and argument throughout this domain. Signed and complex banks have entire solutions, but the positive-bank growth theorem is not asserted for them.

The weak-tap example now has both sides quantified

For the bank with scales $(1/4, 1/4)$ and $(3/4, 3/4)$, weights $1-\varepsilon, \varepsilon$, the functions converge on every compact set as $\varepsilon \downarrow 0$. The preceding envelope gives a linear bound in ε. At every $\varepsilon > 0$, the order is $\log 2 / \log(4/3)$, while at zero it is $1/2$.

The new lower-type theorem does not contradict this: its lower constant depends on the active faster weight and can tend to zero as that channel vanishes. For $\varepsilon = 10^{-3}$ one constructive lower constant is about 1.4496×10^{-9}; a conservative upper constant is about 90.4392.

Identifying a bank has unavoidable equivalences

Permuting channels, swapping the scales within a channel, or merging duplicate scale pairs by adding their weights leaves the function unchanged. The two-scale single-channel inverse is exact up to swapping. A general minimal-bank identifiability theorem beyond these equivalences is not proved.

The resulting research target is specific: determine optimal growth type, possible logarithmic oscillations, and minimal-bank identifiability. A finite plot cannot settle any of those questions.

PART II

Arithmetic depth and signed measures

Complex parameters, positive kernels and the boundaries of positivity.

CHAPTER II

Arithmetic at complex depth

2.1 Arithmetic energy at complex depth

For real $a > 1/2$, $\beta > 0$, and integer $Q \geq 1$, define

$$A_{a,\beta,Q}(s) = \sum_{\substack{n \geq 2 \\ (n,Q)=1}} \mu(n)^2 n^{-2a} (1 - n^{-\beta})^{2s}, \qquad s \in \mathbb{C}.$$

The complex power uses the real logarithm of $1 - n^{-\beta} > 0$. The atom $n = 1$ is excluded because its logarithm is undefined. At positive integer depths its omitted contribution would be zero. At depth zero the corresponding mass-one atom is absent. In particular, $A(0) = Z_Q(2a) - 1$, where

$$Z_Q(v) = \sum_{\substack{n \geq 1 \\ (n,Q)=1}} \mu(n)^2 n^{-v} = \frac{\zeta(v)}{\zeta(2v)} \prod_{p \mid Q} (1 + p^{-v})^{-1}, \qquad v > 1.$$

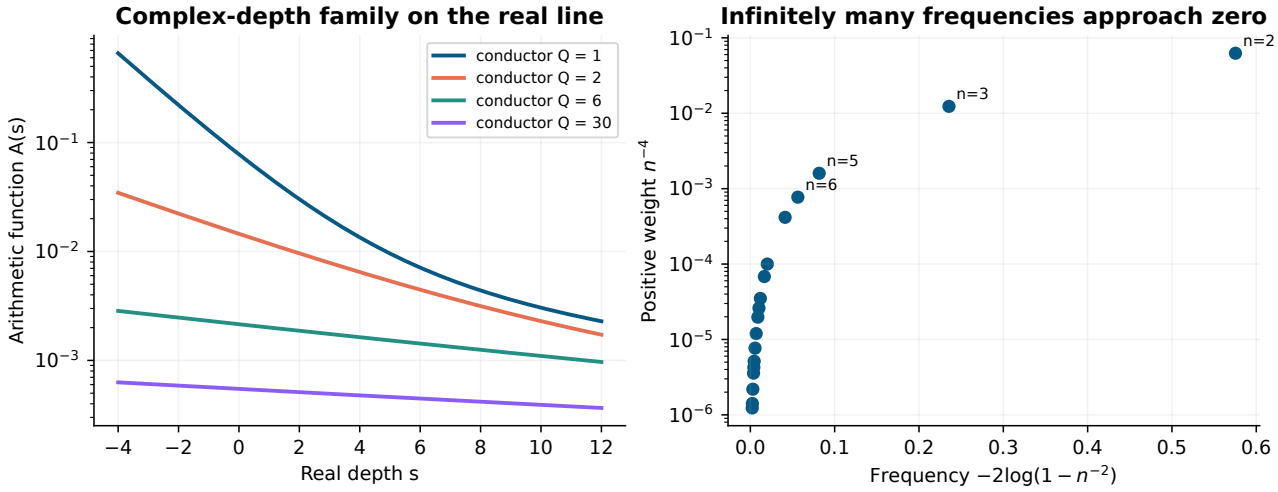


Figure 2.1. Left: $a = \beta = 2$ at real depths, using the exact zeta–Newton representation at 90-digit working precision. Right: initial squarefree frequencies and weights for $Q = 1$. Only finitely many atoms are shown; the proof uses the infinite support.

Let $\mathcal{S}_Q = \{n \geq 2 : \mu(n)^2 = 1,\ (n, Q) = 1\}$ and $\lambda_n = -2\log(1 - n^{-\beta})$. Then

$$A(s) = \sum_{n \in \mathcal{S}_Q} w_n e^{-\lambda_n s}, \qquad w_n = n^{-2a}.$$

The positive weights are summable, and the distinct support frequencies decrease to zero. If p_* is the least prime not dividing Q, then

$$\tau = -2\log(1 - p_*^{-\beta}), \qquad M = Z_Q(2a) - 1,$$

$$|A(s)| \leq M e^{\tau \max(-\Re s, 0)}.$$

This proves local uniform convergence and entire continuation. The first atom dominates $A(-t)$ as $t \to \infty$, so the entire function has exact order one and exponential type τ.

2.2 Closed shifts, infinite differential complexity

The Euler product for Z_Q shows that only $\mathrm{rad}(Q) = \prod_{p|Q} p$ matters. Expansion of the depth factor gives

$$\boxed{A_{a,\beta,Q}(s+1) = A_{a,\beta,Q}(s) - 2A_{a+\beta/2,\beta,Q}(s) + A_{a+\beta,\beta,Q}(s).}$$

The fractional transfer and Newton formulas are

$$A_{a,\beta,Q}(s+t) = \sum_{j \geq 0} (-1)^j \binom{2t}{j} A_{a+j\beta/2,\beta,Q}(s),$$

$$A_{a,\beta,Q}(t) = \sum_{j \geq 0} (-1)^j \binom{2t}{j} [Z_Q(2a + j\beta) - 1].$$

They converge absolutely and locally uniformly: binomial coefficients have at most polynomial growth on compact parameter sets, while the shifted sums decay geometrically. The subtraction of one is essential at noninteger depth.

No polynomial-coefficient linear ODE

Suppose $\sum_{j=0}^{r} P_j(s) A^{(j)}(s) = 0$, where the P_j are polynomials and are not all zero. At $s = -t$, divide by the exponential of the first support atom. The remaining tail is exponentially smaller, so the polynomial $\sum_j P_j(-t)(-\lambda_{p_*})^j$ tends to zero exponentially and must vanish identically. Remove that atom and repeat. Every support frequency therefore satisfies $\sum_j P_j(s)(-\lambda_n)^j = 0$ for all s. For fixed s, this polynomial in λ has infinitely many distinct roots. All its coefficients vanish. Thus all P_j are zero, a contradiction.

The function is **not D-finite in depth**. This excludes identification in the depth variable with fixed finite-parameter hypergeometric or Meijer G functions and ordinary finite D-finite combinations. It does not exclude nonalgebraic substitutions or representations by known non-D-finite functions.

Strict positive complex kernel

For distinct complex points s_i, $K_{ij} = A(s_i + \overline{s_j})$ is strictly positive definite. A zero quadratic form would force a finite exponential sum to vanish at every λ_n. Their accumulation at zero invokes the identity theorem; derivatives at zero then give a nonsingular Vandermonde system. On the real axis, $(-1)^j A^{(j)}(s) > 0$ for every $j \geq 0$.

2.3 An arithmetic sector law

The negative real direction is governed by the first admissible prime. The positive direction is governed by the density of infinitely many squarefree integers. These are different pieces of the same entire function.

Let

$$\alpha = \frac{2a-1}{\beta}, \qquad \delta_Q = \frac{1}{\zeta(2)} \prod_{p \mid Q} \frac{p}{p+1}.$$

As $|s| \to \infty$ in any closed sector $|\arg s| \leq \pi/2 - \epsilon$ with $0 < \epsilon < \pi/2$,

$$\boxed{A_{a,\beta,Q}(s) = \frac{\delta_Q}{\beta} B(\alpha, 2s+1) + O_{a,\beta,Q,\epsilon}\left(|s|^{-(2a-1/2)/\beta}\right).}$$

In particular,

$$A_{a,\beta,Q}(s) \sim \frac{\delta_Q \Gamma(\alpha)}{\beta} (2s)^{-\alpha}.$$

The principal power is used in the right half-plane. The beta expression is an asymptotic continuous-density model, not an identity with the arithmetic sum.

Proof mechanism

Squarefree inclusion–exclusion gives

$$\sum_{\substack{n \leq x \\ (n,Q)=1}} \mu(n)^2 = \delta_Q x + O_Q(\sqrt{x}).$$

Integrate against $g_s(x) = x^{-2a}(1 - x^{-\beta})^{2s}$ on $[1, \infty)$. The density term becomes the beta integral after $y = x^{-\beta}$. Partial integration bounds the error by $C_Q \int_1^\infty \sqrt{x} |g_s'(x)|\, dx$. The two derivative terms are beta integrals with decay exponent $(2a - 1/2)/\beta$; $|s|/\Re s$ stays bounded in the stated sector. This gives the error term and then the leading asymptotic.

One complex example

At $a = \beta = 2$, $Q = 1$,

$$A(1/2 + i/4) \approx 0.06033183289343401791658 - 0.00741238405378543625 1981\, i.$$

Direct finite sums and a zeta–Newton evaluation agree within the recorded omitted-tail envelope. This is an ordinary high-precision example, not an interval certificate.

Mixed Dirichlet-character weights provide matrix-valued positive kernels. Individual off-diagonal entries may be signed or complex, so complete monotonicity is asserted only for the positive principal family.

2.4 The function encodes its parameters

The complete exact analytic germ determines

$$\boxed{a, \quad \beta, \quad \mathrm{rad}(Q).}$$

Precisely, two admissible triples define the same germ if and only if these three quantities agree. Prime powers in Q are invisible because the terms use only coprimality. A finite Taylor polynomial or noisy measurements are different inputs from the complete germ in this theorem.

Let the support integers be $n_1 < n_2 < \cdots$, frequencies $\lambda_j = -2\log(1 - n_j^{-\beta})$, and weights $w_j = n_j^{-2a}$. Starting at $R_1 = A$, peel the ordered atoms:

$$\lambda_j = \lim_{t\to\infty} \frac{\log R_j(-t)}{t}, \qquad w_j = \lim_{t\to\infty} e^{-\lambda_j t} R_j(-t),$$

$$R_{j+1}(s) = R_j(s) - w_j e^{-\lambda_j s}.$$

Every limit follows from the isolated largest remaining frequency and the positive summable tail. Thus the exact function determines its spectral list.

The counting law $N_Q(x) = \delta_Q x + O_Q(\sqrt{x})$ gives

$$\lambda_j = 2\delta_Q^{\beta} j^{-\beta}[1 + O_{Q,\beta}(j^{-1/2} + j^{-\beta})], \quad \beta = -\lim_{j\to\infty} \frac{\log \lambda_j}{\log j}.$$

Once β is recovered,

$$n_j = (1 - e^{-\lambda_j/2})^{-1/\beta}, \qquad a = -\frac{\log w_j}{2\log n_j}.$$

Prime membership in this integer support then recovers the excluded prime set. The reconstruction is exact from infinite data; it does not certify that a finite search has found every excluded prime.

Classical Laplace uniqueness provides a comparison for the inverse mechanism. The parameter-specific extraction, frequency-rank law, and explicit instability are proved locally in the complete arithmetic route.

2.5 Separation improves while subtraction worsens

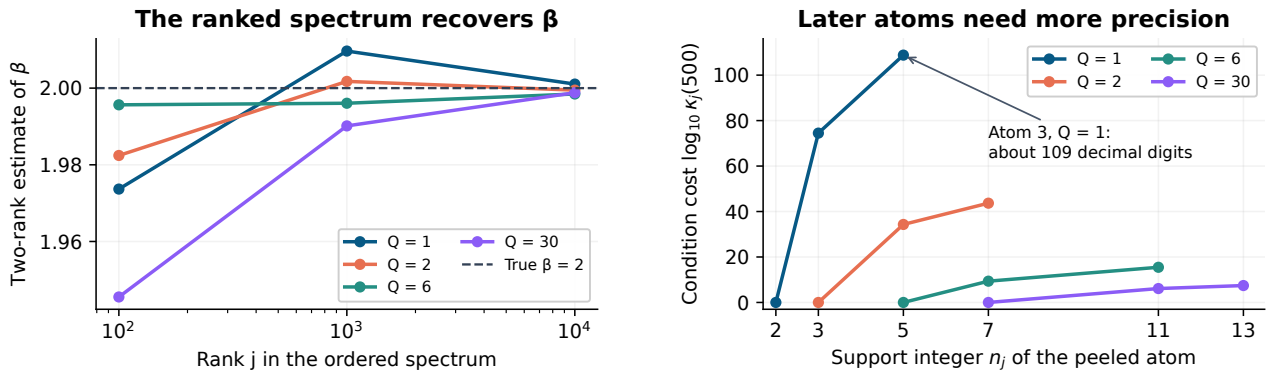


Figure 2.2. The frequency-rank estimates converge toward the depth exponent. Later-atom peeling at large negative depth also has a rapidly growing subtraction condition factor. These are finite examples from the checked arithmetic run, not certified floating-point intervals.

If earlier atoms have been removed exactly, set $\Delta_j = \lambda_j - \lambda_{j+1} > 0$, $M_{j+1} = \sum_{k>j} w_k$. The logarithmic secant

$$\widehat{\lambda}_j(t,h) = \frac{\log R_j(-t-h) - \log R_j(-t)}{h}$$

obeys, for $t \geq 0$, $h > 0$,

$$0 \leq \lambda_j - \widehat{\lambda}_j(t,h) \leq \frac{1}{h} \log\left(1 + \frac{M_{j+1}}{w_j} e^{-\Delta_j t}\right).$$

This improves with negative depth. But relative error in $A(-t)$ can be amplified after subtraction by

$$\kappa_j(t) = \frac{A(-t)}{R_j(-t)} \sim \frac{w_1}{w_j} e^{(\lambda_1 - \lambda_j)t}.$$

For the displayed $Q = 1$ example, the third-atom subtraction at $t = 500$ has a condition factor of roughly $10^{108.8}$. Exact uniqueness therefore does not promise easy recovery from ordinary precision.

2.6 A large prime can hide in every finite window

For a prime $p \nmid Q$, any $R \geq 0$, and integer $k \geq 0$,

$$\boxed{\sup_{|s| \leq R} |A^{(k)}_{a,\beta,Q}(s) - A^{(k)}_{a,\beta,Qp}(s)| \leq \lambda_p^k e^{R\lambda_p} \frac{Z_Q(2a)}{p^{2a}+1}.}$$

The difference consists of the p-divisible admissible squarefree atoms. Their frequencies are at most λ_p and their total weight is the Euler-factor expression on the right. Termwise differentiation proves the bound for every derivative.

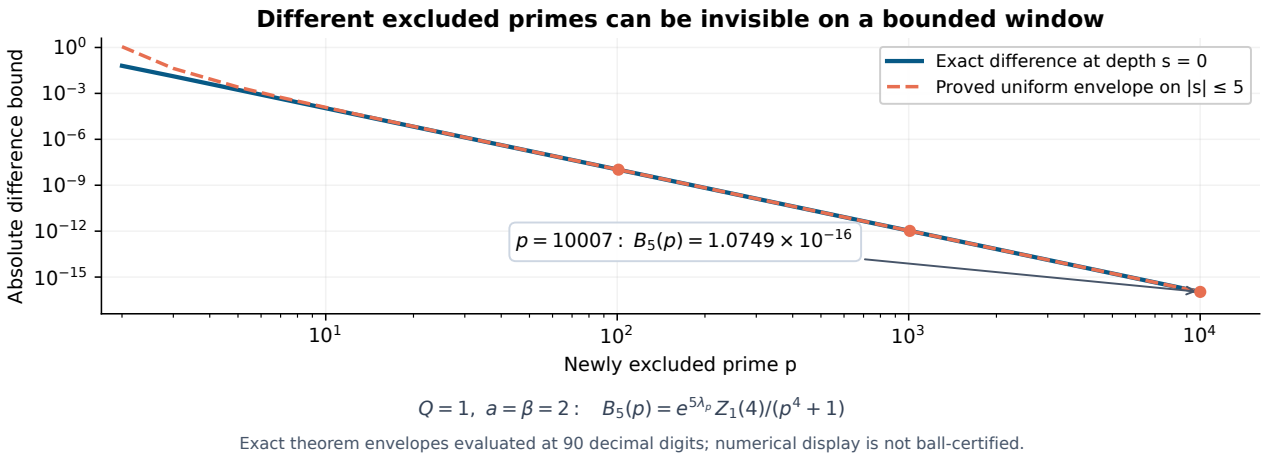


Figure 2.3. The proved compact-window envelope shrinks as the excluded prime increases. At $a = \beta = 2$, $Q = 1$, $R = 5$, excluding $p = 10007$ changes the entire window by at most approximately 1.0749×10^{-16}. The depth-zero difference is known exactly.

The radical differs for every such prime, while all bounded-window derivatives converge to those of A_Q. Without a bound on excluded primes, there is no uniformly stable inverse from these windows to the radical parameter.

The same distinction appears in weak taps: exact structural invariants can change under perturbations that are small at finite resolution.

2.7 An infinite feature space with arithmetic labels

For the ordered support, define $\phi_s(j) = \sqrt{w_j} e^{-\lambda_j s}$. The kernel $A(s + \bar{t})$ is its weighted ℓ^2 Gram kernel. Summability and bounded frequencies make every feature vector well defined.

If a weighted ℓ^2 combination produces the zero entire function, Cauchy–Schwarz makes its coefficients absolutely summable. Successive dominant-frequency peeling then forces every coefficient to vanish. This gives an injective Hilbert realization, and all finite derivative Hankel matrices have full rank: a nonzero polynomial in λ cannot vanish on the infinite frequency support.

Fixed-modulus character resolution

For characters χ, ψ modulo a fixed Q, let $\eta = \chi\overline{\psi}$. When η is nonprincipal, the elementary square-free character sum is $O_Q(\sqrt{x})$, with no density term. The same sector partial-integration argument therefore gives

$$A_{\chi,\psi}(s) = O_{a,\beta,Q,\epsilon}\big(|s|^{-(2a-1/2)/\beta}\big), \qquad |\arg s| \le \pi/2 - \epsilon.$$

Compared with the principal $|s|^{-(2a-1)/\beta}$ scale, this is faster by $|s|^{-1/(2\beta)}$. The modulus is fixed; the constants are not asserted uniform as Q grows. Individual off-diagonal functions can be complex and are not asserted completely monotone.

CHAPTER III

Prime sieves and signed measures

3.1 An infinite prime shelf changes the packets

For a prime p and $\lambda \geq -1$, let

$$x_n = (1 - n^{-2})^2, \qquad \nu_{p,\lambda} = \sum_{n \geq 1} \mu(n)^2 n^{-4} (1 + \lambda \mathbf{1}_{p \mid n}) \delta_{x_n}.$$

Define monic orthogonal polynomials $P_m^{(k;p,\lambda)}$ for the measure $x^k \, d\nu_{p,\lambda}$, $k \geq 0$ integer. The zero atom has mass one at $k = 0$ and is annihilated when $k \geq 1$.

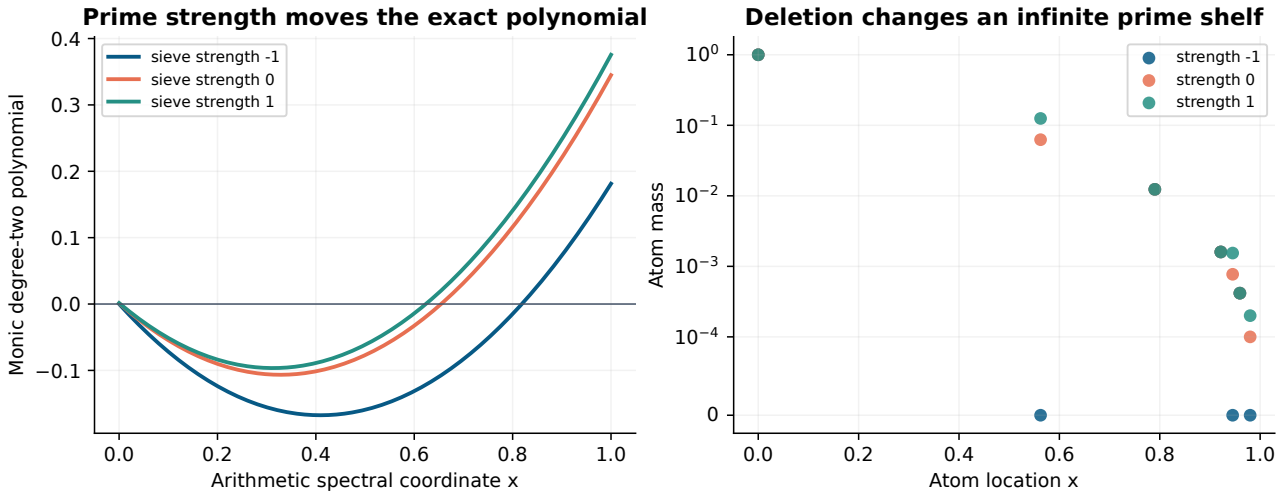


Figure 3.1. Left: degree-two packets for $p = 2$, depth zero. Right: initial atom masses. Strength -1 deletes every even squarefree atom; strength 0 is the original measure; strength 1 doubles that shelf.

The exact moments are finite zeta stencils:

$$M_j^{p,\lambda} = \sum_{r=0}^{2j} (-1)^r \binom{2j}{r} \frac{\zeta(4 + 2r)}{\zeta(8 + 4r)} \left(1 + \frac{\lambda}{p^{4+2r} + 1}\right).$$

All polynomial coefficients belong to $\mathbb{Q}(\pi^{-2}, \lambda)$. With $\Delta = M_0 M_2 - M_1^2$,

$$P_1 = x - \frac{M_1}{M_0}, \qquad P_2 = x^2 - \frac{M_0 M_3 - M_1 M_2}{\Delta} x + \frac{M_1 M_3 - M_2^2}{\Delta}.$$

The infinitely many positive nodes make every Hankel matrix strictly positive definite throughout $\lambda \geq -1$. Hence all degrees exist, with positive norms, real simple zeros in $(0, 1)$, and interlacing.

3.2 Finite positivity can conceal a signed defect

Let $\nu_{\mathrm{non}p}$ and ν_p be the restrictions of the undeformed measure $\nu_{p,0}$ to indices not divisible by p and divisible by p, respectively. Then $\nu_{p,\lambda} = \nu_{\mathrm{non}p} + (1+\lambda)\nu_p$. Let A_m, B_m be the order-m Hankel matrices of these two unscaled positive measures. Both are positive definite. Thus

$$\tau_m(\lambda) = \det(A_m + (1+\lambda)B_m) = \det A_m \prod_{i=1}^{m} [1 + (1+\lambda)\eta_i],$$

where $\eta_i > 0$ are the eigenvalues of $A_m^{-1/2} B_m A_m^{-1/2}$. Every determinant root is real and below -1; possible coefficient poles occur there, although numerator cancellation is possible.

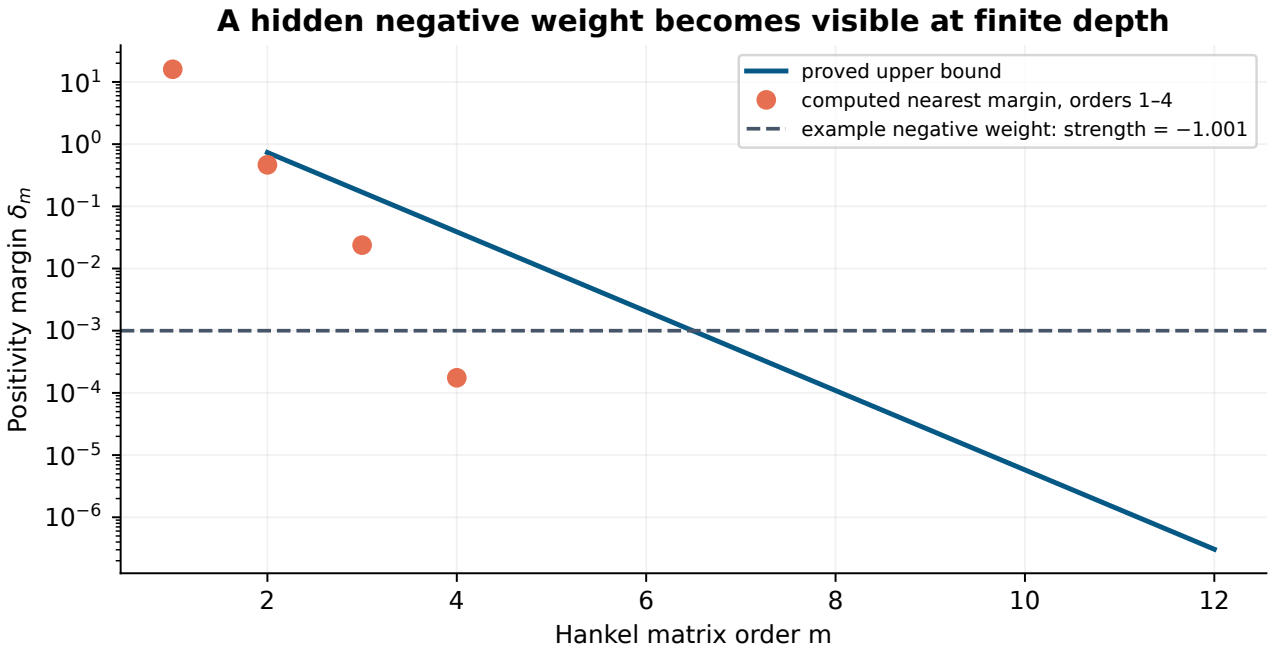


Figure 3.2. The line is a proved bound for $p = 2$; dots are ordinary high-precision pencil roots. A defect $\lambda = -1.001$ eventually violates positivity even though it can pass low-order checks.

The nearest root is $-1 - \delta_m$, with

$$\delta_m = \min_{\substack{f \in \mathbb{R}[x] \setminus \{0\} \\ \deg f < m}} \frac{\int f^2 \, d\nu_{\mathrm{non}p}}{\int f^2 \, d\nu_p} > 0, \qquad \delta_m \downarrow 0.$$

To prove the limit, approximate a continuous bump supported at the isolated node x_p by polynomials on $[0,1]$. The numerator tends to zero while the denominator retains the p^{-4} atom. Hence every $\lambda < -1$ eventually produces a negative finite-degree quadratic form.

For $p = 2$, test with $f(x) = x(1-x)^{m-2}$, $m \geq 2$:

$$\delta_m \leq \frac{4096}{81}\left(\frac{16M_0}{17} - 1\right)\left(\frac{272}{567}\right)^{2(m-2)}, \qquad M_0 = 105\pi^{-4}.$$

This follows from $x_2 = 9/16$ and $x_n \geq 64/81$ at nonzero odd nodes. Exactly $\delta_1 = p^4$; the limit is an infinite-resolution phenomenon.

3.3 Classical operations with arithmetic coordinates

The depth tilt x^k is a Christoffel transformation. Suppressing p, λ,

$$P_m^{(k+1)}(x) = \frac{P_{m+1}^{(k)}(x) - [P_{m+1}^{(k)}(0)/P_m^{(k)}(0)]P_m^{(k)}(x)}{x}.$$

The numerator vanishes at zero. All roots are positive, so the displayed denominator coefficient is nonzero. For shifted Hankel determinants $\tau_m^{(k)} = \det[M_{k+i+j}]_{i,j<m}$, with $\tau_0^{(k)} = 1$,

$$\tau_m^{(k)}\tau_m^{(k+2)} - (\tau_m^{(k+1)})^2 = \tau_{m+1}^{(k)}\tau_{m-1}^{(k+2)} > 0, \qquad m \geq 1.$$

This is the Desnanot–Jacobi identity applied to exact arithmetic moments. The construction mechanism is classical.

An endpoint mass is numerically delicate

For the undeformed depth-zero measure, set $\nu_\theta = \nu + \theta\delta_0$, $\theta \geq -1$. Write $h_j = \int P_j(x)^2\, d\nu(x)$ and $K_m(x,y) = \sum_{j=0}^m P_j(x)P_j(y)/h_j$. The Uvarov formula [5] is

$$P_m^{[\theta]}(x) = P_m(x) - \frac{\theta P_m(0)}{1 + \theta K_{m-1}(0,0)}K_{m-1}(x,0),$$

with $K_{-1} = 0$ for degree zero. The mass at zero is recovered by

$$1 \leq \frac{1}{K_m(0,0)} \leq 1 + (M_0 - 1)(7/16)^{2m}.$$

The lower bound comes from the zero atom, whose mass is one. The test polynomial $(1-x)^m$ gives the upper bound since every other node is at least $9/16$. At finite degree $K_m(0,0) < 1$, because no nonzero polynomial can vanish at all the other infinitely many nodes. Complete mass removal is valid, while $1 - K_m(0,0)$ becomes very small. This explains the conditioning problem.

The resolvent is non-D-finite

For $\lambda \geq -1$, the Stieltjes function $S_{p,\lambda}(z) = \int (z-x)^{-1}\, d\nu_{p,\lambda}(x)$ has infinitely many isolated poles at the positive-weight nodes $x_n \to 1$. A solution of a finite rational-coefficient linear ODE has only

finitely many possible finite singular points. The germ at $z = 2$ therefore is not D-finite. This is a general infinite-atomic-resolvent mechanism, specialized here to arithmetic data.

The full packet sequence also cannot be an affine copy of a continuous Jacobi sequence: compact moment determinacy would equate a purely atomic measure with a continuous one. An inherited Laguerre scaling limit remains compatible with this separation of the complete families.

3.4 Overlap is part of the arithmetic

For a finite set F of distinct primes, define

$$\nu_{F,\lambda} = \sum_{n\geq 1} \mu(n)^2 n^{-4} \prod_{p\in F} (1 + \lambda_p \mathbf{1}_{p|n}) \delta_{x_n}, \quad x_n = (1 - n^{-2})^2.$$

For real strengths, the exact positivity domain is

$$\boxed{\lambda_p \geq -1 \quad \text{for every } p \in F.}$$

Sufficiency is termwise positivity. If one strength is below -1, the atom $n = p$ isolates its negative factor. The other strengths do not occur at that atom. At every simultaneous deletion endpoint, primes outside F still supply infinitely many positive nodes, so all Hankel matrices remain strictly positive definite.

The exact coordinate formula is

$$M_j(\lambda) = \sum_{r=0}^{2j} (-1)^r \binom{2j}{r} \frac{\zeta(4+2r)}{\zeta(8+4r)} \prod_{p\in F} \left(1 + \frac{\lambda_p}{p^{4+2r}+1}\right).$$

Coefficients of the monic families lie in $\mathbb{Q}(\pi^{-2}, \lambda_p : p \in F)$. For two primes, the overlap term is visible:

$$M_j = M_j(0,0) + \lambda_p U_{p,j} + \lambda_q U_{q,j} + \lambda_p \lambda_q U_{pq,j}.$$

Here $U_{pq,j} > 0$ is the pq-divisible submeasure moment. The family does not reduce to adding separate prime responses without their overlap.

3.5 Moment positivity is a weaker requirement

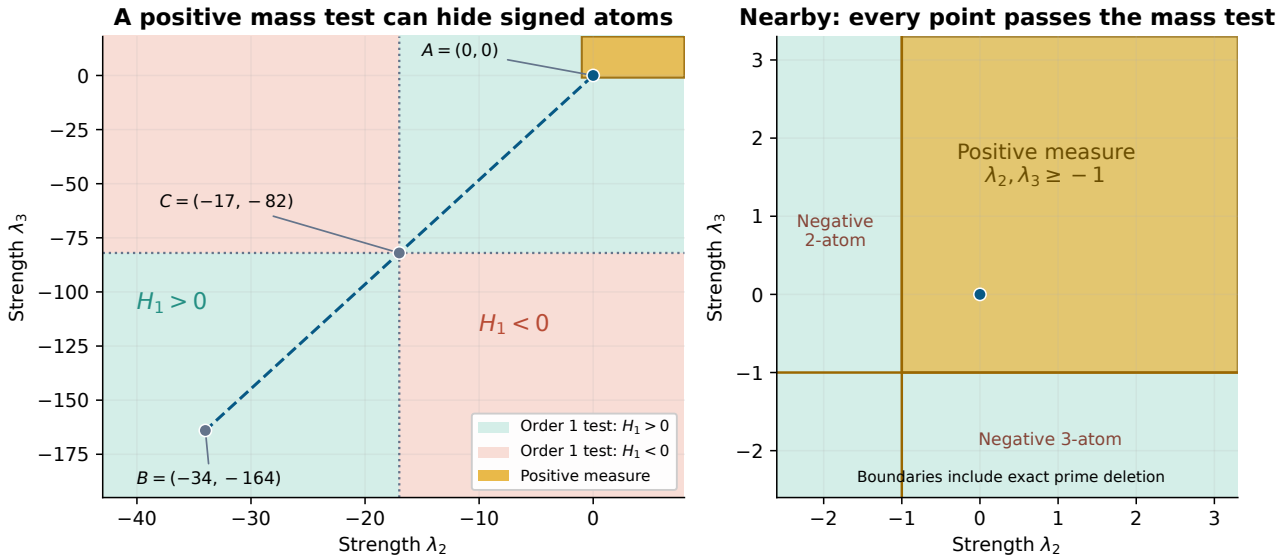


Figure 3.3. The exact positive-measure domain and the order-one moment test have different parameter geometry. Regions passing a finite test outside the safe orthant still contain negative atoms.

For primes two and three,

$$M_0 = 105\pi^{-4}(1 + \lambda_2/17)(1 + \lambda_3/82).$$

Both $(0, 0)$ and $(-34, -164)$ have positive total mass. Their midpoint $(-17, -82)$ has zero mass. Thus the parameter set passing the order-one positive-definiteness test is nonconvex. This particular midpoint argument does not establish nonconvexity of the semidefinite test, which permits zero. For that test, take the two points $(0, 0)$ and $(-34, -246)$. The normalized masses $M_0/(105\pi^{-4})$ there are 1 and 2. Their convex combination with weights $3/5$ and $2/5$ is $(-68/5, -492/5)$, where the normalized mass is $-1/25$. Thus the order-one semidefinite feasible set is also nonconvex, by a separate counterexample.

A separate additive family has different geometry

For weights $1 + \sum_{p \in F} \gamma_p \mathbf{1}_{p|n}$, positivity is equivalent to

$$1 + \sum_{\gamma_p < 0} \gamma_p \geq 0.$$

Every prime subset appears at its squarefree product, proving necessity. Checking each atom proves sufficiency. Its finite Hankel matrices are affine in γ, so the semidefinite feasible sets are convex spectrahedra. The multiplicative family has genuine overlap terms and polynomial parameter dependence. These are two distinct deformations, with distinct domains.

3.6 Every negative prime atom has a finite detector

For an integer $a \geq 2$, let

$$L_a(x) = \prod_{n=1}^{a-1} \frac{x - x_n}{x_a - x_n}, \quad C_a = L_a(1), \quad r_a = \frac{1 - x_{a+1}}{1 - x_a} < 1,$$

$$f_{a,m}(x) = L_a(x) \left(\frac{1 - x}{1 - x_a} \right)^m.$$

This polynomial kills every lower node, equals one at x_a, and has absolute value at most $C_a r_a^m$ at every higher node.

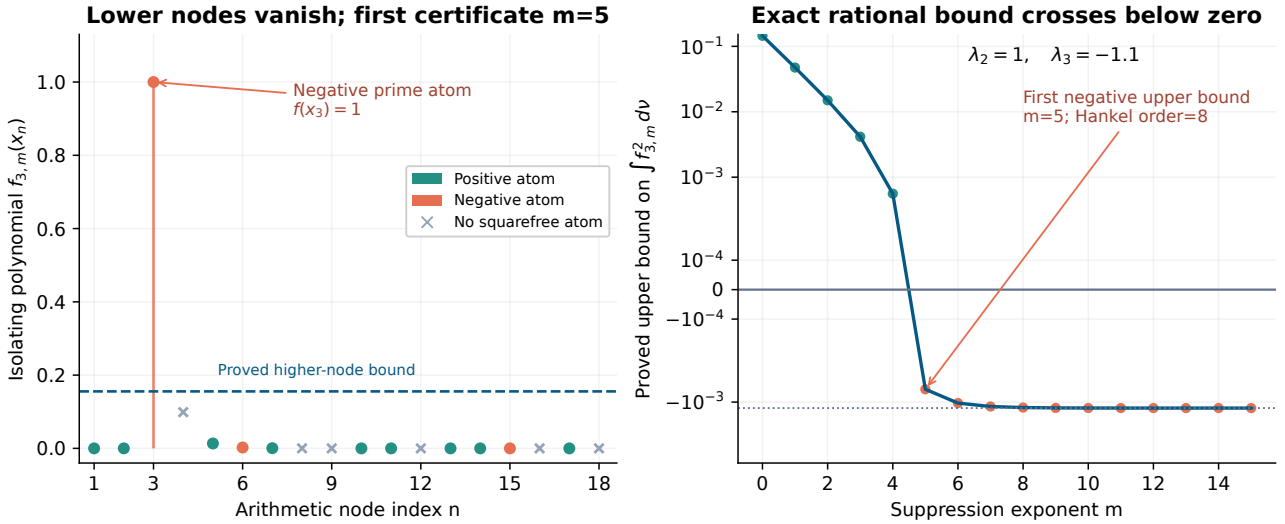


Figure 3.4. A rational detector for $p = 3$, $\lambda_3 = -1.1$, $\lambda_2 = 1$. The first exact bound proving negativity is $m = 5$, so a Hankel matrix of order eight detects the signed defect.

Set $C_F = \prod_{q \in F} \max(1, |1 + \lambda_q|)$. The summable tail gives

$$\int f_{p,m}^2 \, d\nu \leq \frac{1 + \lambda_p}{p^4} + \frac{C_F C_p^2}{3p^3} r_p^{2m}.$$

Hence the quadratic form is negative whenever $pC_F C_p^2 r_p^{2m}/3 < -(1 + \lambda_p)$. For rational strengths this is an exact rational certificate. It needs no numerical eigenvalue calculation. A depth tilt x^k replaces the negative atom contribution by $(1 + \lambda_p) x_p^k / p^4$.

3.7 Real singularities survive multiple deletions

Fix all strengths except λ_p, with the others at least -1. The remaining moment matrix has the form $A_m + (1 + \lambda_p) B_m$, where A_m is the p-free part and B_m the p-divisible part. Both are positive definite, even at other deletion endpoints: primes outside F supply the first support, and integers $p\ell$ the second.

Thus every one-variable determinant fiber has exact degree m and all roots real below -1. Its nearest margin satisfies

$$\delta_m = \min_{\substack{f \in \mathbb{R}[x]\setminus\{0\} \\ \deg f < m}} \frac{\int f^2 \, d\nu_{p\text{-free}}}{\int f^2 \, d\nu_{p\text{-divisible}}}, \qquad \delta_m \downarrow 0.$$

The detector yields, for $C_\kappa = \prod_{q \neq p} \max(1, 1 + \lambda_q)$,

$$\delta_{p+m} \leq \frac{p C_\kappa C_p^2}{3} r_p^{2m}.$$

The denominator retains the atom p; all lower nodes in the numerator are killed. This extends the prime-two bound to every prime and to simultaneous positive or deletion strengths. It does not assert simple roots or global multivariate real stability.

If at least two positive-domain strengths are nonzero, the complete monic sequence cannot equal a one-prime sequence on the same variable and nodes. Compact moment determinacy equates normalized measures; the fixed mass at zero fixes their scale; atom weights at the individual primes then read off every strength. An arbitrary affine change of variable is outside this separator.

PART III

Orbit spectra and exact coordinates

Spectral continuation and the coefficient language of polyphase transforms.

CHAPTER IV

Spectral functions of zero orbits

4.1 One spectral address for each rotation orbit

For integer $N \geq 2$, define the classical Mittag–Leffler seed [4, §10.46]

$$d_N(w) = \sum_{n \geq 0} \frac{(-1)^n w^n}{(Nn)!} = E_{N,1}(-w), \qquad D_N(z) = d_N(z^N).$$

Let w_j be the nonzero zeros of d_N, counted with multiplicity. Each corresponds to one rotation orbit of N zeros of D_N. Using $\operatorname{Arg} w \in (-\pi, \pi]$, define

$$\boxed{\mathcal{Z}_N(s) = \sum_j w_j^{-s}, \qquad \Re s > 1/N.}$$

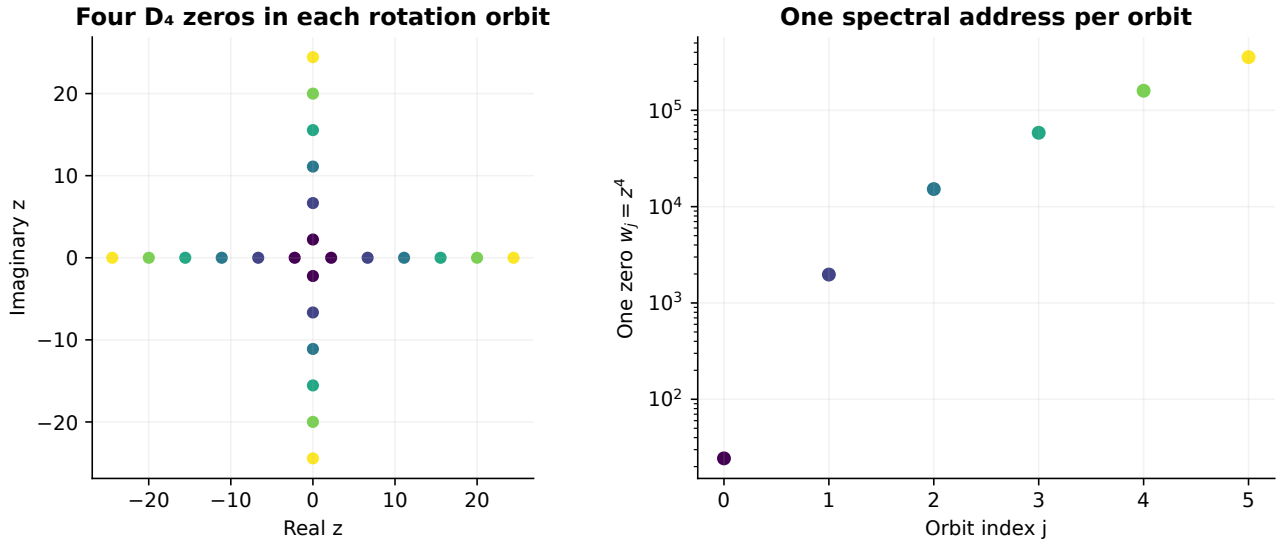


Figure 4.1. For $N = 4$, the four real/imaginary zeros in each orbit share one positive coordinate $w = z^4$. The plot shows the first six orbits. Multiplicity is retained by the definition; simplicity is not assumed in general.

The bound $|d_N(w)| \le e^{|w|^{1/N}}$ and the finite-order zero-counting theorem give absolute local uniform convergence in the stated half-plane. Since the order is below one and $d_N(0) = 1$, the Hadamard factorization has genus zero:

$$d_N(w) = \prod_j (1 - w/w_j).$$

At positive integers, a log derivative gives

$$-w\frac{d_N'(w)}{d_N(w)} = \sum_{k\ge 1} \mathcal{Z}_N(k) w^k.$$

If $a_n = (-1)^n/(Nn)!$ and $b_k = \mathcal{Z}_N(k)$, then

$$b_k = -ka_k - \sum_{j=1}^{k-1} a_j b_{k-j}.$$

Thus every positive integer value is rational without numerical zero finding.

4.2 Classical anchors and the open spectral frontier

The first values are

$$\mathcal{Z}_N(1) = \frac{1}{N!},$$
$$\mathcal{Z}_N(2) = \frac{1}{(N!)^2} - \frac{2}{(2N)!},$$
$$\mathcal{Z}_N(3) = \frac{1}{(N!)^3} - \frac{3}{N!(2N)!} + \frac{3}{(3N)!}.$$

N	$\mathcal{Z}_N(1)$	$\mathcal{Z}_N(2)$	$\mathcal{Z}_N(3)$
2	1/2	1/6	1/15
3	1/6	1/40	53/13440
4	1/24	17/10080	691/9979200
5	1/120	5/72576	997/1743565824

Two exact Hurwitz-zeta reductions

For $N = 2$, $d_2(w) = \cos\sqrt{w}$, whose zeros are $w_j = \pi^2(j + 1/2)^2$, $j \ge 0$. Therefore

$$\mathcal{Z}_2(s) = \pi^{-2s}\zeta(2s, 1/2).$$

For $N = 4$,

$$D_4(z) = \cos(z/\sqrt{2})\cosh(z/\sqrt{2}),$$

and the rotation quotient has one zero $w_j = (\sqrt{2}\pi)^4(j + 1/2)^4$ per orbit. Hence

$$\mathcal{Z}_4(s) = (\sqrt{2}\pi)^{-4s}\zeta(4s, 1/2).$$

These anchors are classical reductions. The general spectral-zeta mechanism also has substantial antecedents, including hypergeometric zero zeta functions.

Global meromorphic continuation

The half-plane definition has a meromorphic extension to the whole complex plane. The following sections prove its sole pole, special values, and regularized product using a branch-safe Mellin representation. These are worked spectral results from established analytic mechanisms. Residue-weighted sums involving derivatives at zeros remain a separate question, especially when multiplicities occur.

4.3 Global meromorphic continuation

For every integer $N \geq 2$, the orbit zeta has a meromorphic continuation to the whole complex plane with exactly one pole:

$$\boxed{s = 1/N, \qquad \operatorname{Res}_{s=1/N} \mathcal{Z}_N(s) = \frac{\sin(\pi/N)}{N\pi}.}$$

Its exact absolute-convergence abscissa is $1/N$. At nonpositive integers,

$$\boxed{\mathcal{Z}_N(-m) = 0 \quad (m \geq 0), \qquad \mathcal{Z}_N'(0) = -\log N.}$$

The zeta-regularized product of the orbit coordinates is consequently $\exp[-\mathcal{Z}_N'(0)] = N$.

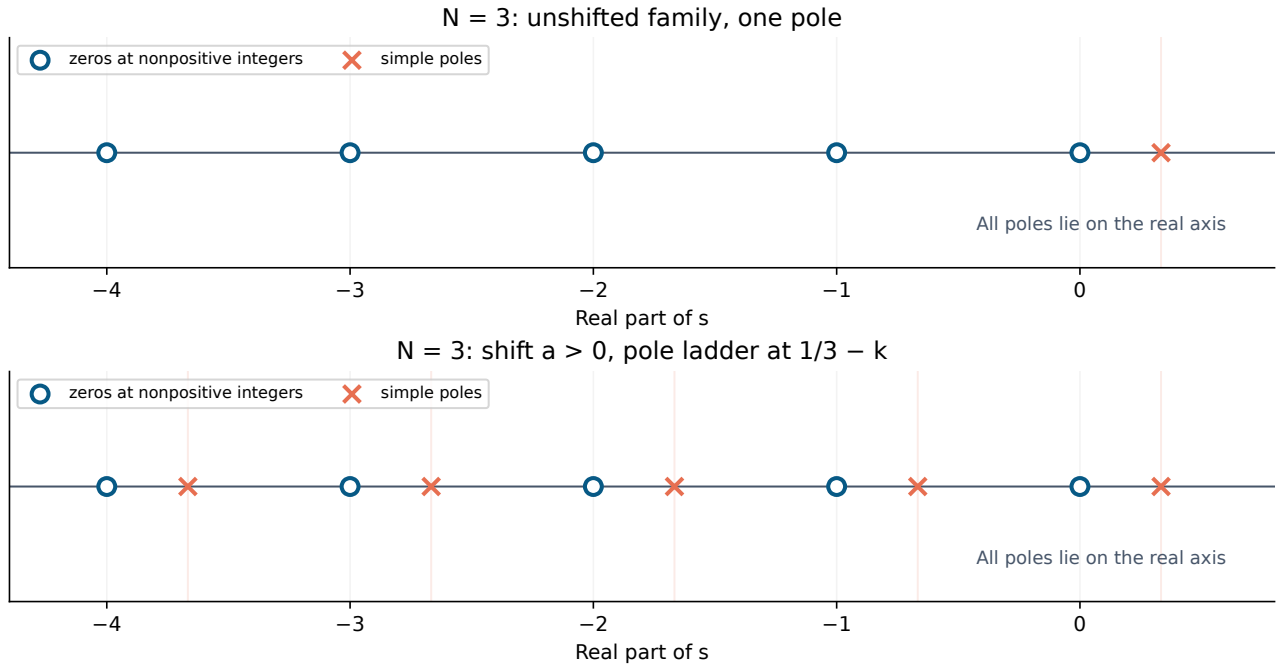


Figure 4.2. Pole and zero locations follow from the proved continuation. The second panel shows the shifted extension, where a pole ladder appears. These are exact structural locations rather than fitted roots.

The continuation uses classical Mellin regularization. The contribution here is a complete local application with multiplicities, principal branches, and all convergence hypotheses checked.

4.4 A finite exponential sum controls the tail

Put $E_N(t) = d_N(-t) = \sum_{n\geq 0} t^n/(Nn)!$ and $\omega = e^{2\pi i/N}$. For $x \geq 0$,

$$E_N(x^N) = \frac{1}{N}\sum_{j=0}^{N-1} e^{\omega^j x}.$$

Root filtering proves this identity term by term: only powers divisible by N remain. The positive real exponential is dominant, so

$$\log E_N(t) = t^{1/N} - \log N + O(e^{-\kappa_N t^{1/N}}), \quad \kappa_N = 1 - \cos(2\pi/N) > 0,$$

with corresponding differentiated estimates on the positive ray.

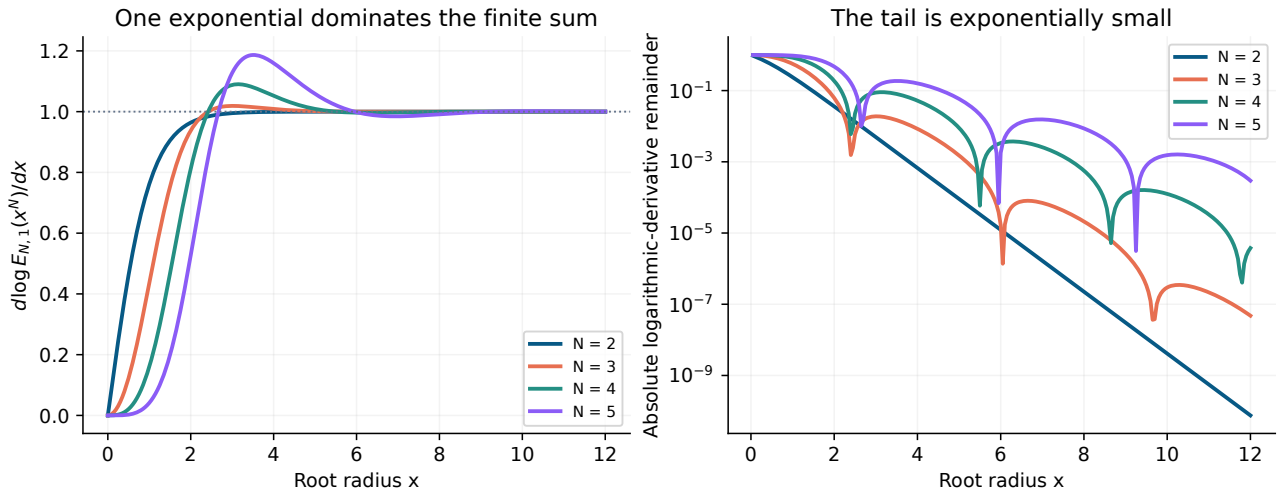


Figure 4.3. Computed logarithmic derivatives of the finite exponential sum approach one in the root-radius variable. The decaying remainder supplies the Mellin continuation's large-radius input.

Why complex zero arguments do not break the integral

In a sufficiently narrow sector around negative w, choose the root $x = (-w)^{1/N}$ near the positive real ray. The first exponential dominates the other $N-1$ terms by a uniform real-part gap at large radius, so this sector is eventually zero free. The finitely many remaining zeros avoid the negative real ray because $d_N(-t) > 0$ for $t \geq 0$. Thus all zero arguments have a uniform gap from the branch cut. In particular $|t + w_j| \geq c_N(t + |w_j|)$ for $t \geq 0$.

4.5 The two ends have different jobs

For $1/N < \Re s < 1$, the genus-zero log derivative and the angular gap give absolute interchange in

$$\mathcal{Z}_N(s) = \frac{\sin \pi s}{\pi}\int_0^\infty t^{-s}\frac{d}{dt}\log E_N(t)\,dt.$$

Each term uses the principal-branch beta integral $\int_0^\infty t^{-s}(t+w)^{-1}\,dt = \pi w^{-s}/\sin \pi s$. The denominator estimate bounds the absolute integral by a constant times $|w|^{-\Re s}$, whose sum converges in this strip.

Near zero write $f(t) = (\log E_N)'(t) = \sum_{k\geq 1} \alpha_k t^{k-1}$, where $\alpha_k = (-1)^{k+1}\mathcal{Z}_N(k)$. For any integer $K \geq 1$, subtract K terms on $[0,1]$:

$$I_K(s) = \int_0^1 t^{-s}\left[f(t) - \sum_{k=1}^{K} \alpha_k t^{k-1}\right] dt + \sum_{k=1}^{K} \frac{\alpha_k}{k-s} + \int_1^\infty t^{-s}\left[f(t) - \frac{1}{N}t^{1/N-1}\right] dt + \frac{1}{N(s-1/N)}.$$

The first integral is holomorphic for $\Re s < K+1$. The second is entire because its remainder decays exponentially in $t^{1/N}$. The factor $\sin \pi s$ cancels the positive-integer poles. Increasing K covers the plane, leaving only $1/N$. At nonpositive integers I_K is regular, so the sine factor gives zero.

At zero the finite parts give $I_K(0) = \lim_{T\to\infty}[\log E_N(T) - T^{1/N}] = -\log N$. Since $(\sin \pi s/\pi)'_{s=0} = 1$, this equals $\mathcal{Z}'_N(0)$. Absolute convergence at a smaller real exponent would give a holomorphic series across $1/N$, contradicting the pole and proving the exact abscissa.

4.6 A Hurwitz-type deformation and its determinant

For real $a \geq 0$, define initially

$$\mathcal{Z}_N(s;a) = \sum_j (w_j + a)^{-s}, \qquad \Re s > 1/N.$$

The rightward shift preserves avoidance of the negative branch cut. Normalize the product with $E_N(a)$ and use $\log E_N(a+t)$ in the Mellin argument. For $a > 0$ there are genuine simple poles at $s = 1/N - k$, $k \geq 0$:

$$\boxed{\operatorname{Res}_{s=1/N-k} \mathcal{Z}_N(s;a) = \frac{\sin(\pi/N)}{N\pi}\frac{(1-1/N)_k}{k!}a^k.}$$

Indeed the large-radius derivative expands as

$$\frac{1}{N}(a+t)^{1/N-1} = \frac{1}{N}\sum_{k\geq 0} \frac{(-1)^k(1-1/N)_k}{k!}a^k t^{1/N-1-k}$$

as an asymptotic series. The alternating sign is canceled by $\sin(\pi(1/N-k)) = (-1)^k \sin(\pi/N)$. At $a = 0$ all secondary residues vanish.

The negative-integer values remain zero, and

$$\mathcal{Z}'_N(0;a) = -\log[NE_N(a)], \qquad \boxed{\prod_j{}^{\mathrm{reg}}(w_j + a) = NE_{N,1}(a).}$$

The finite part $-\log N$ and normalization $-\log E_N(a)$ give a zeta-regularized product, not an ordinary product. At $N = 2$ it is $2\cosh\sqrt{a}$, the classical half-integer spectral determinant reproduced by the four shifted benchmarks. Functional equations and derivative-weighted zero sums remain open here.

CHAPTER V

Sequences, trees and polyphase

5.1 Integer coordinates for the nonlinear family

Normalize the Taylor coefficients by

$$A_n(q,r) = (2n+1)!c_n(q,r), \qquad A_0 = 1.$$

The recurrence becomes

$$\boxed{A_n = \sum_{i=0}^{n-1} \binom{2n}{2i+1} q^{2i+1} r^{2(n-1-i)+1} A_i A_{n-1-i}, \quad n \geq 1.}$$

Therefore $A_n \in \mathbb{Z}[q,r]$ has nonnegative coefficients and is symmetric in its two variables. The first coordinates are

$$A_1 = 2qr,$$
$$A_2 = 8q^2r^2(q^2+r^2),$$
$$A_3 = q^3r^3[48(q^2+r^2)(q^4+r^4) + 80q^2r^2].$$

At $(q,r) = (1,1)$ these are the tangent numbers $1, 2, 16, 272, 7936, \ldots$, the known OEIS A000182 anchor. At $(1,2)$ the exact sequence begins $1, 4, 160, 35200, 38041600, \ldots$.

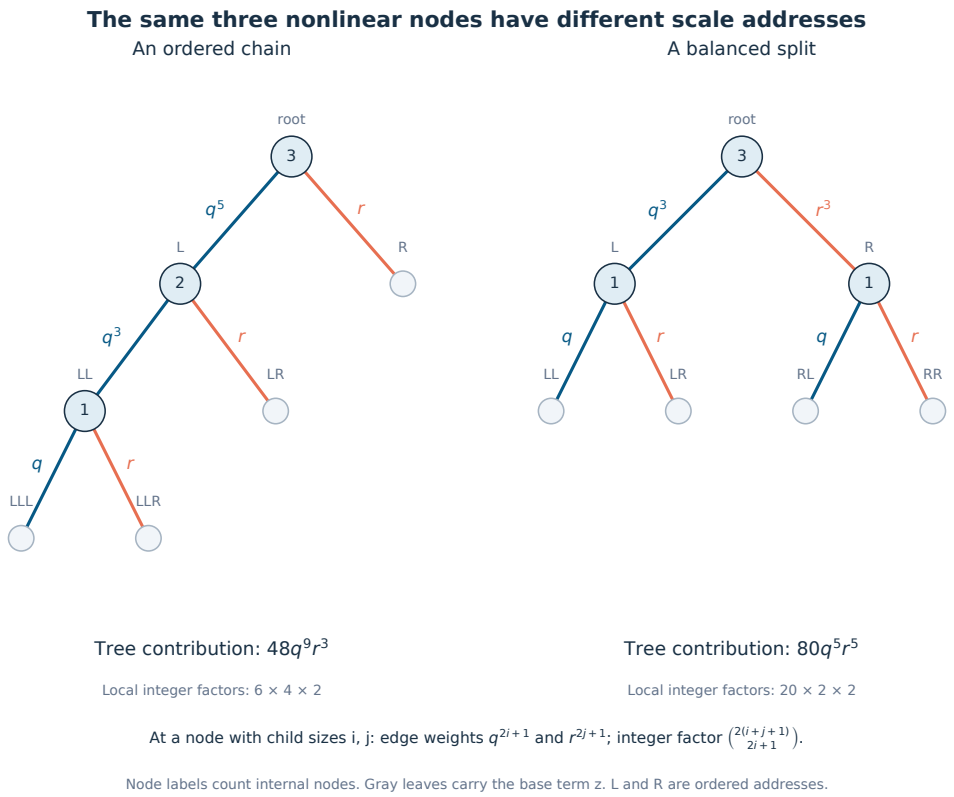


Figure 5.1. Ordered trees retain left/right path information. The two displayed shapes contribute different monomials to the same factorial-normalized coefficient. Their labels are exact tree data.

At rational scales, an integer denominator clearing is available. If D clears every contraction denominator and H clears every bank weight,

$$H^n D^{n(n+1)} A_n \in \mathbb{Z}.$$

The maximum root-path exponent sum over a full binary tree is $n(n+1)$. The clearing provides exact sequence exports without implying a new OEIS entry.

5.2 A formal sequence is not always an analytic germ

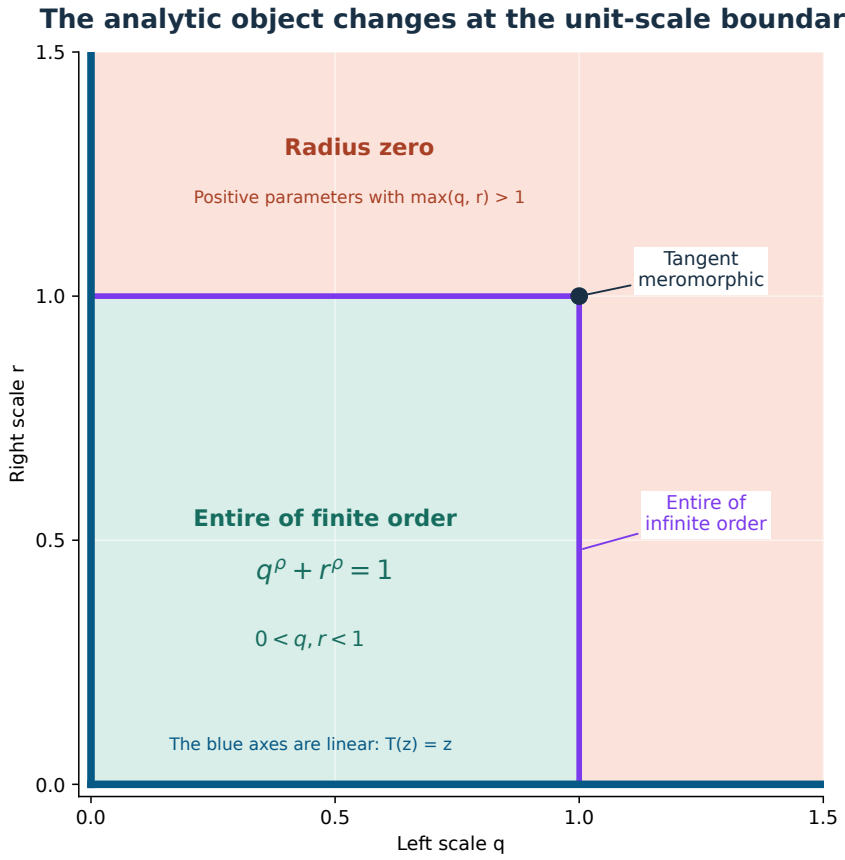


Figure 5.2. The full nonnegative real parameter map separates finite-order entire functions, infinite-order entire edges, tangent, and zero-radius formal series. Zero scales give the linear function.

If $q > 0$, $r > 1$, the recurrence includes its $i = 0$ term and gives

$$c_n \geq \frac{q^n r^{n^2}}{3 \cdot 5 \cdots (2n+1)}.$$

The root test proves zero radius. By symmetry this covers either scale above one, provided the other is positive. The exported positive integer asymmetric rows belong to this formal regime.

If $0 < q < 1$, $r = 1$, the equation is linear in the uncontracted value: $T' = 1 + T(qz)T(z)$. A known coefficient on $|z| < R/q$ gives a linear ODE there, so disk bootstrapping proves entire extension. On the positive ray, $(\log T)' = T(qR) + 1/T(R) \geq qR$, giving an exponential lower bound for T. Substitution back gives, for $R \geq 2/q$,

$$\log T(R) \geq \frac{R}{2} \exp(q^3 R^2/8 - q/2).$$

Thus the entire order is infinite. The corner $(1, 1)$ is tangent with poles. These exact boundaries protect the analytic interpretation of the catalog.

5.3 Polyphase sections preserve the full sequence

For an ordinary generating function $G(z) = \sum_{m \geq 0} a_m z^m$ and integer $b \geq 1$, write

$$G(z) = \sum_{j=0}^{b-1} z^j G_j(z^b), \qquad G_j(t) = \sum_{n \geq 0} a_{bn+j} t^n.$$

The root projector is

$$P_{b,j} G(z) = \frac{1}{b} \sum_{k=0}^{b-1} \omega^{-jk} G(\omega^k z) = z^j G_j(z^b), \qquad \omega = e^{2\pi i / b}.$$

The same projector works on an EGF, but the section retains its original factorials: $\sum_n a_{bn+j} z^{bn+j}/(bn+j)!$. Removing those denominators changes the representation and requires an explicit transport. Root filtering does not do it automatically.

For causal FIR taps h_ℓ, $b_m = \sum_\ell h_\ell a_{m-\ell}$ with zero extension to negative indices, split $A(z)$ and $B(z)$ into b phases. Then $B_i(t) = \sum_j H_{ij}(t) A_j(t)$, where

$$\boxed{H_{ij}(t) = \sum_{\substack{\ell \geq 0 \\ j+\ell \equiv i \pmod b}} h_\ell t^{(j+\ell-i)/b}.}$$

The exponent is the nonnegative carry to the next phase block. This is an exact coefficient law, with no approximation or loss of terms.

5.4 The carry matrix is part of the filter

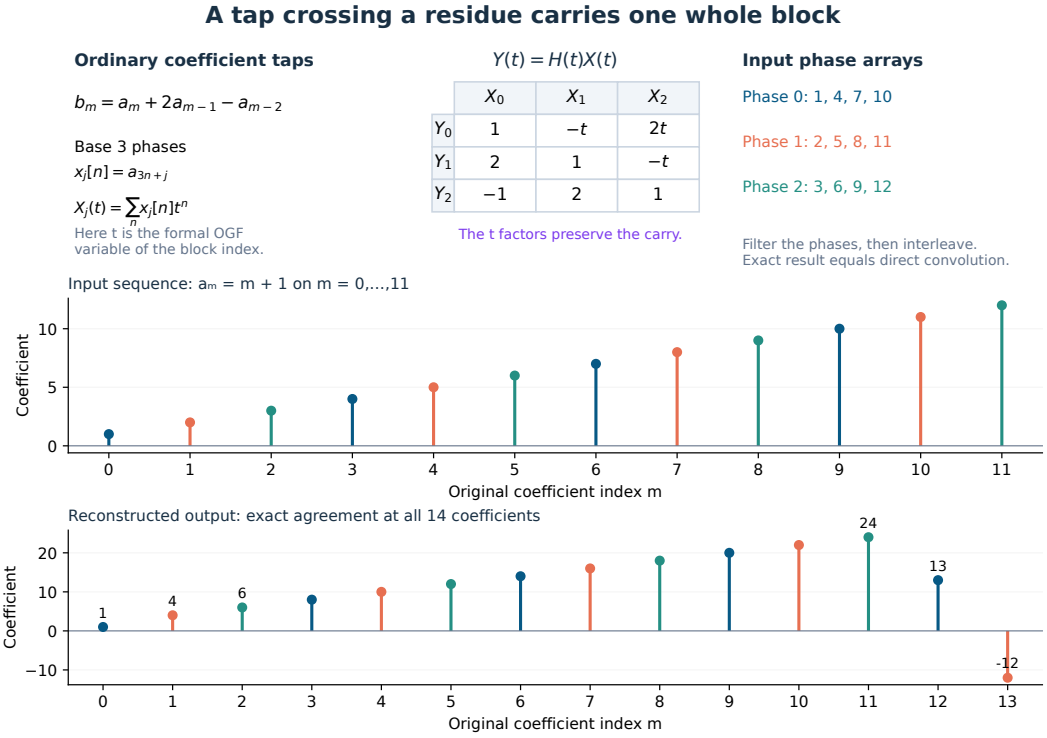


Figure 5.3. A three-phase filter with taps $[1, 2, -1]$. The matrix carries terms across block boundaries. Interleaving its output reproduces the direct scalar FIR calculation exactly.

With these taps and $b = 3$,

$$H(t) = \begin{pmatrix} 1 & -t & 2t \\ 2 & 1 & -t \\ -1 & 2 & 1 \end{pmatrix}.$$

The entries arise from the same congruence condition. For instance an input in phase two shifted by one lands in phase zero of the next block, contributing $2t$ to $H_{0,2}$.

Three operations that must be kept distinct

For an EGF $E_a(z) = \sum_m a_m z^m / m!$, differentiation transports future coefficients: $E_a^{(k)} = \sum_m a_{m+k} z^m / m!$. Causal ordinary taps instead act by repeated zero-constant integration:

$$E_b = \sum_\ell h_\ell I^\ell E_a.$$

Multiplication of two EGFs gives Hurwitz convolution, $b_m = \sum_{k=0}^{m} \binom{m}{k} a_k h_{m-k}$. It is not ordinary sequence FIR convolution. Intrinsic nonlinear feedback taps alter the defining family and are a fourth operation with their own coefficient recurrence.

5.5 A catalog with explicit provenance

The standard-library `family_lab.py` exposes exact coefficient polynomials, normalized sequences, positive-bank coefficients, rational denominator clearing, root sections, Hurwitz products, ordinary FIR taps, and polyphase filter matrices. The catalog contains 18 rows through index 12.

Every row records parameters, coefficient normalization, arithmetic regime, and whether its entries are integers or rationals. Eight positive integer asymmetric specializations are labeled zero-radius formal sequences. Entire interior examples and an infinite-order edge are labeled separately.

Example	First normalized coordinates	Interpretation
$(1,1)$	$1,2,16,272,7936$	Known tangent anchor
$(1,2)$	$1,4,160,35200,38041600$	Integer, formal radius zero
$(1/2,1/2)$	$1,1/2,1/4,1/8,1/16$	Scaled sinh, entire order one
$(1/3,2/3)$	$1,4/9,160/729,18560/177147,\ldots$	Asymmetric entire order one

Implementation boundaries are enforced

Phase residues and bases must be integers, and a phase bank cannot be empty. The independent review found that fractional residues and zero phases were previously accepted. Both domain-validation defects were fixed and covered by regression assertions before publication.

The 8,038 exact API checks compare separate constructions: Picard integration, sine/cosine tangent division, root filters in a cyclotomic quotient, direct and phase-matrix taps, and coefficient-level antiderivatives. They verify finite implementation ranges. The algebraic laws above have separate proofs in Appendix E.

The catalog is ready for comparison with OEIS, with known anchors identified. It makes no claim that an unmatched prefix establishes a new sequence, and no sequence is represented here as a submitted or independently assigned OEIS entry.

PART IV

Coupled systems and finite resolution

Interacting channels, global growth and finite observation.

CHAPTER VI

Coupled contraction functions

6.1 Coupled growth and the cost of resolution

The coupled family consists of two entire functions whose derivatives depend on contracted values of both components. Its growth exponent is the unique positive number ρ for which

$$\operatorname{spr}\begin{pmatrix} q^{\rho} & r^{\rho} \\ a^{\rho} & b^{\rho} \end{pmatrix} = 1, \qquad 0 < q, r, a, b < 1.$$

Both functions have positive lower type and finite upper type at this order. The positive eigenvector fixes the proportions of both type vectors. The existence of an ordinary type limit remains open.

Local coefficients reveal the coupling

Two explicit parameter surfaces describe exactly when one normalized component is an amplitude and argument rescaling of the other. Outside these surfaces, the coefficients through degree seven recover all four ordered scales. This provides an exact local inverse for the labeled pair.

Three ways finite observations can miss structure

The resolution atlas compares a weak tap, a large excluded prime, and a negative sieve atom. Each example links a structural change to a concrete observation scale and a proved certificate.

Example	Observation	What the certificate gives
Weak feedback tap	Values on a complex disk	An explicit compact error and a sufficient radius for separation
Excluded prime	Values and derivatives	Exact disk bounds and a negative-depth visibility bracket
Negative sieve atom	All polynomial tests up to a degree	Positive quadratic forms through degree four and a negative degree-seven witness

The computed figures follow in this chapter and Chapter 7. Complete derivations accompany the full monograph, and the source archive contains the alternative growth proof, exact laboratory, and review records. The six-source literature comparison identifies classical antecedents. Historical priority of the specific coupled results remains unresolved.

How to read the figures

An exact rational bound supplies a certificate. A decimal display illustrates its size. Numerical curves retain their stated truncation and precision, and the universal growth and recovery statements rest on their proofs.

6.2 Two functions exchange growth

For four real contractions $0 < q, r, a, b < 1$, define the normalized pair

$$\boxed{\begin{aligned} U'(z) &= 1 + U(qz)V(rz), \\ V'(z) &= 1 + U(az)V(bz), \qquad U(0) = V(0) = 0. \end{aligned}}$$

Each equation combines one value of U with one value of V. The four scales specify where that exchange occurs. Both functions begin with the same unit slope, while later coefficients retain the two equations' different scale addresses.

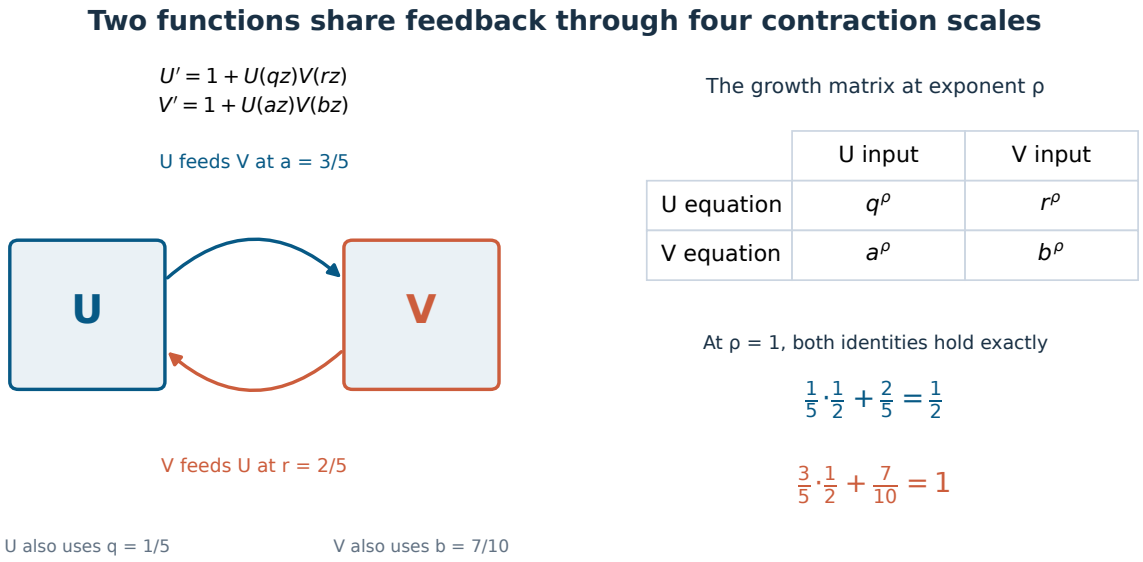


Figure 6.1. The worked pair $(q, r, a, b) = (1/5, 2/5, 3/5, 7/10)$ has exact order one. The two displayed identities give the positive growth vector $(1/2, 1)^T$.

There is a unique entire solution pair. Both functions are odd, and every odd Taylor coefficient is positive. The common order is governed by the positive matrix

$$P(s) = \begin{pmatrix} q^s & r^s \\ a^s & b^s \end{pmatrix}, \qquad \operatorname{spr} P(\rho) = 1.$$

The eigenvector supplies the relative weights that a row sum misses. In the example, the row sums at $s = 1$ are $3/5$ and $13/10$. The coupled system nevertheless has order exactly one in both components.

6.3 The coefficients preserve both addresses

Write $U(z) = \sum_{n\geq 0} u_n z^{2n+1}$ and $V(z) = \sum_{n\geq 0} v_n z^{2n+1}$, with $u_0 = v_0 = 1$. The first equation gives the exact recursion

$$u_n = \frac{1}{2n+1} \sum_{i+j=n-1} q^{2i+1} r^{2j+1} u_i v_j, \qquad n \geq 1.$$

The second replaces (q, r) by (a, b) while retaining the same products $u_i v_j$. Thus each new coefficient uses the shared history of the pair.

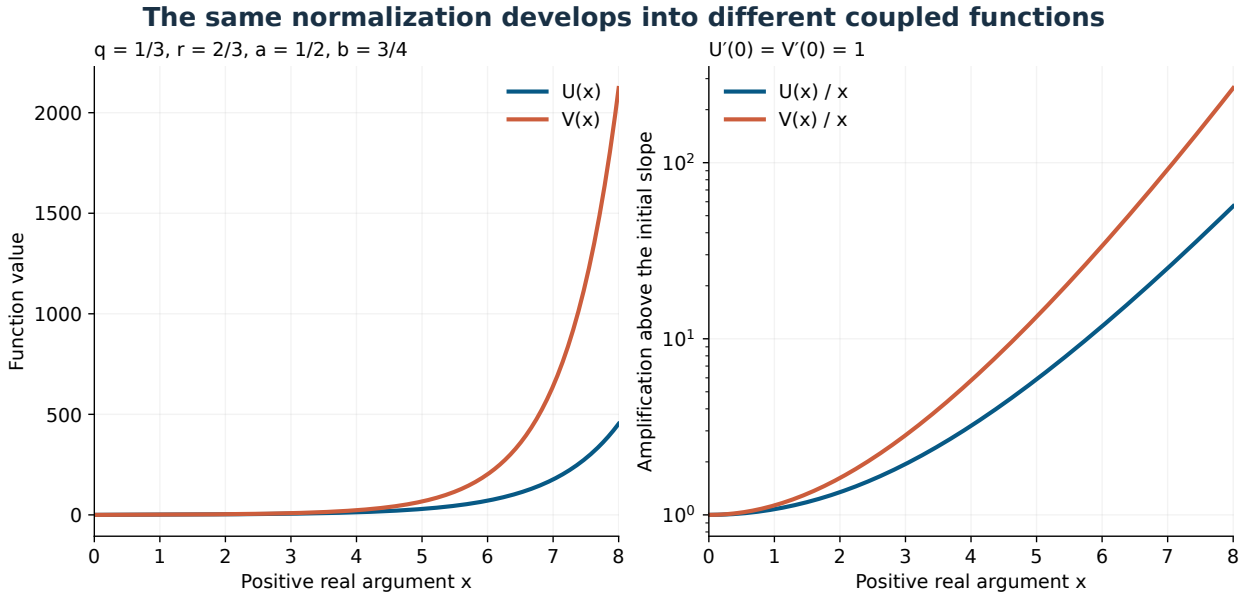


Figure 6.2. For $(q, r, a, b) = (1/3, 2/3, 1/2, 3/4)$, the components separate despite their common initial slope. These numerical curves use odd indices through 240. The two truncations at indices 120 and 240 agree at $x = 8$ to displayed double precision.

The first distinction already appears at degree three:

$$U(z) = z + \frac{qr}{3} z^3 + O(z^5), \qquad V(z) = z + \frac{ab}{3} z^3 + O(z^5).$$

Induction gives $0 < u_n, v_n \leq 2^{-n}$, which supplies a convergent germ. If both functions are known on a disk of radius R, their integral equations extend them to radius R/Q, where $Q = \max(q, r, a, b) < 1$. Repeating this step reaches every finite disk.

The numerical agreement above checks the plotted approximation. The later certificate page supplies an exact bound on the omitted tail.

6.4 One order, two exact type proportions

The entire functions have the same order ρ, with positive lower type and finite upper type. Positivity places the maximum modulus on the positive real axis, so $M_U(R) = U(R)$ and $M_V(R) = V(R)$.

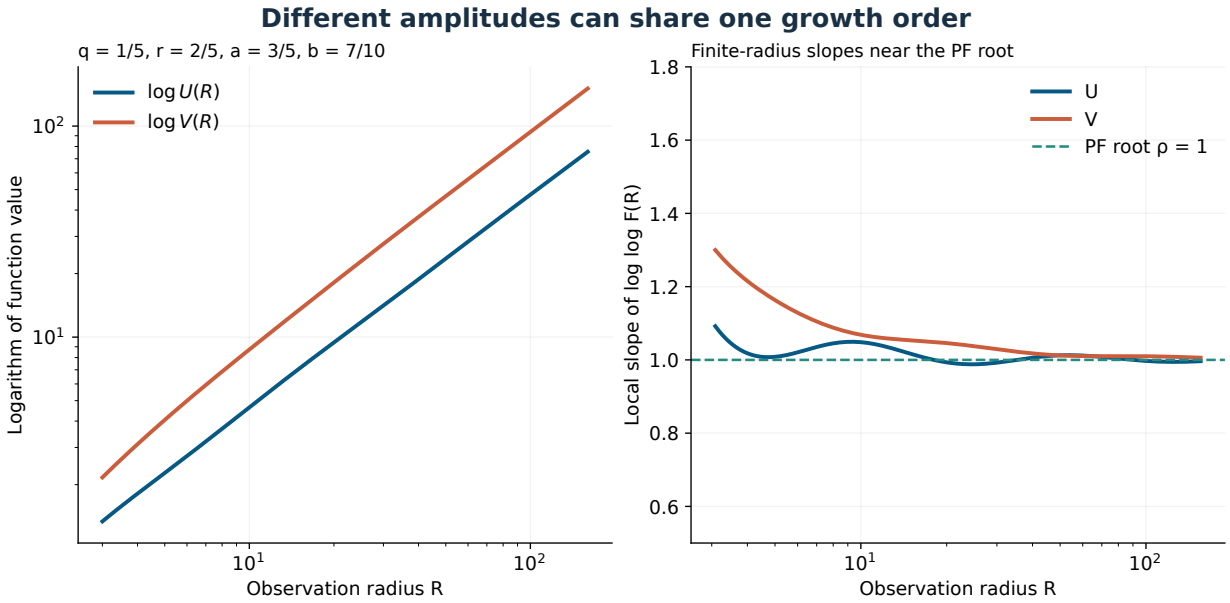


Figure 6.3. The order-one example has different component amplitudes. The right panel shows finite-radius slopes near one. The curves use odd indices through 800. Agreement with index 400 is a numerical diagnostic, and the order itself follows from the analytic proof.

For $F_1 = U$ and $F_2 = V$, define

$$\underline{\tau}_i = \liminf_{R\to\infty} \frac{\log M_{F_i}(R)}{R^\rho}, \qquad \overline{\tau}_i = \limsup_{R\to\infty} \frac{\log M_{F_i}(R)}{R^\rho}.$$

If $P(\rho)w = w$ with $w > 0$, then both type vectors have precisely these Perron proportions:

$$\boxed{\underline{\boldsymbol{\tau}} = \underline{\tau}\, w, \qquad \overline{\boldsymbol{\tau}} = \overline{\tau}\, w, \qquad 0 < \underline{\tau} \le \overline{\tau} < \infty.}$$

For the worked pair, both the lower type and the upper type of V are twice the corresponding type of U. Either both ordinary type limits exist or neither does. Equality of the lower and upper types remains open. The finite-radius slope picture does not decide that question.

6.5 Growth follows a spectral surface

The order is the unique positive solution of

$$\boxed{(1-q^\rho)(1-b^\rho)=(ar)^\rho.}$$

The left side increases from zero to one as ρ increases. The right side decreases from one to zero. Their unique crossing determines the growth exponent without fitting a truncated Taylor curve.

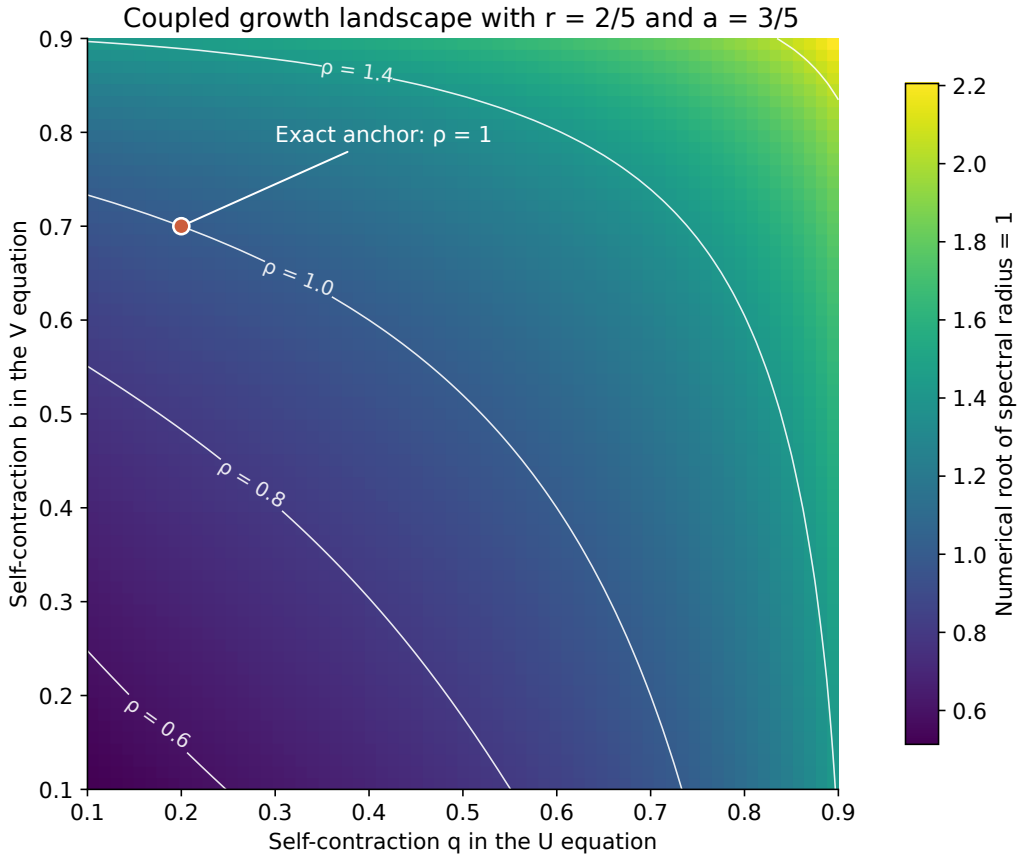


Figure 6.4. Numerical solutions of the proved characteristic equation, with $r = 2/5$ and $a = 3/5$. The highlighted pair $(q, b) = (1/5, 7/10)$ has order exactly one by rational arithmetic.

The order depends on the self scales q, b and on the product ar of the cross scales. Holding q, b, ar fixed preserves the order, while changing the cross scales separately generally changes the functions and their type proportions:

$$\frac{w_1}{w_2}=\frac{r^\rho}{1-q^\rho}=\frac{1-b^\rho}{a^\rho}.$$

Consequently, equal order does not determine the family member. It fixes one growth exponent within a larger parameter space. The coefficients carry enough additional information to recover all four ordered scales away from the reduction surfaces described below.

6.6 A coefficient list with a certified tail

A finite Taylor list becomes an exact approximation certificate when it is paired with a bound on a larger disk. Let F be either component, and let F_N retain the odd indices $0, \dots, N$.

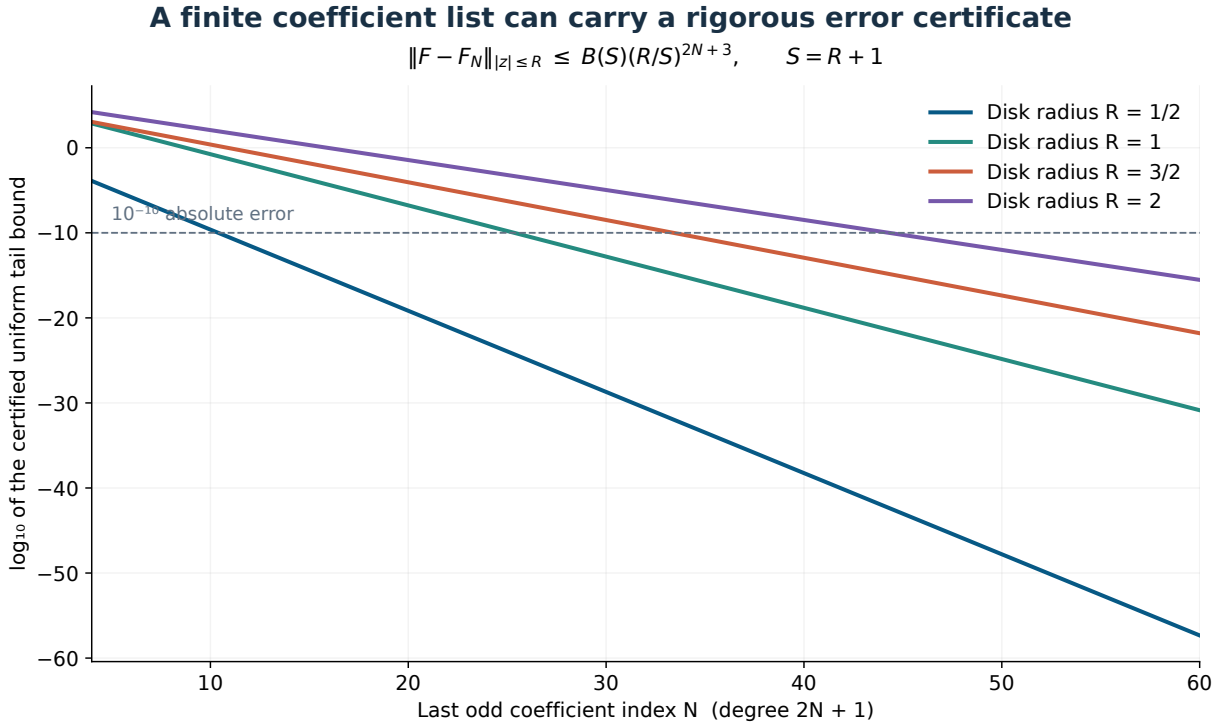


Figure 6.5. Each curve is computed from an exact rational upper bound for the same worked pair. Increasing the coefficient count certifies a smaller uniform error on the stated complex disk. The logarithmic plotting coordinates are rounded.

Put $Q = \max(q, r, a, b)$. One elementary majorant starts with $B(x) = x/(1 - x^2)$ for $0 \le x < 1$ and works outward through the finite contraction ladder using

$$B(x) = x\big(1 + B(Qx)^2\big).$$

The integral equations show that this bounds both components on the disk $|z| \le x$. For $S > R \ge 0$, positivity then gives

$$\boxed{\max_{|z| \le R} |F(z) - F_N(z)| \le B(S) \left(\frac{R}{S}\right)^{2N+3}.}$$

The exponent is the first omitted odd degree. Every later term has an even smaller ratio between its values at radii R and S. For the worked pair, $N = 30$, $R = 1$ and $S = 2$ give an error below 1.600×10^{-13} for both functions. The laboratory returns rational interval endpoints, so the certificate survives decimal rounding.

6.7 The phase calculus transports the pair

Use the derivative normalization $A_n = (2n+1)!u_n$, $B_n = (2n+1)!v_n$. Its recurrence has integer binomial weights:

$$A_n = \sum_{i+j=n-1} \binom{2n}{2i+1} q^{2i+1} r^{2j+1} A_i B_j, \qquad n \geq 1.$$

The second component again replaces (q, r) by (a, b).

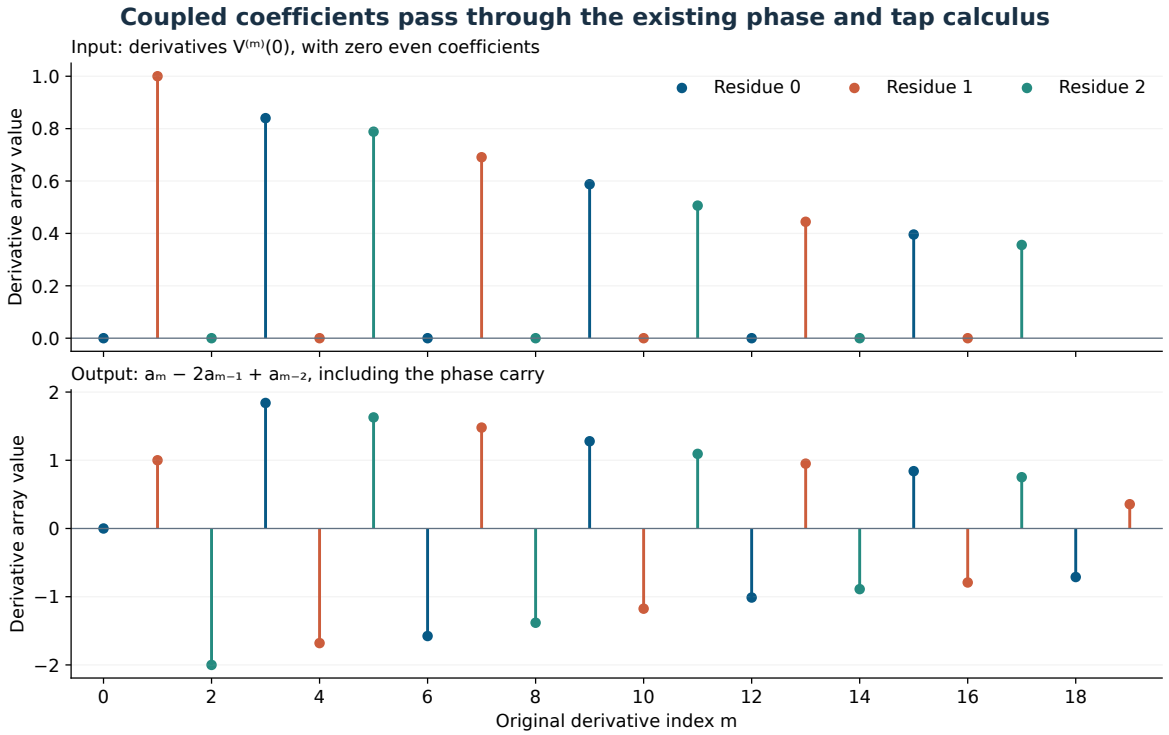


Figure 6.6. The full derivative array of V is split into three residue lanes. Applying taps $(1, -2, 1)$ with the correct block carries, then interleaving, agrees exactly with direct convolution.

These derivative arrays are polynomials with nonnegative integer coefficients in the four scale variables. Their total degree is at most $n(n+1)$. If every parameter denominator divides D_0, then

$$D_0^{n(n+1)} A_n, \qquad D_0^{n(n+1)} B_n \quad \text{are integers.}$$

This uniform clearing factor makes exact rational families available to integer sequence experiments. It need not be the smallest possible factor.

Ordinary taps on a derivative array correspond to repeated integration shifts of its exponential generating function. Multiplication of two exponential generating functions instead requires binomial convolution. The catalog preserves that distinction and marks generic integer and signed scale examples as formal series outside the proved analytic domain.

6.8 Two surfaces where one component rescales to the other

Set $p = qr$, $k = ab$, and use the ordinary Taylor coefficients u_2, v_2 at degree five. The exact separation quantity factors as

$$\boxed{D = k^2 u_2 - p^2 v_2 = \frac{pkar}{15}(q^2 - b^2)(qb - ar).}$$

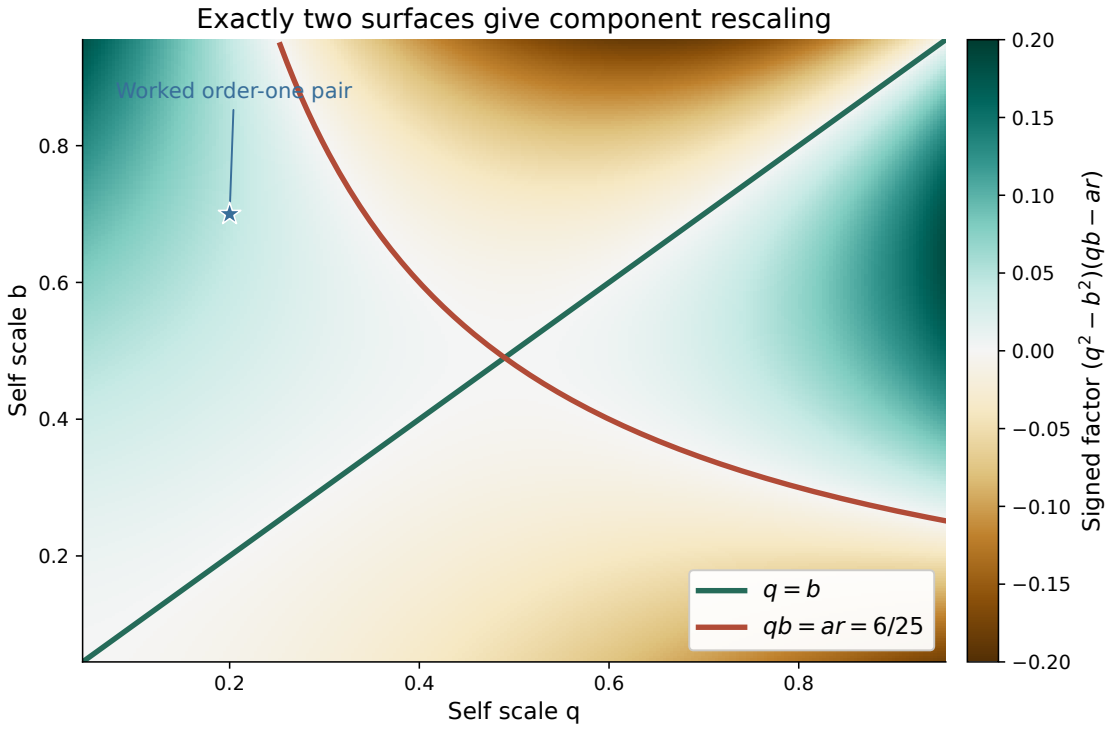


Figure 6.7. The two reduction surfaces are $q = b$ and $qb = ar$. Their union is exactly the zero set of D in the positive contraction domain. Outside this union, the components cannot be obtained from each other by amplitude and argument rescaling.

There exist nonzero complex constants A, B with $V(z) = A\,U(Bz)$ if and only if $D = 0$. On either surface, put $s = \sqrt{k/p} > 0$. The scalar family is defined by $T'_{x,y}(z) = 1 + T_{x,y}(xz)T_{x,y}(yz)$, $T_{x,y}(0) = 0$. It gives the explicit reduction

$$U(z) = \sqrt{s}\, T_{q,sr}(z/\sqrt{s}), \qquad V(z) = s^{-1/2} T_{q,sr}(\sqrt{s}\, z).$$

Both effective scales lie in $(0, 1)$. Equality $U = V$ is more restrictive: it occurs exactly when $\{q, r\} = \{a, b\}$.

This classifies relations between the normalized components. Separately, no invertible constant linear coordinate change decouples the defining operator into two autonomous scalar equations on every analytic input. That operator statement does not exclude nonlinear changes of variables or other special-function identities.

6.9 Degree seven identifies the four scales

Away from $D = 0$, the six coefficients $(u_1, v_1, u_2, v_2, u_3, v_3)$ uniquely recover the ordered parameters (q, r, a, b) in $(0,1)^4$. These are the coefficients at degrees three, five and seven of the two labeled functions.

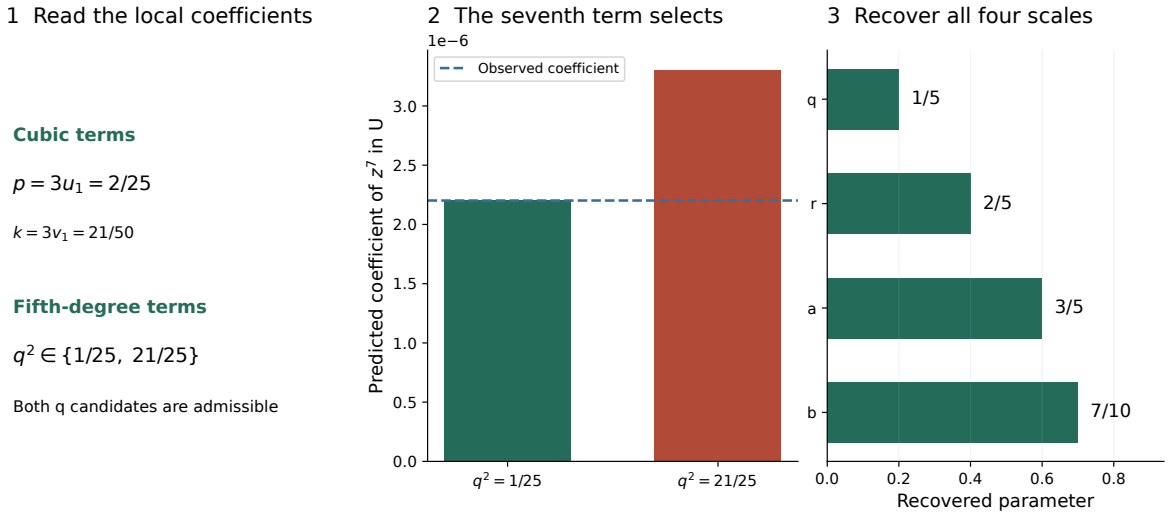


Figure 6.8. Cubic terms recover the two scale products. Fifth-degree terms leave at most two candidates for each remaining scale. The seventh-degree terms select the unique admissible candidates when $D \neq 0$. Repeated quadratic roots are already unique.

First $p = 3u_1$ and $k = 3v_1$. The possible values $x = q^2$ and $y = a^2$ satisfy

$$px^2 - \frac{15u_2}{p}x + kp^2 = 0, \qquad py^2 - \frac{15v_2}{k}y + k^3 = 0.$$

For two distinct positive candidates x, x', the predicted seventh coefficients differ by

$$u_3(x) - u_3(x') = \frac{pD}{7k^2}(x^2 - x'^2) \neq 0.$$

The second component supplies the analogous separation for y. Finally take the positive square roots and recover $r = p/q$, $b = k/a$.

This is an exact-data inverse theorem. Near a reduction surface, small D can make candidate predictions close, so a uniform stable inverse does not follow. The degree-seven recovery and the reduction classification are proved statements. Historical priority of these particular results is addressed separately by the bounded literature comparison.

CHAPTER VII

Limits of finite observation

7.1 A small change can alter the global order

A feedback channel may be almost invisible on a fixed disk and still determine the eventual growth of the function. Consider the normalized entire solution

$$F_\varepsilon'(z) = 1 + (1-\varepsilon)F_\varepsilon(z/4)^2 + \varepsilon F_\varepsilon(3z/4)^2, \qquad F_\varepsilon(0) = 0.$$

Here $0 \le \varepsilon \le 1$. At $\varepsilon = 0$, its entire order is $1/2$. At every positive weight, the order becomes $\rho = \log 2/\log(4/3) \approx 2.40942084$.

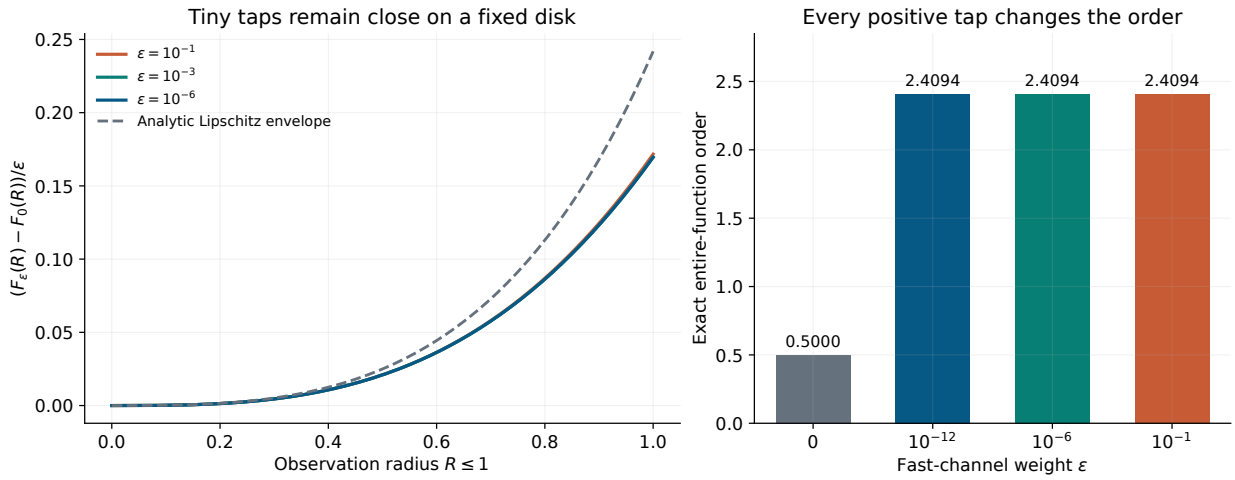


Figure 7.1. Left: divide the compact difference by the tap weight to compare its shape. Right: the proved order jumps at zero. The dashed curve is an analytic envelope. The function curves use 100-digit arithmetic and have a normalized omitted-series bound below 5.26×10^{-23} on $0 \le R \le 1$. Floating rounding is separate from that tail bound.

The unit disk comes with an exact error certificate

Let $f_{3/4} = F_1$, with $f_{3/4}(z) = \sum_{n\geq 0} d_n z^{2n+1}$. Positive coefficients give

$$\sup_{|z|\leq R} |F_\varepsilon(z) - F_0(z)| \leq \varepsilon \sum_{n\geq 1} n d_n R^{2n+1}.$$

A rational coefficient sum and a positive-tail estimate prove that, on the unit disk, the multiplier is less than 0.241890267. For $\varepsilon = 10^{-12}$, the entire disk therefore changes by less than $2.41890267 \times 10^{-13}$.

The observation window and the global invariant answer different questions. Exact measurements can distinguish the functions. With an absolute error allowance at least half the displayed bound, midpoint data can fit both. The order concerns the limit through arbitrarily large radii, where the active faster channel eventually matters.

7.2 How far is far enough to guarantee separation?

The growth theorem supplies positive lower type for the weak-tap function and finite upper type for the slow function. For $0 < \varepsilon \leq 1$ and $R \geq e$,

$$\log F_\varepsilon(R) \geq c_\varepsilon R^\rho, \qquad \log F_0(R) \leq C_0\sqrt{R},$$

$$c_\varepsilon = \frac{\log 2}{(4/\varepsilon + 8/3)^\rho}, \qquad C_0 = e^{-1/2}(1 + 22\log 2).$$

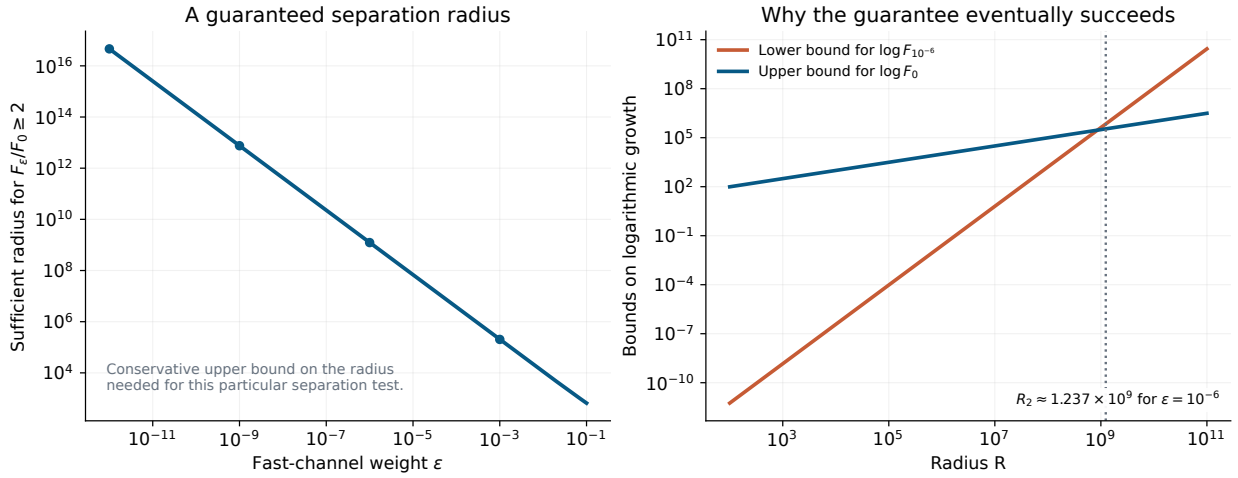


Figure 7.2. The left curve is a sufficient radius obtained from conservative comparison constants. The right panel shows why the lower bound for the perturbed function eventually exceeds the upper bound for the slow one. These are bounds on logarithmic growth, rather than numerical evaluations at the large plotted radii.

An explicit sufficient radius

Put

$$R_2(\varepsilon) = \max\left\{e, \left(\frac{2C_0}{c_\varepsilon}\right)^{1/(\rho-1/2)}, \left(\frac{2\log 2}{c_\varepsilon}\right)^{1/\rho}\right\}.$$

Then $F_\varepsilon(R) \geq 2F_0(R)$ for every $R \geq R_2(\varepsilon)$. The formula makes $c_\varepsilon R^\rho$ at least both $2C_0\sqrt{R}$ and $2\log 2$, and therefore at least their half-sum. Exponentiating gives the factor of two.

For $\varepsilon = 10^{-6}$, the formula is approximately 1.237×10^9. This large radius is a guaranteed sufficient choice. It is not the first radius at which a useful difference appears, and it does not establish failure of every observation at smaller radii. The exact formula carries the guarantee. Rounded figures illustrate its scale.

7.3 A large excluded prime hides in a fixed window

Use the squarefree arithmetic family

$$A_Q(s) = \sum_{\substack{n\geq 2\\ \mu(n)^2=1\\ (n,Q)=1}} n^{-4}(1-n^{-2})^{2s}, \qquad D_p(s) = A_1(s) - A_p(s),$$

where p is prime. The difference contains exactly the squarefree atoms divisible by p. Its largest frequency is $\lambda_p = -2\log(1-p^{-2})$, and its total mass is $D(4)/(p^4+1)$, with $D(4) = 105/\pi^4$.

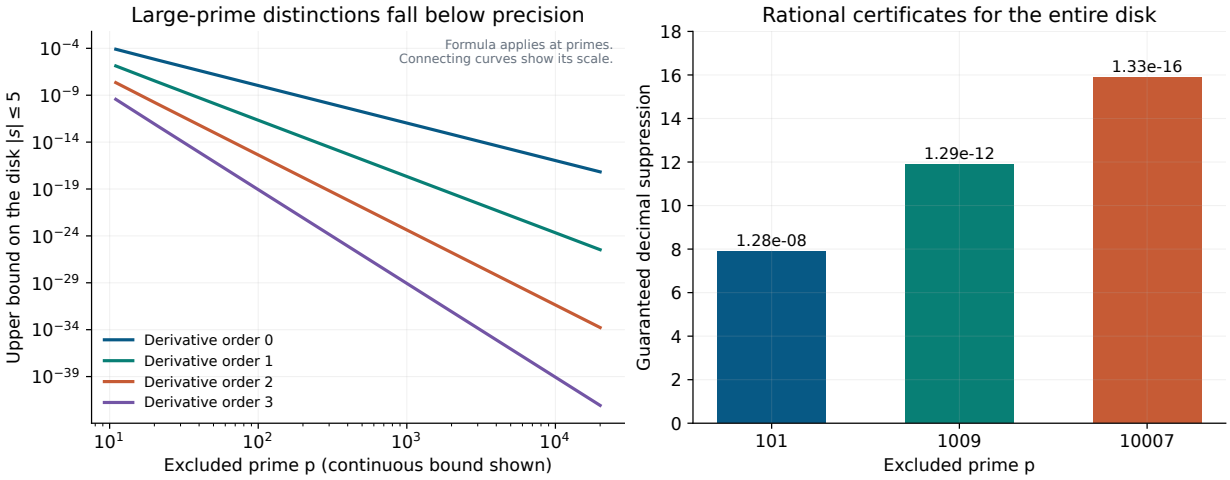


Figure 7.3. Left: analytic bounds for the function and three derivatives on $|s| \leq 5$. The connecting curves show scale, while the arithmetic statement applies at primes. Right: rational bounds for three particular excluded primes. The bar height is the negative base-ten logarithm of the bound, not a count of recovered digits.

The full complex disk has a rational certificate

For integer $k \geq 0$,

$$\sup_{|s|\leq 5} |D_p^{(k)}(s)| < \frac{4(1-p^{-2})^{-10}}{3(p^4+1)} \left(\frac{2}{p^2-1}\right)^k.$$

The inequality uses $D(4) < 4/3$ and $\lambda_p \leq 2/(p^2-1)$. Every quantity on the right is rational. For $k = 0$, upward decimal bounds are 1.283×10^{-8} at $p = 101$, 1.287×10^{-12} at $p = 1009$, and 1.330×10^{-16} at $p = 10007$.

The excluded prime changes the exact inverse of the function. Nevertheless, its effect becomes arbitrarily small on every fixed disk, including in every fixed derivative order. A bounded error model therefore needs an arithmetic parameter bound if it is to promise uniform recovery.

7.4 Seeing the prime can make subtraction harder

At negative real depth, the difference grows. The prime atom alone supplies a lower bound, while the entire removed shelf supplies an upper bound:

$$p^{-4}e^{\lambda_p T} \le D_p(-T) \le \frac{D(4)}{p^4+1}e^{\lambda_p T}, \qquad T \ge 0.$$

Choose a tolerance $\eta > D(4)/(p^4+1)$. Its unique crossing occurs between

$$T_- = \frac{\log\big(\eta(p^4+1)/D(4)\big)}{\lambda_p}, \qquad T_+ = \frac{\log(\eta p^4)}{\lambda_p}.$$

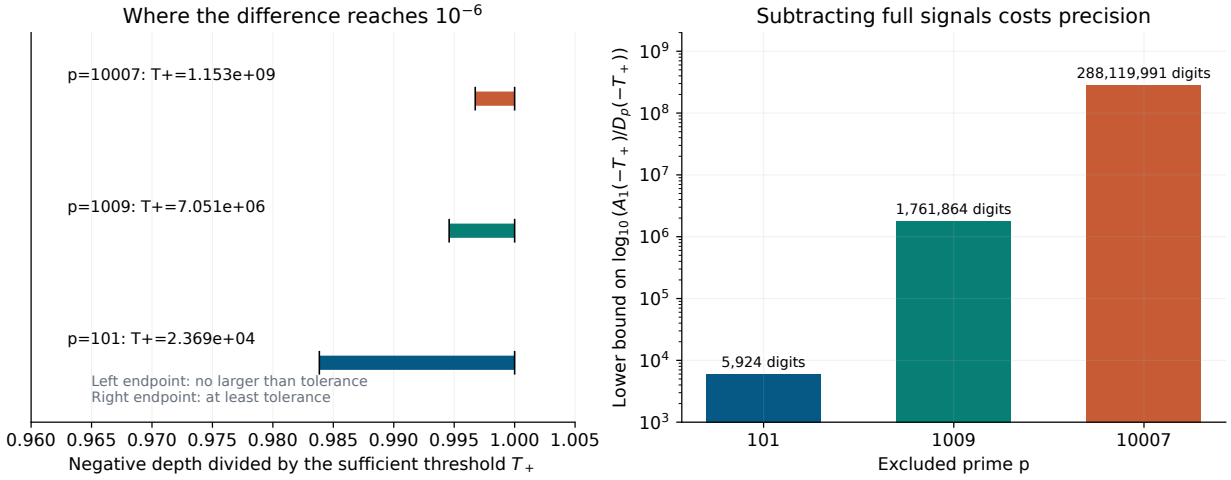


Figure 7.4. At tolerance 10^{-6}, the left panel shows the analytic crossing brackets after rescaling each row by T_+. The right panel shows a lower bound on the decimal cancellation scale when subtracting full functions. Displayed endpoints and labels are ordinary floating evaluations of exact formulas.

For $p = 101$, the difference is no larger than 10^{-6} through $T_- = 23307.789\ldots$, and at least that large by $T_+ = 23690.516\ldots$. The decimals illustrate the formulas and are not rounded interval certificates.

The direct positive difference and subtraction have different costs

The $n = 2$ atom in the full function proves

$$\frac{A_1(-T)}{D_p(-T)} \ge \frac{p^4+1}{16D(4)}e^{(\lambda_2-\lambda_p)T}.$$

At T_+ for $p = 101$, the base-ten logarithm of this lower bound is about 5924. Subtracting independently approximated full functions can therefore amplify relative errors enormously. Evaluating the known positive difference series is a different procedure. These conditioning figures impose no universal precision requirement on every possible recovery algorithm.

7.5 A degree-seven witness exposes a signed defect

Let $x_n = (1 - n^{-2})^2$, and change the prime-two sieve strength to $\lambda_2 = -1 - \delta$. For a real polynomial f, the associated quadratic form is

$$Q_\delta(f) = \sum_{\substack{n\geq 1\\ \mu(n)^2=1\\ n \text{ odd}}} \frac{f(x_n)^2}{n^4} - \delta \sum_{\substack{n\geq 1\\ \mu(n)^2=1\\ n \text{ even}}} \frac{f(x_n)^2}{n^4}.$$

Every even squarefree atom has negative mass. At $\delta = 10^{-12}$, the polynomial below certifies that this is detectable at finite degree.

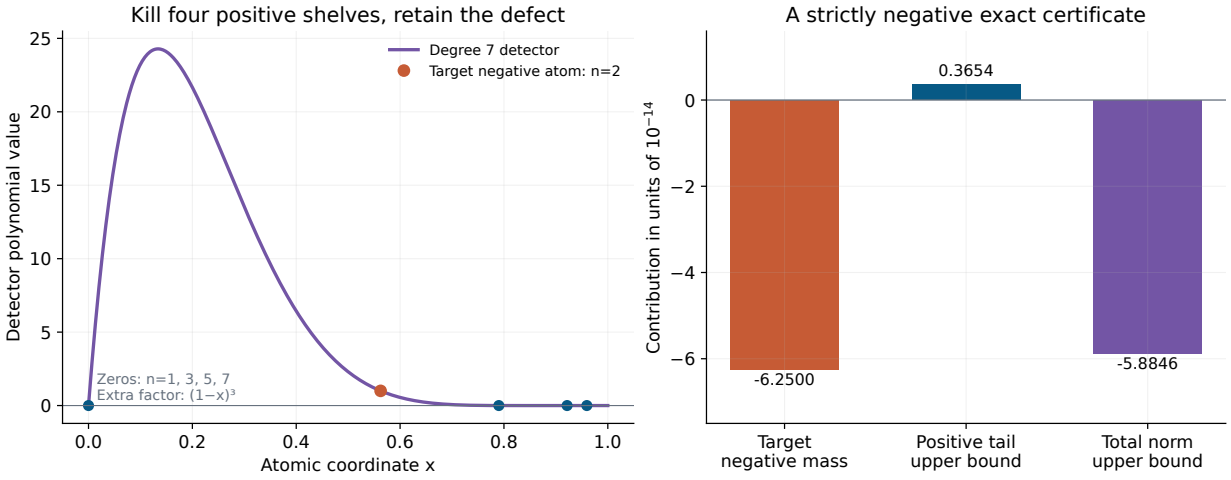


Figure 7.5. The detector vanishes on the first four positive shelves and equals one at the negative atom $n = 2$. The positive bar is an upper bound for the entire remaining positive tail. The total upper bound is negative, so no omitted atom can reverse the conclusion.

The certificate uses rational arithmetic throughout

Take $S = \{1, 3, 5, 7\}$ and define

$$P(x) = \prod_{n\in S} \frac{x - x_n}{x_2 - x_n} \left(\frac{1 - x}{1 - x_2}\right)^3.$$

Its degree is seven. All remaining positive nodes begin at $n = 11$. With $C = 756482048/20777538825$ and $r = 3856/102487$, a complete tail bound gives

$$Q_{10^{-12}}(P) \leq -\frac{10^{-12}}{16} + \frac{C^2 r^6}{3 \cdot 7^3} < -5.8845708899 \times 10^{-14}.$$

The inequality is certified as a comparison of exact rational numbers. The first four zeros remove the dominant positive contributions. The factor $(1 - x)^3$ suppresses the remaining cluster near one. The construction exhibits a detecting degree, without asserting that degree seven is the smallest possible choice.

7.6 Passing every coarse test can still miss the defect

The previous witness would be less informative without a converse guarantee at lower resolution. For the same defect $\delta = 10^{-12}$, every nonzero polynomial of degree at most four has strictly positive quadratic form. This quantifies the information that the coarse test actually misses.

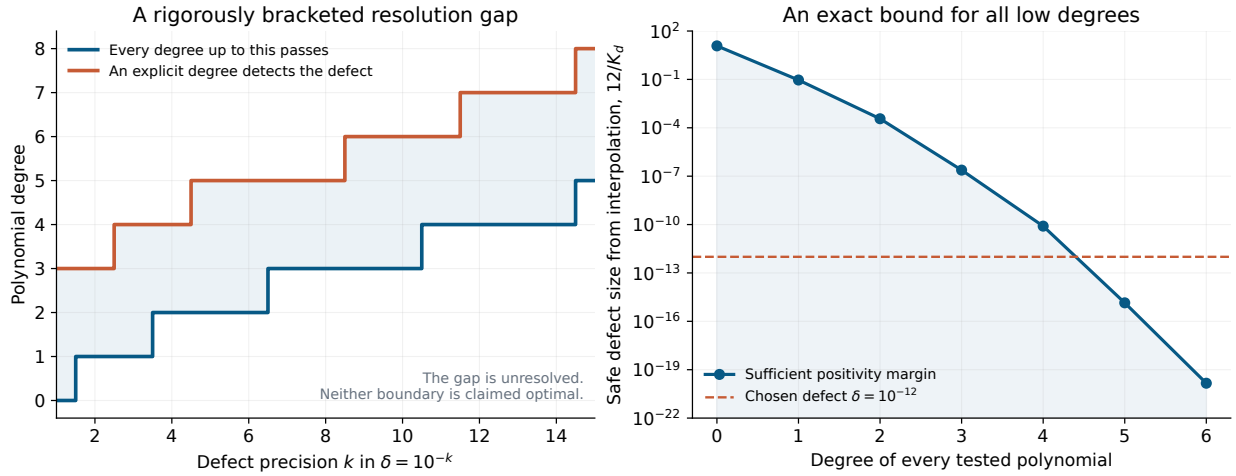


Figure 7.6. The blue boundary certifies positivity for every polynomial through that degree. The orange boundary gives an explicit detecting polynomial. The shaded gap remains unresolved by these certificates. At $\delta = 10^{-12}$, degrees through four pass, degree seven fails, and degrees five and six are undecided here.

Interpolation controls the whole polynomial space

Choose the odd squarefree labels $n_i = 1, 3, 5, 7, 11$, write $y_i = x_{n_i}$, and put

$$b_i = \prod_{j \neq i} \frac{\max(y_j, 1 - y_j)}{|y_i - y_j|}, \qquad K_4 = \sum_{i=0}^{4} n_i^4 b_i^2.$$

Lagrange interpolation and weighted Cauchy–Schwarz show that, for every polynomial f of degree at most four,

$$Q_\delta(f) \geq \left(1 - \frac{\delta K_4}{12}\right) \sum_{i=0}^{4} n_i^{-4} f(y_i)^2.$$

Exact rational comparison gives $12/K_4 > 7.9790 \times 10^{-11} > 10^{-12}$. A nonzero polynomial cannot vanish at all five selected nodes, so the right side is strictly positive. Thus the order-five Hankel matrix is positive definite, while the degree-seven witness makes the order-eight matrix fail positive semidefiniteness.

The complete atlas contains the general interpolation and detector bounds. Its reproducible check records 985 exact assertions and 16 floating algebra checks. The proofs establish the universal statements. The tests verify the stated finite certificates and implementations.

PART V

Proofs and mathematical evidence

Complete arguments, reproducible calculations and their precise limits.

The proof architecture

The illustrated chapters develop the definitions, decisive proof steps, and worked examples. The appendices provide the complete derivations, explicit constants, computational contracts, source comparisons, and unresolved questions. Editable source files accompany the monograph.

Appendix	Proof chapter	Main dependencies
A	Dilation type and continuity	Positive coefficient recurrence, radius bootstrap, translated-radius comparison
B	Arithmetic inverse and character resolution	Summable positive atoms, squarefree counting, Euler factors, sector partial integration
C	Multiple-prime geometry and detectors	Exact moments, isolated-node polynomials, definite matrix pencils
D	Orbit continuation and shifts	Genus-zero product, branch separation, exponential sums, two-end Mellin subtraction
E	Integer sequences and polyphase laws	Factorial recurrence, ordered trees, root filtering, carry arithmetic
F	Coupled entire growth and type	Positive coupled recurrence, characteristic matrix, translated powers, left eigenvector
G	Component reduction and exact inverse	Cubic and fifth coefficients, factorization, seventh-coefficient separation
H	Constant linear operator structure	Projection fibers, polynomial interpolation, monomial tests
I	Quantitative resolution atlas	Tap type bounds, removed-prime mass, exact interpolation and tail certificates
J	Coupled exact laboratory	Derivative recurrence, denominator clearing, positive disk majorants

APPENDIX A

Positive lower type and quantitative tap continuity

This chapter sharpens the entire-growth theorem for nonlinear contraction families. The symmetric definition has the antecedent identified in the reading map.

A.1 The exact growth exponent has positive lower type

Let

$$F'(z) = 1 + \sum_{j=1}^{J} h_j F(q_j z) F(r_j z), \qquad F(0) = 0,$$

where $h_j > 0$, $\sum_j h_j = 1$, and $0 < q_j, r_j < 1$. Zero-weight channels may instead be allowed if they are removed from the active bank before defining its growth exponent. Put

$$\rho = \max_{j:h_j>0} \rho_j, \qquad q_j^{\rho_j} + r_j^{\rho_j} = 1.$$

The inherited coefficient recurrence gives nonnegative coefficients, entire extension, and $M(R) = \max_{|z|=R} |F(z)| = F(R) \geq R$ for $R > 0$.

Theorem A.1. There are explicit constants $0 < c_- \leq c_+ < \infty$ such that

$$c_- \leq \liminf_{R\to\infty} \frac{\log M(R)}{R^\rho} \leq \limsup_{R\to\infty} \frac{\log M(R)}{R^\rho} \leq c_+.$$

In particular the bank has positive lower type and finite upper type at its exact order, including when $0 < \rho < 1$. Furthermore

$$\lim_{R\to\infty}\frac{\log\log M(R)}{\log R}=\rho.$$

This last radial growth-exponent limit does not assert a type limit or uniform angular growth.

A.1.1 Explicit lower constants and proof

Select any active maximizing channel and abbreviate it to (h,q,r), so $q^\rho+r^\rho=1$. Define

$$L=\frac{1}{h},\qquad C=\max\left(\frac{qL}{1-q},\frac{rL}{1-r}\right),\qquad B=L+\frac{2}{\min(q,r)},\qquad c_-=\frac{\log 2}{(B+C)^\rho}.$$

We prove the stronger bound

$$\boxed{\log M(R)\ge c_-(R+C)^\rho\quad\text{for every } R\ge 2.}$$

Write $H(R)=\log M(R)$. On the seed interval $[2,B]$, $H(R)\ge\log R\ge\log 2\ge c_-(R+C)^\rho$. For $R\ge B$, integrate the positive feedback over the fixed-width interval $[R-L,R]$:

$$\begin{aligned}M(R)&\ge h\int_{R-L}^{R}M(qt)M(rt)\,dt\\&\ge hLM(q(R-L))M(r(R-L))\\&=M(q(R-L))M(r(R-L)).\end{aligned}$$

The two child radii are at least two because $R\ge B$. Moreover

$$q(R-L)+C\ge q(R+C),\qquad r(R-L)+C\ge r(R+C),$$

because respectively $(1-q)C\ge qL$ and $(1-r)C\ge rL$. If the comparison bound is known at both child radii, it follows that

$$\begin{aligned}H(R)&\ge H(q(R-L))+H(r(R-L))\\&\ge c_-\{[q(R-L)+C]^\rho+[r(R-L)+C]^\rho\}\\&\ge c_-(q^\rho+r^\rho)(R+C)^\rho=c_-(R+C)^\rho.\end{aligned}$$

For a rigorous propagation, put $Q_*=\max(q,r)<1$ and $d=(1-Q_*)B+Q_*L>0$. Every child of every $R\ge B$ is at most $R-d$. Induction on the intervals $[B+kd,B+(k+1)d]$, beginning with the already controlled seed, proves the comparison for all larger radii. Continuity deals with common endpoints. All power comparisons use only monotonicity of x^ρ for positive x; no convexity assumption is made, so the argument also covers $\rho<1$.

A.1.2 Explicit finite upper constants

For all channels set

$$Q = \max_j \max(q_j, r_j), \quad m = \min_j \min(q_j, r_j), \quad \Delta = \log(1/m), \quad B_+ = \max_j \log \frac{1}{q_j r_j} + \log 2.$$

Choose an integer $N \geq 0$ with $Q^{-N} \geq 3/m$, and put

$$V_N = (2^{N+1} - 1)\log 2 + (2^{N+1} - N - 2)\log(1/Q),$$

$$c_+ = e^{-\rho}(V_N + 1 + \Delta + B_+).$$

These constants are intentionally conservative, and require no numerical evaluation of an unknown solution. The tangent majorant gives $M(1) < 2$. At $R_k = Q^{-k}$, the integral equation gives

$$M(R_k) \leq R_k[1 + M(R_{k-1})^2].$$

Define $U_0 = 2$, $U_k = Q^{-k}(1 + U_{k-1}^2)$. Then $M(R_k) \leq U_k$, $U_k \geq 1$, and $\log U_k \leq k \log(1/Q) + \log 2 + 2 \log U_{k-1}$. Summing this elementary recurrence gives $\log U_N \leq V_N$. Since $e < 3$, the logarithmic-radius seed $1 \leq t \leq 1 + \Delta$ has $e^t \leq e/m < 3/m \leq R_N$, and therefore $\log M(e^t) \leq V_N$.

Let $a_j = \log(1/q_j)$, $b_j = \log(1/r_j)$, and $G(t) = \log M(e^t) + t + B_+$. For $t \geq 1 + \Delta$, all child moduli are at least one, so the positive integral and weight normalization give

$$\log M(e^t) \leq t + \log 2 + \max_j \{\log M(e^{t-a_j}) + \log M(e^{t-b_j})\}.$$

The definition of B_+ implies

$$G(t) \leq \max_j \{G(t - a_j) + G(t - b_j)\}.$$

On the seed, $G(t) \leq V_N + 1 + \Delta + B_+ \leq c_+ e^{\rho t}$. Each channel satisfies $q_j^\rho + r_j^\rho \leq 1$. Induction in intervals of length $\min_j \min(a_j, b_j) > 0$ therefore propagates the seed comparison, giving the explicit upper bound

$$\boxed{\log M(R) \leq c_+ R^\rho - \log R - B_+ \quad (R \geq e).}$$

Dividing the two bounds by R^ρ, then taking logarithms of their positive logarithmic-growth bounds, proves all assertions of Theorem A.1. The theorem leaves open whether $\log M(R)/R^\rho$ has a limit. Lattice resonances or logarithmic oscillations are possible research directions, not results here.

A.2 Joint holomorphic dependence on parameters

Fix the number J of channels. Allow complex weights h_j, without normalization, and complex contractions satisfying $|q_j|, |r_j| < 1$. The same formal recurrence defines coefficients

$$c_n(h, q, r) \in \mathbb{Q}[h_1, \dots, h_J, q_1, r_1, \dots, q_J, r_J].$$

Each is homogeneous of degree n in the weights. If a parameter set has $|q_j|, |r_j| \le Q < 1$ and $\sum_j |h_j| \le W$, with $W > 0$, coefficient induction gives

$$|c_n(h, q, r)| \le W^n d_n(Q),$$

where $f_Q(z) = \sum d_n(Q) z^{2n+1}$ is the established diagonal function. Consequently, on every disk $|z| \le R$,

$$\sum_{n \ge 0} |c_n(h, q, r)| R^{2n+1} \le W^{-1/2} f_Q(\sqrt{W} R) < \infty.$$

Every compact subset of the complex parameter domain has such Q, W. The series therefore converges normally on compact sets of the joint domain, and its sum is jointly holomorphic in the weights, contractions, and z. This proves parameter continuity at zero weights, although the growth order can jump there. Complex or signed parameters do not inherit the positive-bank growth theorem merely from holomorphic dependence.

A.3 A quantitative compact bound for changing tap weights

Keep fixed real contractions $0 < q_j, r_j \le Q < 1$, and let h, g be nonnegative normalized weight vectors. Zero weights are permitted. Let $d = \|h - g\|_1$. Then for every $R \ge 0$,

$$\boxed{\sup_{|z| \le R} |F_h(z) - F_g(z)| \le \frac{d}{4} \{R f_Q'(R) - f_Q(R)\}.}$$

Proof. Regard c_n as a polynomial in the real weight variables with the contractions fixed. Its coefficients are nonnegative. Induction in the recurrence gives the coefficientwise polynomial bound

$$0 \preceq c_n(h) \preceq d_n(Q) \Big(\sum_j h_j \Big)^n.$$

Here $\preceq$ compares every monomial coefficient. Differentiation preserves this comparison, so on the normalized nonnegative simplex

$$0 \le \partial_{h_j} c_n \le n d_n(Q).$$

Put $v = h - g$. Its positive and negative parts both have sum $d/2$, since $\sum_j v_j = 0$. At every point of the segment between g and h, all partial derivatives lie in the interval $[0, nd_n(Q)]$. Hence

$$|v \cdot \nabla c_n| \le \frac{d}{2} n d_n(Q), \qquad |c_n(h) - c_n(g)| \le \frac{d}{2} n d_n(Q).$$

Multiply by R^{2n+1} and sum. Entire convergence justifies the sum, and

$$R f_Q'(R) - f_Q(R) = 2 \sum_{n \ge 0} n d_n(Q) R^{2n+1},$$

proving the claim. The same argument applies to the closed simplex and needs no positive minimum weight.

A.3.1 A vanishing tap and discontinuous order

Take the two diagonal channels $(q, r) = (1/4, 1/4)$ and $(3/4, 3/4)$, with weights $1 - \varepsilon$ and ε, respectively. For $0 \le \varepsilon \le 1$, write the resulting function as F_ε. The quantitative bound gives

$$\sup_{|z| \le R} |F_\varepsilon(z) - f_{1/4}(z)| \le \frac{\varepsilon}{2} \{R f_{3/4}'(R) - f_{3/4}(R)\}.$$

Thus convergence to $f_{1/4}$ is uniform on every fixed disk, at an explicit linear rate in ε. Yet

$$\rho(F_0) = \frac{1}{2}, \qquad \rho(F_\varepsilon) = \frac{\log 2}{\log(4/3)} \quad (0 < \varepsilon \le 1).$$

For the faster active channel the lower constants become $L = 1/\varepsilon$, $C = 3/\varepsilon$, $B = 1/\varepsilon + 8/3$. Its certified lower-type constant is

$$c_-(\varepsilon) = \frac{\log 2}{(4/\varepsilon + 8/3)^{\log 2 / \log(4/3)}} > 0.$$

It tends to zero as the faster tap vanishes. These are proved growth and compact-convergence statements. They do not determine an actual crossover radius or leading asymptotic constant.

APPENDIX B

Arithmetic depth: an exact inverse, its conditioning, and character resolution

The entire squarefree depth function determines its arithmetic parameters exactly, with one precise equivalence: powers of the primes in the modulus are invisible. This is a local mathematical theorem. It does not assert historical priority for Laplace inversion or for this particular arithmetic application.

B.1 Definitions and conventions

For real $a > 1/2$, real $\beta > 0$, and integer $Q \geq 1$, write

$$A_{a,\beta,Q}(s) = \sum_{\substack{n \geq 2 \\ \mu(n)^2 = 1 \\ (n,Q)=1}} n^{-2a} \exp(-\lambda_n s), \qquad \lambda_n = -2\log(1 - n^{-\beta}).$$

The logarithm is real. The omitted $n = 1$ atom is not restored in any inverse formula. Let $n_1 < n_2 < \cdots$ be the support integers, and abbreviate $\lambda_j = \lambda_{n_j}$, $w_j = n_j^{-2a}$. Then $\lambda_1 > \lambda_2 > \cdots > 0$, $\lambda_j \to 0$, and $\sum_j w_j = M = Z_Q(2a) - 1 < \infty$, where

$$Z_Q(v) = \frac{\zeta(v)}{\zeta(2v)} \prod_{p \mid Q} (1 + p^{-v})^{-1}, \qquad v > 1.$$

Here a germ means the complete exact analytic germ, equivalently all exact derivatives at a point, rather than a finite Taylor polynomial or noisy measurements. The base route proves that this germ has a unique entire continuation, with $|A(s)| \leq M \exp(\lambda_1 \max\{-\Re s, 0\})$.

B.2 Exact inverse theorem

Theorem B.1 (AI-1). Two admissible parameter triples define the same analytic germ if and only if

$$a = a', \qquad \beta = \beta', \qquad \operatorname{rad}(Q) = \operatorname{rad}(Q').$$

The function itself therefore encodes the weight exponent, the depth exponent, and the finite excluded prime set. It does not encode valuations $v_p(Q)$.

B.2.1 Step 1: recover the ordered spectral atoms

Starting with $R_1 = A$, define successively

$$\lambda_j = \lim_{t\to\infty} \frac{\log R_j(-t)}{t}, \qquad w_j = \lim_{t\to\infty} e^{-\lambda_j t} R_j(-t), \qquad R_{j+1}(s) = R_j(s) - w_j e^{-\lambda_j s}.$$

Every limit exists and recovers exactly the j-th support frequency and weight. Indeed, if $M_{j+1} = \sum_{k>j} w_k$, then for every $t \geq 0$,

$$R_j(-t) = w_j e^{\lambda_j t}(1 + r_j(t)), \qquad 0 \leq r_j(t) \leq \frac{M_{j+1}}{w_j} e^{-(\lambda_j - \lambda_{j+1})t}.$$

The bound follows by replacing every tail frequency by its largest value λ_{j+1}. Taking logarithms and dividing by t proves the first limit. Multiplying by $e^{-\lambda_j t}$ proves the second. Removing this exact entire atom leaves the same hypotheses for the next step. Thus the complete ordered atom list is intrinsic to the entire function.

No approximation to a large negative-depth value is used in this uniqueness proof. It is an exact limiting argument.

B.2.2 Step 2: recover β without knowing the integer support

Put

$$\delta_Q = \frac{1}{\zeta(2)} \prod_{p \mid Q} \frac{p}{p+1} > 0.$$

The base route establishes the elementary counting estimate

$$N_Q(x) := \#\{2 \leq n \leq x : \mu(n)^2 = 1, (n, Q) = 1\} = \delta_Q x + O_Q(\sqrt{x}).$$

Since $N_Q(n_j) = j$, it follows that

$$n_j = \frac{j}{\delta_Q}\left(1 + O_Q(j^{-1/2})\right), \quad \lambda_j = 2\delta_Q^{\beta} j^{-\beta}\left(1 + O_{Q,\beta}(j^{-1/2} + j^{-\beta})\right).$$

For completeness, the first estimate follows initially from $j = \delta_Q n_j + O_Q(\sqrt{n_j})$, which gives $n_j \asymp_Q j$; substituting this back improves the error to $O_Q(\sqrt{j})$. The second uses $-\log(1-u) = u(1+O(u))$ as $u \downarrow 0$.

Consequently the already recovered frequencies determine

$$\boxed{\beta = -\lim_{j\to\infty} \frac{\log \lambda_j}{\log j}.}$$

A rank ratio avoids the slowly decaying constant divided by $\log j$: for every fixed real $c > 1$,

$$-\frac{\log(\lambda_{\lfloor cj \rfloor}/\lambda_j)}{\log c} = \beta + O_{Q,\beta,c}(j^{-1/2} + j^{-\beta}).$$

The floor contributes an additional $O(j^{-1})$, which is absorbed by the displayed error. These are fixed-parameter asymptotics. They do not give a constant uniform in arbitrary moduli.

B.2.3 Step 3: recover the support integers and the weight exponent

Once β is known, every spectral atom gives its exact integer label:

$$\boxed{n_j = (1 - e^{-\lambda_j/2})^{-1/\beta}, \qquad a = -\frac{\log w_j}{2 \log n_j}.}$$

The recovered real number in the first formula is an integer by the family definition; rounding is not part of the exact theorem. Since $n_j \geq 2$, the denominator in the second formula is nonzero. Every recovered atom yields the same value of a.

B.2.4 Step 4: recover the excluded primes

A prime p lies in the recovered integer support exactly when $p \nmid Q$: primes are squarefree, and no other restriction is imposed. Hence

$$\boxed{\operatorname{rad}(Q) = \prod_{\substack{p \text{ prime} \\ p \notin \{n_j : j \geq 1\}}} p.}$$

The product is finite because the parameters are assumed to come from this family. This formula is an exact reconstruction from infinite data, not an algorithm that can certify completion of the prime list after finitely many observations. Conversely, equal a, β and equal radicals produce exactly the same terms. This proves both directions of AI-1.

B.2.5 A constructive counting envelope

The rank asymptotic can be made effective without an RH input. Write $\omega(Q) = \#\{p : p \mid Q\}$. For real $x \geq 4$, inclusion and exclusion gives

$$|N_Q(x) - \delta_Q x| \leq C_Q\sqrt{x} + 1, \qquad C_Q = 2^{\omega(Q)} + 2\frac{\varphi(Q)}{Q}.$$

To verify the constants, expand $\mu(n)^2 = \sum_{d^2|n} \mu(d)$. For $(d, Q) = 1$, the number of $m \leq x/d^2$ coprime to Q differs from $(\varphi(Q)/Q)x/d^2$ by at most $2^{\omega(Q)}$. Summing over at most $\sqrt{x}$ values of d gives the first part of C_Q. The omitted main-term tail is at most $(\varphi(Q)/Q)x/\lfloor\sqrt{x}\rfloor \leq 2(\varphi(Q)/Q)\sqrt{x}$. Removing $n = 1$ adds one. The main-term density is $(\varphi(Q)/Q)\sum_{(d,Q)=1} \mu(d)d^{-2} = \delta_Q$ by its absolutely convergent Euler product.

For $j \geq 3$, therefore,

$$\left(\frac{\sqrt{C_Q^2 + 4\delta_Q(j-1)} - C_Q}{2\delta_Q}\right)^2 \leq n_j \leq \left(\frac{\sqrt{C_Q^2 + 4\delta_Q(j+1)} + C_Q}{2\delta_Q}\right)^2.$$

The lower and upper bounds are the positive solutions of the corresponding quadratic inequalities in $\sqrt{n_j}$. At $j \geq 3$, all possible supports have $n_j \geq 5$, so the $x \geq 4$ counting envelope applies.

B.3 What finite negative-depth measurements can recover

Theorem B.2 (AI-2), gap bound. Suppose the first $j-1$ atoms have already been removed exactly, put $\Delta_j = \lambda_j - \lambda_{j+1} > 0$, and fix $h > 0$. Define

$$\widehat{\lambda}_j(t, h) = \frac{\log R_j(-t-h) - \log R_j(-t)}{h}.$$

Then for every $t \geq 0$,

$$0 \leq \lambda_j - \widehat{\lambda}_j(t, h) \leq \frac{1}{h}\log\left(1 + \frac{M_{j+1}}{w_j}e^{-\Delta_j t}\right),$$

and

$$0 \leq e^{-\lambda_j t}R_j(-t) - w_j \leq M_{j+1}e^{-\Delta_j t}.$$

Proof. The preceding positive remainder formula gives $\widehat{\lambda}_j = \lambda_j + h^{-1}[\log(1 + r_j(t+h)) - \log(1 + r_j(t))]$. Each tail factor decreases, so $0 \leq r_j(t+h) \leq r_j(t)$. The two inequalities now follow from the bound on $r_j(t)$. For the amplitude, multiply the positive tail bound by $e^{-\lambda_j t}$.

In particular, to guarantee frequency error at most $\varepsilon > 0$ from exact residual values, it suffices to take

$$t \geq \max\left\{0, \frac{1}{\Delta_j}\log\frac{M_{j+1}}{w_j(e^{h\varepsilon}-1)}\right\}.$$

The parameters in this certificate are properties of the true tail. If they are only estimated from data, this is a conditional recovery bound rather than an independent numerical certificate.

B.3.1 Positive tail envelopes for reproducible examples

For integer $L \geq n_j$, a direct sum through $n \leq L$ at depth $-t$, $t \geq 0$, omits at most

$$E_L(t) = e^{t\lambda_{L+1}}\frac{L^{1-2a}}{2a-1}.$$

Indeed all omitted frequencies are at most λ_{L+1}, and $\sum_{n>L} n^{-2a} \leq \int_L^\infty x^{-2a}\,dx$. Ignoring squarefreeness and coprimality makes this a valid upper bound. If r_0, r_1 are the two positive truncated residual sums at $t, t+h$, the true secant belongs to

$$\left[\frac{\log r_1 - \log(r_0 + E_L(t))}{h}, \frac{\log(r_1 + E_L(t+h)) - \log r_0}{h}\right].$$

This interval treats truncation exactly at the mathematical level. Its displayed floating-point endpoints are not directed-rounding certificates.

B.3.2 Cancellation is a real limitation

Evaluating a residual by subtracting previous atoms is different from evaluating its known positive series. If an observation of $A(-t)$ has relative error at most η and the previous atoms are exact, then the residual error can have relative size

$$\eta\,\kappa_j(t), \qquad \kappa_j(t) = \frac{A(-t)}{R_j(-t)} \sim \frac{w_1}{w_j}e^{(\lambda_1-\lambda_j)t}.$$

Thus the large negative depth that separates nearby atoms also worsens cancellation for later atoms. Uncertain previously subtracted frequencies introduce further error. The computation evaluates residuals as positive sums and reports $\log_{10}\kappa_j$ so this conditioning cost remains visible.

B.4 Exact uniqueness does not imply uniform prime recovery

Theorem B.3 (AI-3), bounded-window instability. Let p be a prime not dividing Q, and let $R \geq 0$. For every integer $k \geq 0$,

$$\boxed{\sup_{|s|\le R} |A^{(k)}_{a,\beta,Q}(s) - A^{(k)}_{a,\beta,Qp}(s)| \le \lambda_p^k e^{R\lambda_p} \frac{Z_Q(2a)}{p^{2a}+1}.}$$

Consequently adding larger and larger excluded primes gives convergence in every derivative on every bounded complex-depth window, even though the recovered radical changes each time.

Proof. The difference consists exactly of the squarefree integers divisible by p and coprime to Q, all of which satisfy $n \ge p$. Their frequencies are at most λ_p. The Euler factor at p shows that their total weight is

$$\sum_{\substack{n\ge 1\\ \mu(n)^2=1,(n,Q)=1\\ p\mid n}} n^{-2a} = \frac{Z_Q(2a)}{p^{2a}+1}.$$

There is no $n = 1$ term in this difference. Bound the k-th derivative of every exponential by $\lambda_p^k e^{R\lambda_p}$ and sum. Since $\lambda_p \to 0$ and $p^{-2a} \to 0$, the bound tends to zero. This proves the derivative convergence and the claimed instability.

More explicitly, for any bounded window and positive measurement tolerance, two distinct radicals in this family can produce functions closer than that tolerance throughout the window. This defeats a recovery guarantee uniform over unbounded excluded primes. It does not refute recovery under an a priori modulus bound or from complete exact analytic data.

For $a = \beta = 2, Q = 1$, the mass removed by p is exactly $105/[\pi^4(p^4+1)]$. The examples $p = 101, 1009, 10007$ quantify how quickly large-prime distinctions disappear on $|s| \le 5$.

B.5 The function as an arithmetic Hilbert feature space

This section spells out the classical feature-space construction for this arithmetic spectrum. It supplies a precise space in which the complex-depth packets live.

For $c = (c_j) \in \ell^2$, define

$$(Uc)(s) = \sum_{j\ge 1} c_j \sqrt{w_j}\, e^{-\lambda_j s}.$$

The Cauchy–Schwarz inequality gives uniform convergence on bounded complex sets and

$$|(Uc)(s)| \le \|c\|_{\ell^2} \sqrt{A(2\Re s)}.$$

The map is injective: $\sum |c_j|\sqrt{w_j} \le \|c\|\sqrt{M} < \infty$, so the same spectral peeling argument, now for complex coefficients, forces the first coefficient and then every coefficient to vanish whenever $Uc = 0$. Positivity was needed to recover unknown frequencies in AI-1; injectivity here only needs absolute summability and the known ordered support. Specifically, after dividing by the largest remaining exponential, the tail is bounded by $e^{-\Delta_j t} \sum_{k>j} |c_k|\sqrt{w_k}$, which tends to zero.

The image $\mathcal{H}_{a,\beta,Q} = U\ell^2$, with $\|Uc\|_{\mathcal{H}} = \|c\|_{\ell^2}$, is therefore a complete Hilbert space of entire functions. Its reproducing kernel is

$$K(s,t) = A(s+\bar{t}).$$

Using an inner product linear in the first argument, the coefficient vector of $K(\cdot,t)$ is $(\sqrt{w_j}e^{-\lambda_j \bar{t}})_j$, so $\langle Uc, K(\cdot,t)\rangle = (Uc)(t)$. This also verifies the sign and conjugation convention directly. Arbitrarily large finite Gram matrices at distinct complex depths are strictly positive, as proved in the base route. Thus the feature space has infinite rank, not a finite-dimensional Prony model.

The monomial moment matrices also have infinite rank: $m_k = (-1)^k A^{(k)}(0) = \sum_j w_j \lambda_j^k$, and for every nonzero polynomial P, $\sum_j w_j |P(\lambda_j)|^2 > 0$, because a nonzero polynomial cannot vanish at infinitely many distinct frequencies. All finite derivative Hankel matrices are strictly positive definite.

B.6 Complete fixed-modulus character resolution

Let χ, ψ be Dirichlet characters modulo the same fixed integer Q, extended by zero outside the units, and put $\eta = \chi\overline{\psi}$. The base extension is

$$A_{\chi,\psi}(s) = \sum_{n\geq 2} \mu(n)^2 \eta(n) n^{-2a}(1-n^{-\beta})^{2s}.$$

The endpoint subtraction in its Newton expansion is still exactly one:

$$A_{\chi,\psi}(s) = \sum_{j\geq 0} (-1)^j \binom{2s}{j} \left[\frac{L(2a+j\beta,\eta)}{L(4a+2j\beta,\eta^2)} - 1\right].$$

Every character takes the value one at $n = 1$; at primes dividing Q, it is zero. The Euler product identity is valid even when η is imprimitive, because the actual Dirichlet character and its actual modulus are retained. All arguments of L lie in $\Re v > 1$, where its Euler product converges absolutely and is nonzero. No unproved zero-free-region hypothesis is used.

Theorem B.4 (AI-4), character sector decay. Fix $a > 1/2, \beta > 0, Q$, and a closed sector $|\arg s| \leq \pi/2 - \varepsilon$, $0 < \varepsilon < \pi/2$. If $\chi \neq \psi$, then uniformly in that sector,

$$A_{\chi,\psi}(s) = O_{a,\beta,Q,\varepsilon}\big(|s|^{-(2a-1/2)/\beta}\big), \qquad \frac{A_{\chi,\psi}(s)}{A_{a,\beta,Q}(s)} = O_{a,\beta,Q,\varepsilon}\big(|s|^{-1/(2\beta)}\big).$$

These statements are uniform over the finite character set of this fixed modulus. They are not uniform as Q grows.

Proof. Distinct characters give a nonprincipal η. Its sum over a complete period is zero, so $|\sum_{m\leq y} \eta(m)| \leq Q$. Hence

$$\sum_{n\leq x} \mu(n)^2 \eta(n) = \sum_{d\leq \sqrt{x}} \mu(d)\eta(d)^2 \sum_{m\leq x/d^2} \eta(m) = O_Q(\sqrt{x}).$$

Use partial integration against $g_s(x) = x^{-2a}(1-x^{-\beta})^{2s}$, whose endpoint values vanish when $\Re s > 0$. The counting bound reduces the magnitude to a constant times $\int_1^\infty \sqrt{x}\,|g_s'(x)|\,dx$. Writing $u = \Re s$ and $\gamma = (2a-1/2)/\beta > 0$, direct substitution $y = x^{-\beta}$ bounds its two derivative terms by

$$\frac{2a}{\beta}B(\gamma, 2u+1) + 2|s|B(\gamma+1, 2u),$$

which is $O_{a,\beta,\varepsilon}(|s|^{-\gamma})$ because $u \geq |s|\sin\varepsilon$. The principal diagonal has the nonzero leading term $\delta_Q\Gamma(\alpha)\beta^{-1}(2s)^{-\alpha}$, $\alpha = (2a-1)/\beta$, by the base sector theorem. Its modulus is bounded below by a positive fixed-sector multiple of $|s|^{-\alpha}$ for sufficiently large $|s|$. Division gives the second bound, since $\gamma - \alpha = 1/(2\beta)$.

At real positive depth, the matrix $(A_{\chi,\psi}(s))$ on any d distinct characters is positive semidefinite and has identical diagonal $A_{a,\beta,Q}(s)$. Its normalized matrix tends to I_d, with operator norm error $O_{a,\beta,Q,d}(s^{-1/(2\beta)})$. Indeed, the off-diagonal entry bound controls the maximum row and column sums, and thus the operator norm. This gives quantitative separation of a fixed character bank. It is consistent with a complex or signed off-diagonal entry and makes no complete-monotonicity assertion for that entry.

B.7 Classical comparison and limits of novelty

Uniqueness of a positive measure from its Laplace transform is classical. Schilling, Song and Vondraček [15, Proposition 1.2 and Theorem 1.4] give the uniqueness and Bernstein representation results. Here the measure is $\sum_j w_j\delta_{\lambda_j}$, the transform variable is real depth $s > 0$, and finiteness follows from $\sum_j w_j < \infty$. The exact recovery of a, β and $\mathrm{rad}(Q)$, the rank asymptotic and the large-prime instability estimates are proved above. They are not attributed to that reference.

The Hilbert feature-space construction and finite Prony reconstruction are also classical. This chapter supplies their realization for the arithmetic spectrum. It does not claim historical priority for these mechanisms or for the parameter-specific inverse and character results. A bounded literature comparison cannot establish the absence of earlier work.

B.8 Computational verification

`checks/arithmetic_inverse.py` is deterministic. Its exact checks use rational finite atomic surrogates with $2a = 4$, integer $\beta = 1, 2, 3$, $Q = 1, 2, 6, 30$, and one through five atoms. They independently construct the annihilating polynomial from moments and from its known rational nodes, verify the positive Vandermonde formula for Hankel determinants, reconstruct weights, recover integer labels at known β, and test further exact recurrence moments. These surrogates do not turn the infinite family's Hankel matrices into finite-rank matrices.

The high-precision examples use 180 decimal digits. They show two-rank β estimates at ranks 100, 1000, and 10000, conditional negative-depth peeling for the first three atoms at $t = 20, 100, 500$, and

large-prime bounded-window envelopes. Positive direct sums use $n \leq 5000$, with the analytic omitted-tail envelope above. Rank enumeration uses $n \leq 100000$. Actual cancellation factors are reported. Numerical values and floating-point endpoints are illustrations, not ball-arithmetic certificates.

From the package's `research/` directory, run `python checks/arithmetic_inverse.py` in a Python environment with `mpmath` installed. Results are written to `evidence/arithmetic_inverse_checks.json`, including input/source hashes, arithmetic conventions, tested ranges, software versions and elapsed time. Earlier retrieval failures remain in the archived run history. Theorems B.1–B.4 rest on the local proofs above. Historical priority remains unresolved.

APPENDIX C

Finite-prime sieve families and explicit detection of signed atoms

The construction extends the one-prime setting to a finite-prime parameter family. The arguments below identify where classical orthogonal-polynomial mechanisms enter the arithmetic construction.

C.1 Definition and exact coordinates

Let F be a finite set of distinct primes, let $\boldsymbol{\lambda} = (\lambda_p)_{p\in F}$, and put

$$x_n = (1-n^{-2})^2, \qquad \kappa_F(n;\boldsymbol{\lambda}) = \prod_{p\in F}(1+\lambda_p \mathbf{1}_{p|n}),$$
$$\nu_{F,\boldsymbol{\lambda}} = \sum_{n\geq 1} \mu(n)^2 n^{-4}\kappa_F(n;\boldsymbol{\lambda})\delta_{x_n}.$$

The mass at $x_1 = 0$ is exactly 1. A strength $\lambda_p = -1$ deletes every squarefree atom divisible by p. Several deletions commute. The depth-k family uses $x^k\,d\nu$, for integers $k \geq 0$.

Write $D(s) = \zeta(s)/\zeta(2s)$. For arbitrary finite complex strengths and $\Re s > 1$, absolute convergence permits expansion of the finite prime product. The local squarefree Euler factors give

$$Z_F(s;\boldsymbol{\lambda}) = \sum_{n\geq 1}\mu(n)^2 n^{-s}\kappa_F(n;\boldsymbol{\lambda}) = D(s)\prod_{p\in F}\left(1+\frac{\lambda_p}{p^s+1}\right).$$

Equivalently, expansion in subsets $S \subseteq F$ gives the coefficient $D(s)/\prod_{p\in S}(p^s+1)$ for $\prod_{p\in S}\lambda_p$. This is an independently useful coordinate formula for prime overlap.

Consequently

$$M_j(\boldsymbol{\lambda}) = \int x^j\,d\nu_{F,\boldsymbol{\lambda}} = \sum_{r=0}^{2j}(-1)^r\binom{2j}{r}D(4+2r)\prod_{p\in F}\left(1+\frac{\lambda_p}{p^{4+2r}+1}\right). \tag{1}$$

Depth-k moments are M_{k+j}. With $v = \pi^{-2}$, the even-zeta formula makes every $D(4+2r)$ a rational multiple of v^{r+2}. Thus the moments belong to $\mathbb{Q}[v, \lambda_p : p \in F]$, and monic orthogonal-polynomial coefficients belong to $\mathbb{Q}(v, \lambda_p : p \in F)$. This is an exact field statement, with no decimal recognition step.

For two primes the interaction term is explicit:

$$M_j(\lambda_p, \lambda_q) = M_j(0,0) + \lambda_p U_{p,j} + \lambda_q U_{q,j} + \lambda_p \lambda_q U_{pq,j},$$

where $U_{pq,j} = \sum_{pq|n} \mu(n)^2 n^{-4} x_n^j > 0$. More generally, with all other strengths at least -1, every mixed moment derivative in a set of distinct primes is strictly positive. It is the integral over atoms divisible by those primes, with the remaining nonnegative prime factors. Infinitely many such atoms remain after any finite collection of deletions. Pure second derivatives in any one strength vanish because the moments are separately affine.

C.2 The exact positivity domain

Theorem C.1. For real strengths, $\nu_{F,\lambda}$ is a positive measure if and only if $\lambda_p \geq -1$ for every $p \in F$. On this closed orthant, every finite Hankel matrix of every nonnegative integer depth is strictly positive definite.

Proof. The stated inequalities make each atom weight nonnegative. The primes outside F supply infinitely many positive atoms, even when all strengths are deletion endpoints. A nonzero polynomial cannot vanish on infinitely many distinct nodes; therefore its squared norm is strictly positive. Conversely, if $\lambda_p < -1$, the squarefree atom $n = p$ has mass $(1+\lambda_p)p^{-4} < 0$: no other strength appears at that atom. The same argument works after every depth tilt because $x_p > 0$. □

The positive monic families $P_m^{(k;F,\boldsymbol{\lambda})}$ consequently exist at all degrees throughout the closed orthant. Their Hankel determinants never vanish there, including at simultaneous deletion endpoints. Each finite-degree coefficient is analytic in a neighborhood of every point of that orthant. This neighborhood is a finite-degree statement; the next theorem explains why no common enlargement of the positivity domain works at all degrees.

Together, Theorems C.1 and C.2 also prove the exact equivalence: every finite Hankel matrix is positive semidefinite if and only if every strength is at least -1. Thus this is a complete positivity-domain result, not only a sufficient condition.

C.3 An explicit polynomial detector for every bad strength

For an integer $a \geq 2$, define

$$L_a(x) = \prod_{n=1}^{a-1} \frac{x - x_n}{x_a - x_n}, \qquad C_a = L_a(1) = \prod_{n=1}^{a-1} \frac{1 - x_n}{x_a - x_n} > 0,$$

$$r_a = \frac{1-x_{a+1}}{1-x_a} = \frac{a^4\big(2(a+1)^2-1\big)}{(a+1)^4(2a^2-1)} \in (0,1),$$

$$f_{a,m}(x) = L_a(x)\left(\frac{1-x}{1-x_a}\right)^m, \qquad m = 0,1,2,\dots. \tag{2}$$

The degree is $a-1+m$; all lower nodes are killed exactly; $f_{a,m}(x_a) = 1$. At every higher node, $|f_{a,m}(x_n)| \le C_a r_a^m$, because each factor of L_a increases on $[x_a, 1]$ and $1 - x_n \le 1 - x_{a+1}$.

Set $C_F = \prod_{q\in F} \max(1, |1+\lambda_q|)$. Then $|\kappa_F(n)| \le C_F$, and the elementary decreasing-series bound gives

$$\sum_{n>a} |\mu(n)^2 n^{-4} \kappa_F(n)| \le \frac{C_F}{3a^3}. \tag{3}$$

Theorem C.2. If $\lambda_p < -1$, then

$$\int f_{p,m}(x)^2 \, d\nu_{F,\lambda}(x) \le \frac{1+\lambda_p}{p^4} + \frac{C_F C_p^2}{3p^3} r_p^{2m}. \tag{4}$$

Hence the Hankel matrix of order $p+m$ is not positive semidefinite whenever

$$\boxed{\frac{pC_F C_p^2}{3} r_p^{2m} < -(1+\lambda_p).} \tag{5}$$

All quantities in (5) are rational when the strengths are rational. It provides an exact finite certificate without calculating Hankel eigenvalues or relying on floating-point root finding. A suitable finite m exists because $r_p < 1$.

Proof. The polynomial kills all atoms below p, equals 1 at the negative atom p, and has the stated uniform bound above p. Replacing all higher signed contributions by their absolute values and applying (3) proves (4). The coefficients of $f_{p,m}$ then supply a negative quadratic form for $[M_{i+j}]_{i,j<p+m}$ when (5) holds. □

For depth k, the same polynomial satisfies

$$\int x^k f_{p,m}(x)^2 \, d\nu \le \frac{(1+\lambda_p)x_p^k}{p^4} + \frac{C_F C_p^2}{3p^3} r_p^{2m}.$$

Replace the right side of (5) by $-(1+\lambda_p)x_p^k$ to obtain an explicit depth-k detector. This proof extends to any finite signed atomic measure with these nodes and the same summable weight envelope. Its mechanism is an isolating polynomial followed by exponential suppression of the higher nodes.

C.4 Conditional prime fibers and all-prime margin bounds

Fix $p \in F$, with all other strengths at least -1, and write $\kappa(n) = \prod_{q\in F\setminus\{p\}} (1+\lambda_q \mathbf{1}_{q|n})$. Separate the positive measure into its p-free and p-divisible parts:

$$A_m = [\sum_{p\nmid n} \mu(n)^2 n^{-4} \kappa(n) x_n^{i+j}]_{i,j<m}, \quad B_m = [\sum_{p\mid n} \mu(n)^2 n^{-4} \kappa(n) x_n^{i+j}]_{i,j<m}.$$

Both matrices are positive definite. For A_m, use infinitely many primes outside F; for B_m, use infinitely many squarefree integers $p\ell$, with primes ℓ outside F. This remains true at every deletion endpoint of the other strengths.

Theorem C.3. The one-variable fiber

$$\tau_m(\lambda_p) = \det\big(A_m + (1+\lambda_p)B_m\big)$$

has exact degree m, and all its roots, with multiplicity, are real and strictly less than -1. The root nearest the positivity boundary is $-1-\delta_m$, with

$$\delta_m = \min_{0\neq f\in\mathbb{R}[x],\ \deg f<m} \frac{\int f^2\, d\nu_{p\text{-free}}}{\int f^2\, d\nu_{p\text{-divisible}}} > 0. \tag{6}$$

The sequence δ_m is nonincreasing, and, with $C_\kappa = \prod_{q\neq p} \max(1, 1+\lambda_q)$,

$$\boxed{\delta_{p+m} \le \frac{pC_\kappa C_p^2}{3} r_p^{2m}.} \tag{7}$$

Proof. The definite pencil is congruent to $I + (1+\lambda_p)A_m^{-1/2} B_m A_m^{-1/2}$, whose eigenvalues have positive slopes. Its roots are $-1-1/\eta_i$, with $\eta_i > 0$. This proves the degree and root statements, and the reciprocal largest eigenvalue is exactly (6). Polynomial-space inclusion proves monotonicity. Test (6) at order $p+m$ with (2). The denominator includes the atom p, of mass p^{-4}, because $\kappa(p) = 1$. The numerator kills every lower atom, has no atom at p, and its higher tail is bounded by $C_\kappa C_p^2 r_p^{2m}/(3p^3)$. This proves (7) and therefore $\delta_m \to 0$. □

A sharper arithmetic bound uses the exact remaining tail mass

$$A_{\text{tail}} = D(4)\frac{p^4}{p^4+1}\prod_{q\neq p}\left(1+\frac{\lambda_q}{q^4+1}\right) - \sum_{1\le n<p} \mu(n)^2 n^{-4}\kappa(n) > 0,$$

and replaces (7) by $\delta_{p+m} \le p^4 C_p^2 A_{\text{tail}} r_p^{2m}$. Every finite-degree coefficient can have poles only at the fiber's Hankel roots; numerator cancellations can remove a possible pole. The theorem does not assert simple roots or global multivariate real stability.

At depth zero, the initial margin is exactly $\delta_1 = p^4$, independently of all other safe strengths: the total p-free and p-divisible masses have ratio p^4, since all the other Euler factors cancel. The higher-order margins contain the arithmetic overlap information.

The same argument applies to every nonnegative depth, replacing each integral by its x^k tilt. The denominator's explicit atom contribution becomes $p^{-4}x_p^k$, and (7) acquires the factor x_p^{-k}.

C.5 Resolution, nonconvex finite tests, and a different additive family

For $F = \{2,3\}$, the order-one Hankel matrix is the scalar

$$M_0(\lambda_2,\lambda_3) = 105\pi^{-4}\left(1+\frac{\lambda_2}{17}\right)\left(1+\frac{\lambda_3}{82}\right).$$

Thus $(0,0)$ and $(-34,-164)$ have the same positive order-one Hankel matrix. Their midpoint $(-17,-82)$ has zero total mass. The unrestricted real parameter set passing the order-one positive-definiteness test is therefore nonconvex. This is a concrete warning about a finite test, while the true positivity domain in Theorem C.1 is a convex closed orthant.

The positive-semidefinite feasible set is nonconvex as well: the points $(0,0)$ and $(-34,-246)$ have positive mass factors 1 and 2, while their convex combination with weights $3/5$ and $2/5$, namely $(-68/5,-492/5)$, has mass factor $-1/25$.

An additive prime family is a different deformation:

$$\widetilde{\nu}_{F,\gamma} = \sum_{n\ge 1}\mu(n)^2 n^{-4}\left(1+\sum_{p\in F}\gamma_p \mathbf{1}_{p\mid n}\right)\delta_{x_n}.$$

Its exact positivity domain is the polyhedron

$$1+\sum_{p\in S}\gamma_p \ge 0 \quad (S\subseteq F), \quad \text{equivalently} \quad 1+\sum_{\gamma_p<0}\gamma_p \ge 0.$$

Necessity uses the squarefree integer $n=\prod_{p\in S}p$; sufficiency checks every atom's prime subset. Its finite Hankel matrices are affine functions of the strengths, so their positive-semidefinite feasible sets are convex spectrahedra. In contrast, the multiplicative family includes the arithmetic prime-overlap terms and has polynomial parameter dependence. For example, additive strengths $\gamma_2=\gamma_3=-3/4$ leave both individual prime weights positive but make the $n=6$ weight negative; multiplicative strengths $\lambda_2=\lambda_3=-3/4$ remain safely positive.

C.6 A limited nonreduction statement

If at least two strengths in a positive multiplicative family are nonzero, its entire depth-zero monic polynomial sequence cannot equal any one-prime sequence on the same variable and node system. A direct proof avoids importing a determinacy theorem. Write $P_m = x^m + \sum_{j<m} c_{mj}x^j$. The equations $\int P_m\,d\nu = 0$ recursively determine every normalized moment from the monic sequence. Equal sequences therefore give equal normalized Stieltjes series for $|z|>1$. Analytic continuation on the connected complement of the common closed node set makes their Stieltjes functions equal, and residues at each isolated node give equal normalized atom weights. The mass 1 at zero fixes the normalization constant. Finally, the atom at each prime p reads off $1+\lambda_p$, whereas a one-prime deformation

changes at most one such atom. This is a precise separator from the one-prime family. It does not address arbitrary affine variable changes.

The multi-prime Stieltjes kernel also retains infinitely many isolated poles at primes outside F, so the preceding one-prime proof of non-D-finiteness applies unchanged. Orthogonal-polynomial existence, definite-pencil spectral theory, and compact moment determinacy are classical mechanisms. The specific arithmetic coordinates, parameter geometry, and explicit finite-resolution detector are the objects developed here.

C.7 Worked arithmetic examples

For $F = \{2, 3\}$, the following coefficients are rounded high-precision evaluations of (1) and the Hankel formulas. They are not exact decimal constants.

(λ_2, λ_3)	$P_1(x)$	$P_2(x)$
$(-1, -1)$	$x - 0.00200014863265043361$	$x^2 - 0.933902261393426053x + 0.000000921271332319859170$
$(-1/2, 1)$	$x - 0.0377167661732468061$	$x^2 - 0.725293001442481628x + 0.000932648146085806112$
$(1, 1)$	$x - 0.0822907496962840844$	$x^2 - 0.655873200757636623x + 0.00211153000026086129$

Simultaneously deleting $2, 3, 5$ gives $P_1(x) = x - 0.000528721422047782375$ and $P_2(x) = x^2 - 0.966491641778821472x + 0.000000079553141379691051 4$, again rounded. This removes the low prime shelves while retaining the fixed mass at zero and an infinite tail.

For the variable strength at $p = 2$, the nearest conditional margins are:

Hankel order	Other strength $\lambda_3 = -1$	Other strength $\lambda_3 = 3$
1	16, exact	16, exact
2	0.0939109919936561	1.43829172807931
3	0.000302450514004102	0.0346655628067259
4	0.000000528145808944195	0.000223749375519984

The noninteger entries are approximate symmetric-pencil calculations. They show an actual prime-overlap effect beyond the mass test. In these calculations the defect $\lambda_2 = -1.001$ is visible at order 3 when the 3-shelf is deleted, but only at order 4 when that shelf is strengthened to 3. This comparison is a numerical example, not a universal monotonicity theorem.

The separate rational certificates (5) do not depend on those approximate roots. The script constructs negative detectors for primes $2, 3, 5, 7$, at Hankel orders $8, 11, 19, 40$, respectively. These sufficient orders are not asserted to be minimal. In the $p = 7$ example, the other strengths are $\lambda_2 = 1/2$, $\lambda_3 = -1$, $\lambda_5 = 2$, and $\lambda_7 = -1.0001$; the exact rational upper bound on the detector quadratic form is approximately -9.74271×10^{-9}.

C.8 Computation contract

`checks/multi_prime_sieve.py` uses exact rational arithmetic for Euler-factor versus subset-expansion comparisons, Bernoulli-based even-zeta coordinates, isolating-polynomial values, and the rational detection criterion (5). It separately evaluates the infinite moments at high precision, tests positive orthogonality grids, compares them with a direct finite squarefree sum plus a proved tail envelope, calculates conditional definite-pencil roots, and evaluates signed detector quadratic forms. These decimal checks are not interval certificates. Universal positivity and negativity conclusions follow from the displayed proofs and exact rational bounds.

The passing run records 1,019 exact rational assertions, 102 positive parameter/depth cases, 1,395 lower-monomial orthogonality conditions, 381 recurrence identities, 40 conditional-pencil cases, and four exact negative-atom certificates. Working precision is 320 decimal digits. Maximum absolute orthogonality residual was approximately 6.33×10^{-322}, maximum recurrence residual 2.23×10^{-303}, and maximum scale-normalized pencil determinant residual 5.06×10^{-321}. These are finite numerical consistency results, not interval certificates. No execution failure occurred in this route's run.

The script records actual versions, source hash, parameter bounds, finite counts, precision, residuals, examples, and any failed criteria in `evidence/multi_prime_sieve_checks.json`. It accepts an optional output path so a parent bounded runner can place the result inside a fresh evidence directory. No broad priority search was performed for this specific extension; historical novelty remains unresolved.

APPENDIX D

Orbit spectral zeta: continuation, trace zeros, and regularized product

This chapter extends the previously defined orbit family with a self-contained continuation proof. The Mittag–Leffler seed and Mellin continuation mechanism are classical.

D.1 The continuation theorem

Let $N \geq 2$ be an integer, and put $\alpha = 1/N$. Define

$$d_N(w) = \sum_{n=0}^{\infty} \frac{(-1)^n w^n}{(Nn)!} = E_{N,1}(-w).$$

List its nonzero zeros w_j with multiplicity, and use the principal logarithm, with $-\pi < \operatorname{Arg} w_j < \pi$. No zero lies on the omitted negative ray. The orbit zeta function

$$\mathcal{Z}_N(s) = \sum_j e^{-s \operatorname{Log} w_j}$$

converges absolutely exactly when $\Re s > 1/N$. It has a meromorphic continuation to the whole plane, with exactly one pole: a simple pole at $s = 1/N$, of residue

$$\boxed{\operatorname{Res}_{s=1/N} \mathcal{Z}_N(s) = \frac{\sin(\pi/N)}{N\pi}.}$$

At every nonpositive integer,

$$\boxed{\mathcal{Z}_N(-m) = 0 \quad (m = 0, 1, 2, \ldots).}$$

At the origin,

$$\boxed{\mathcal{Z}_N'(0) = -\log N, \qquad \exp[-\mathcal{Z}_N'(0)] = N.}$$

The last equality is the zeta regularized product of the orbit zeros under this branch convention. It is a regularized product, not convergence of the ordinary product of the zeros. Positive integer values retain the exact rational coefficient law established in the preceding construction.

D.2 The exponential packet and its exact asymptotic

Let $\omega = e^{2\pi i/N}$. The finite root-of-unity filter gives, for every $x \in \mathbb{C}$,

$$F_N(x) := d_N(-x^N) = \frac{1}{N} \sum_{j=0}^{N-1} e^{\omega^j x} = \sum_{n=0}^{\infty} \frac{x^{Nn}}{(Nn)!}. \tag{S1}$$

This equality follows by expanding the exponentials and using $N^{-1} \sum_j \omega^{jm} = 1$ when $N \mid m$, and zero otherwise. For real $x \geq 0$, the power series makes $F_N(x) > 0$. Put

$$h_N(x) = \sum_{j=1}^{N-1} e^{(\omega^j - 1)x}, \qquad c_N = 1 - \cos(2\pi/N) > 0.$$

Then

$$F_N(x) = \frac{e^x}{N}(1 + h_N(x)), \qquad |h_N(x)| \leq (N-1)e^{-c_N x}, \qquad |h_N'(x)| \leq 2(N-1)e^{-c_N x}. \tag{S2}$$

Since $1 + h_N(x) = Ne^{-x}F_N(x) > 0$, the real logarithm is well defined for all $x \geq 0$. At infinity,

$$\log F_N(x) = x - \log N + O(e^{-c_N x}), \qquad g_N(x) := \frac{F_N'(x)}{F_N(x)} = 1 + O(e^{-c_N x}). \tag{S3}$$

At the origin $g_N(x) = O(x^{N-1})$. Its only Taylor powers are x^{Nm-1}, with $m \geq 1$.

D.3 The branch and absolute-interchange issue

The pre-existing genus-zero product is

$$d_N(w) = \prod_j (1 - w/w_j). \tag{S4}$$

For completeness, the series bound $|d_N(w)| \le \exp(|w|^{1/N})$ gives order at most $1/N < 1$. Hadamard factorization therefore has genus zero and a constant exponential factor, which equals one because $d_N(0) = 1$. The usual zero-count consequence gives $\sum_j |w_j|^{-\sigma} < \infty$ for every $\sigma > 1/N$. Along the negative real axis (S3) also shows the order is exactly $1/N$.

It is not enough simply to say that no zero lies on the integration contour. We need a uniform angular gap from the branch cut to interchange the Mellin integral with the zero sum. Here is that gap.

For $|\arg(-w)| \le \pi/2$, choose $x = (-w)^{1/N}$ with $|\arg x| \le \pi/(2N)$. For every $j \ne 0$,

$$\Re x - \Re(\omega^j x) \ge \left[\cos\frac{\pi}{2N} - \cos\frac{3\pi}{2N}\right] |x| =: \gamma_N |x| > 0. \tag{S5}$$

Indeed, the nearest competing root is separated from the positive direction by at least $3\pi/(2N)$, while the distinguished root is within $\pi/(2N)$. Cosine decreases on $[0, \pi]$. Thus, once $(N-1)e^{-\gamma_N|x|} < 1$, the distinguished term e^x in (S1) is larger in modulus than the sum of all competitors, and $d_N(w) \ne 0$. Consequently, sufficiently large zeros avoid the entire closed left half-plane. There are only finitely many remaining zeros in a bounded disk. None lies on the negative ray, since $d_N(-t) > 0$ for $t \ge 0$. It follows that some $\eta_N > 0$ satisfies

$$|\operatorname{Arg} w_j| \le \pi - \eta_N \qquad \text{for every } j. \tag{S6}$$

With $c = \sin(\eta_N/2) > 0$, this implies

$$|t + w_j| \ge c(t + |w_j|), \qquad t \ge 0. \tag{S7}$$

To check the elementary estimate, write $w = re^{i\theta}$: $|t + w|^2 = (t + r)^2 - 4tr\sin^2(\theta/2) \ge (t + r)^2\cos^2(\theta/2)$.

D.4 Mellin representation in the original strip

Let $H_N(t) = d_N(-t) = E_{N,1}(t)$, and $G_N(t) = H_N'(t)/H_N(t)$. Logarithmic differentiation of (S4), locally uniformly off the zeros, gives

$$G_N(t) = \sum_j \frac{1}{t + w_j}, \qquad t \ge 0. \tag{S8}$$

For $1/N < \sigma < 1$, (S7) yields

$$\sum_j \int_0^\infty \frac{t^{-\sigma}}{|t + w_j|}\, dt \le \frac{\pi}{c\sin(\pi\sigma)} \sum_j |w_j|^{-\sigma} < \infty. \tag{S9}$$

This is the absolute interchange needed for complex s with $\Re s = \sigma$. Euler's beta integral and the reflection identity give

$$\int_0^\infty \frac{t^{-s}}{t+w}\,dt = \frac{\pi}{\sin(\pi s)} e^{-s\,\mathrm{Log}\,w}, \quad 0 < \Re s < 1, \quad |\arg w| < \pi. \tag{S10}$$

First prove this for positive w by substitution and the beta integral, then extend to the slit w-plane by holomorphic dependence. On compact subsets of that slit plane the denominator estimate supplies the needed local domination.

Combining (S8)–(S10), and substituting $t = x^N$, proves

$$\boxed{\mathcal{Z}_N(s) = \frac{\sin(\pi s)}{\pi} \int_0^\infty x^{-Ns} g_N(x)\,dx, \qquad \frac{1}{N} < \Re s < 1.} \tag{S11}$$

For $x > 0$, $x^{-Ns} = e^{-Ns\log x}$ uses the real logarithm. Multiplicities are already incorporated in (S4), so no simple-zero assumption entered the proof.

D.5 Global continuation and the only pole

One can see directly that d_N has no zero on $|w| \le 1$:

$$|d_N(w) - 1| \le \sum_{n\ge 1} \frac{1}{(Nn)!} \le \cosh(1) - 1 < 1.$$

The strict inequality also gives a slightly larger zero-free disk by continuity. Thus $G_N(t)$ has a Taylor series converging uniformly on $[0,1]$,

$$G_N(t) = \sum_{k\ge 0} a_{N,k} t^k, \qquad g_N(x) = \sum_{m\ge 1} N a_{N,m-1} x^{Nm-1}. \tag{S12}$$

For any integer $K \ge 0$, define

$$\begin{aligned} B_{N,K}(s) = &\int_0^1 x^{-Ns}\left[g_N(x) - \sum_{m=1}^{K} N a_{N,m-1} x^{Nm-1}\right] dx \\ &+ \sum_{m=1}^{K} \frac{a_{N,m-1}}{m-s} + \int_1^\infty x^{-Ns}\big[g_N(x) - 1\big]dx + \frac{1}{Ns-1}. \end{aligned} \tag{S13}$$

The first integral is holomorphic for $\Re s < K+1$. This includes local uniform domination, since the Taylor remainder is $O(x^{N(K+1)-1})$. The last integral is entire in s, because (S3) gives exponential decay against every power of x, uniformly on compact s-sets, including after any number of s-derivatives. The rational terms exhibit the only possible poles: positive integers $1,\dots,K$ and $1/N$.

On their overlapping domains the functions (S13) agree: adding the next Taylor term subtracts its integral and adds precisely the same rational function. They also agree with (S11) in its original strip. Therefore

$$\mathcal{Z}_N(s) = \frac{\sin(\pi s)}{\pi} B_{N,K}(s) \tag{S14}$$

provides compatible meromorphic continuations covering the whole plane as $K \to \infty$. At each positive integer m, the apparent simple pole $a_{N,m-1}/(m-s)$ cancels with the simple zero of $\sin(\pi s)$. The term $1/(Ns-1)$ has residue $1/N$, and its multiplier at $s = 1/N$ is nonzero. This proves the stated unique simple pole and its residue.

It also proves that the original series cannot converge absolutely at $s = 1/N$. If it did, its absolute terms would dominate the series for real $s \downarrow 1/N$, except for finitely many zeros of modulus below one. Dominated convergence would then keep that real limit bounded, contradicting the nonzero pole. Absolute convergence at any smaller real part would imply convergence at $1/N$. The abscissa is consequently exactly $1/N$.

D.6 Trace zeros, rational values, and the origin

For $\Re s < 1$ we may use $K = 0$:

$$B_{N,0}(s) = \int_0^1 x^{-Ns} g_N(x)\, dx + \int_1^\infty x^{-Ns}(g_N(x) - 1)\, dx + \frac{1}{Ns-1}. \tag{S15}$$

This expression is holomorphic at every nonpositive integer. Hence (S14) proves $\mathcal{Z}_N(-m) = 0$. These statements do not assert that every such zero is simple.

At a positive integer m, taking the removable limit in (S14) gives

$$\mathcal{Z}_N(m) = (-1)^{m+1} a_{N,m-1}. \tag{S16}$$

If $c_n = (-1)^n/(Nn)!$, the previous logarithmic-product law therefore remains

$$b_m := \mathcal{Z}_N(m) = -m c_m - \sum_{j=1}^{m-1} c_j b_{m-j}. \tag{S17}$$

In particular all these values are rational. This is the finite coefficient dictionary, independent of numerical zero location.

At $s = 0$, the elementary antiderivatives in (S15) give

$$\begin{aligned} B_{N,0}(0) &= \log F_N(1) + \lim_{R\to\infty} \big[\log F_N(R) - R - \log F_N(1) + 1\big] - 1 \\ &= -\log N. \end{aligned}$$

Since $\sin(\pi s)/\pi = s + O(s^3)$, (S14) implies $\mathcal{Z}_N(0) = 0$ and $\mathcal{Z}_N'(0) = -\log N$.

D.7 Classical benchmarks and numerical examples

The inherited identities

$$\mathcal{Z}_2(s) = \pi^{-2s}\zeta(2s, 1/2), \qquad \mathcal{Z}_4(s) = (\sqrt{2}\pi)^{-4s}\zeta(4s, 1/2)$$

now hold as meromorphic identities, by equality in the original half-plane and uniqueness of continuation. Their pole residues are respectively $1/(2\pi)$ and $1/(4\sqrt{2}\pi)$, agreeing with the general theorem. Their zero values at nonpositive integers follow from the Hurwitz formula, and their regularized products are respectively 2 and 4.

The companion script performs 411 exact rational assertions: independent formal-logarithm and quotient calculations for $2 \le N \le 10$ through degree 40; three explicit integer values for each N; and 12 Bernoulli/Hurwitz anchors each for $N = 2, 4$. It then evaluates (S13) using a truncated local Taylor sum and high-precision exponential-tail quadrature. Sixteen $N = 2, 4$ benchmarks sample both sides of the original convergence boundary, negative real values, and complex values. Values for $N = 3, 5$ and checks of $\mathcal{Z}_N'(0)$ are recorded in the JSON evidence.

Those quadrature results are approximations. Agreement at two precisions and with known functions tests normalization and implementation; it does not replace the proof, certify intervals, or settle historical novelty.

D.8 A worked Hurwitz deformation

There is a concrete shifted family. For a real shift $a \ge 0$, define

$$\mathcal{Z}_N(s; a) = \sum_j (w_j + a)^{-s}, \qquad \Re s > 1/N, \tag{T1}$$

again with the principal logarithm and multiplicities. A rightward shift preserves the angular gap from the negative ray: for each nonreal w, $|\arg(w + a)|$ is nonincreasing in a, and positive real zeros remain positive. The zero sequence is unchanged at infinity up to a bounded translation, so the previous absolute convergence argument applies. The normalized determinant is exactly

$$\frac{H_N(a + t)}{H_N(a)} = \prod_j \left(1 + \frac{t}{w_j + a}\right), \qquad H_N(t) = E_{N,1}(t) > 0 \quad (t \ge 0). \tag{T2}$$

This follows by taking the ratio of the two convergent products in (S4), not by introducing an unverified exponential factor. Its logarithmic derivative is $G_{N,a}(t) = H_N'(a + t)/H_N(a + t)$. The same dominated beta-integral argument gives

$$\mathcal{Z}_N(s; a) = \frac{\sin(\pi s)}{\pi} \int_0^\infty t^{-s} G_{N,a}(t)\, dt, \qquad 1/N < \Re s < 1. \tag{T3}$$

At infinity, (S2)–(S3), with $x = (a + t)^{1/N}$, imply

$$G_{N,a}(t) = \alpha(t+a)^{\alpha-1} + O\Big((t+a)^{\alpha-1}e^{-c_N(t+a)^\alpha}\Big). \tag{T4}$$

For fixed a and any integer $K \geq 0$, the binomial expansion therefore gives

$$G_{N,a}(t) = \sum_{k=0}^{K} \alpha \binom{\alpha-1}{k} a^k t^{\alpha-k-1} + O(t^{\alpha-K-2}). \tag{T5}$$

To be explicit about continuation, choose a finite splitting point $T > 2a+1$. Subtract the first $K+1$ terms of (T5) inside the integral from T to infinity, and add their integrals back as the rational terms

$$\frac{\alpha\binom{\alpha-1}{k}a^k T^{\alpha-k-s}}{s-\alpha+k}. \tag{T6}$$

The remainder integral is holomorphic for $\Re s > \alpha - K - 1$. The integral on any compact interval away from zero is entire. At zero, $G_{N,a}$ is analytic since $H_N(a) > 0$; subtracting any finite Taylor polynomial there extends the other side, with apparent poles only at positive integers. Such Taylor poles cancel against $\sin(\pi s)$, just as in Section D.5. Choosing arbitrarily large subtractions at both ends covers every $s \in \mathbb{C}$. The resulting continuations agree on overlaps because all added terms are exactly the integrals of the terms removed.

For $a > 0$, the complete pole set is consequently

$$\boxed{s = \frac{1}{N} - k, \quad k = 0, 1, 2, \ldots,}$$

and every pole is simple. Its residue is

$$\begin{aligned} \operatorname{Res}_{s=\alpha-k} \mathcal{Z}_N(s;a) &= \frac{\alpha \sin(\pi(\alpha-k))}{\pi} \binom{\alpha-1}{k} a^k \\ &= \boxed{\frac{\sin(\pi/N)}{N\pi} \frac{(1-1/N)_k}{k!} a^k.} \end{aligned} \tag{T7}$$

Here $(b)_0 = 1$ and $(b)_k = b(b+1)\cdots(b+k-1)$. The sign calculation uses both $\sin(\pi(\alpha-k)) = (-1)^k \sin(\pi\alpha)$ and $\binom{\alpha-1}{k} = (-1)^k(1-\alpha)_k/k!$; their signs cancel. All residues are positive when $a > 0$. At $a = 0$, the secondary coefficients vanish, so the only remaining pole is the unshifted pole at $1/N$. As before, its nonzero residue makes the absolute convergence abscissa exactly $1/N$.

None of the pole locations $\alpha - k$ is an integer. Thus the sine factor vanishes at every nonpositive integer without an opposing pole:

$$\boxed{\mathcal{Z}_N(-m;a) = 0 \quad (m \geq 0).} \tag{T8}$$

Finally, the one-term subtraction is already convergent at $s = 0$, since $G_{N,a}(t) - \alpha t^{\alpha-1} = O(t^{\alpha-2})$ and $\alpha < 1$. Let

$$B_{N,a}(0) = \int_0^1 G_{N,a}(t)dt + \int_1^\infty [G_{N,a}(t) - \alpha t^{\alpha-1}]dt - 1.$$

Integrating exactly and using $\log H_N(a+t) - t^\alpha \to -\log N$ gives

$$B_{N,a}(0) = -\log N - \log H_N(a).$$

The multiplier $\sin(\pi s)/\pi$ then gives

$$\boxed{\mathcal{Z}'_N(0;a) = -\log[NE_{N,1}(a)], \qquad \exp[-\mathcal{Z}'_N(0;a)] = NE_{N,1}(a).} \tag{T9}$$

For $N = 2$, the product reduces to $2\cosh\sqrt{a}$. Four direct quadrature checks at $a = 0, 1/4, 2, 9$ agree with $-\log(2\cosh\sqrt{a})$ at 80-digit working precision. They use a local integral, an exactly integrated algebraic leading tail, and an exponentially decaying remainder; the quadrature does not sample numerical zero locations. These are four additional numerical benchmarks, with the original 411 exact assertions unchanged. Results are in `evidence/spectral_continuation_checks.json` under `shifted_N2_product_benchmarks`.

This is a classical Hurwitz-type spectral deformation, with a packet-specific explicit regularized determinant. It is useful because a single shift reveals an entire pole ladder that collapses at the unshifted boundary. No historical-priority claim is made for the deformation or determinant identity.

D.9 Source comparison and bounded search

The continuation proof uses the finite-order Hadamard product and the beta and reflection identities. DLMF [4, §§5.5, 5.12 and 10.46] provides the special-function identities and identifies the seed as a Mittag–Leffler function. The finite-order factorization theorem is also summarized in Elkies's notes [6]. The normalization, zero counts, complex branch gap and domination estimates needed here were proved in Sections D.2–D.5.

Mellin subtraction and spectral regularization are established methods. Voros [8, §§2.1–2.2], with its published erratum [9], provides a related framework. The present proof checks the hypotheses for this Mittag–Leffler seed directly and does not import a theorem about Riemann zeros. The coefficient approach also has antecedents in the hypergeometric zero spectra of Byrnes, Jiu, Moll and Vignat [7].

This comparison establishes methodological context, not priority for the particular specialization. The archived research notes preserve the broader search record. A complete historical review of Mittag–Leffler and hyper-Bessel zero-zeta functions remains outside the scope of this volume.

D.10 Scope and remaining questions

The local proof establishes global continuation for the unweighted orbit family and its nonnegative real shifts. A functional equation is not supplied or presumed. The only-pole theorem concerns the

unshifted case; positive shifts have the full pole ladder in (T7). The pole and trace-zero theorems follow from the exact positive-axis exponential asymptotic, and do not imply an RH-type critical-line property. Residue-weighted sums still require separate multiplicity and convergence analysis. A historical comparison against all Mittag-Leffler and hyper-Bessel zero-zeta literature remains open.

The evidence archive distinguishes exact identities, numerical checks and previously corrected implementation failures. None of the open questions listed above is assumed in the continuation proof.

APPENDIX E

Exact sequence, polyphase and tap laboratory

This chapter connects the nonlinear family to exact sequences and finite filter algebra. Its reusable code implements finite calculations. The analytic results are proved in Chapter 1 and Appendix A. All mathematical sequence indices begin at zero. All finite arrays are zero extended beyond their displayed support. The catalog contains explicit candidates for OEIS lookup. This chapter does not assert an OEIS accession or historical priority for an unsearched row.

E.1 The integer polynomial object

Write the unique odd formal solution as

$$T_{q,r}(z) = \sum_{n\geq 0} c_n(q,r) z^{2n+1} = \sum_{n\geq 0} A_n(q,r) \frac{z^{2n+1}}{(2n+1)!}.$$

The two coefficient systems are related by $A_n = (2n+1)!c_n$. In particular, A_n is the derivative of order $2n+1$ at zero. The coefficient c_n, the derivative A_n, and the full EGF sequence a_m with $a_{2n+1} = A_n, a_{2n} = 0$ are different objects. None of the code silently substitutes one for another.

The nonlinear differential equation gives the recurrence

$$\boxed{A_0 = 1, \qquad A_n = \sum_{i=0}^{n-1} \binom{2n}{2i+1} q^{2i+1} r^{2(n-1-i)+1} A_i A_{n-1-i}, \quad n \geq 1.}$$

Proof. Multiply the ordinary Taylor recurrence by $(2n+1)!$. The factor attached to $A_i A_j$, where $i + j = n-1$, is $(2n)!/[(2i+1)!(2j+1)!] = \binom{2n}{2i+1}$. This also proves the recurrence directly in the EGF convention. □

Polynomial theorem. For every n, $A_n \in \mathbb{Z}[q,r]$, all its nonzero coefficients are positive integers, and $A_n(q,r) = A_n(r,q)$. Every monomial $q^u r^v$ satisfies

$$u, v \geq n, \qquad u \equiv v \equiv n \pmod 2, \qquad u + v \leq n(n+1).$$

Proof. The recurrence is an induction using positive integer binomial coefficients. Swapping q, r and replacing i by $n-1-i$ leaves the sum unchanged. If child indices are i, j, their exponent pairs receive the shifts $(2i+1, 2j+1)$. The lower bounds follow from $i + j + 1 = n$. The two parities are the parity of $i + j + 1$, also n. For the degree bound, a recurrence term has total degree at most

$$2n + i(i+1) + j(j+1) \leq n(n+1), \qquad i + j = n - 1,$$

since $i(i+1) + j(j+1)$ is largest at $(i,j) = (0, n-1)$ or its swap. The base $A_0 = 1$ satisfies every assertion. □

The first four polynomials are

$$\begin{aligned} A_0 &= 1, \\ A_1 &= 2qr, \\ A_2 &= 8q^2r^2(q^2 + r^2), \\ A_3 &= q^3r^3\left[48(q^2 + r^2)(q^4 + r^4) + 80q^2r^2\right]. \end{aligned}$$

Consequently each integer pair (q, r) gives an integer sequence for all n, independently of whether its formal Taylor series converges. For example, the first values of $A_n(1,2)$ are $1, 4, 160, 35200, 38041600$.

E.1.1 Rational feedback banks also admit integer sequences

For rational channel tuples (h_t, q_t, r_t), use

$$F'(z) = 1 + \sum_t h_t F(q_t z) F(r_t z), \qquad F(0) = 0.$$

The preceding recurrence is summed over channels with the factor h_t. In the universal polynomial over the weights and contractions, every term of A_n has weight degree exactly n and total contraction degree at most $n(n+1)$. The weight statement follows from one new weight at each recurrence step and $1 + i + j = n$; the contraction bound uses the same induction.

Let H be a common denominator for all channel weights, and D a common denominator for all channel contractions. Then

$$\boxed{B_n = H^n D^{n(n+1)} A_n \in \mathbb{Z} \quad \text{for all } n.}$$

This is a proved normalization, even with signed rational weights. It is usually not the smallest possible denominator clearing. The catalog records both A_n and B_n, and the exact multiplier, so that a proposed sequence lookup can state its normalization honestly.

E.2 A sharp distinction between sequences and analytic germs

The entire-function theorem uses $0 < q, r < 1$. Specializations with large positive integers produce valid formal and integer sequences but do not necessarily produce analytic functions near zero.

Zero-radius theorem. If $q > 0$ and $r > 1$, the formal series for $T_{q,r}$ has radius of convergence zero. The same holds after swapping the parameters.

Proof. Every coefficient is positive. In the ordinary recurrence keep only the term $i = 0$. This gives

$$c_n \geq \frac{qr^{2n-1}}{2n+1} c_{n-1} \quad \Longrightarrow \quad c_n \geq \frac{q^n r^{n^2}}{3 \cdot 5 \cdots (2n+1)}.$$

Since the denominator is at most $(2n+1)^n$,

$$c_n^{1/(2n+1)} \geq q^{n/(2n+1)} r^{n^2/(2n+1)} (2n+1)^{-n/(2n+1)} \longrightarrow \infty.$$

The Cauchy–Hadamard criterion therefore gives radius zero. □

More generally, a positive feedback bank with a channel satisfying $h > 0, q > 0, r > 1$ has the same obstruction, replacing q^n by $(hq)^n$. Positivity prevents cancellation. No conclusion of this form is asserted for a bank with signed weights.

Parameters or bank	First five A_n	Mathematical status
$(1, 1)$	1, 2, 16, 272, 7936	Known tangent derivatives
$(0, 1)$	1, 0, 0, 0, 0	Known linear boundary
$(1, -1)$	1, −2, 16, −272, 7936	Known hyperbolic tangent derivatives
$(1, 2)$	1, 4, 160, 35200, 38041600	Integer sequence, radius zero
$(1/2, 1/2)$	1, 1/2, 1/4, 1/8, 1/16	Known scaled hyperbolic sine
$(1/4, 3/4)$	1, 3/8, 45/256, 21465/262144, 39833775/1073741824	Entire asymmetric family, order one

The complete catalog contains **18 rows**, each through $n = 12$: three classical or degenerate integer anchors, eight positive integer formal specializations, four rational contractions, one entire edge case of infinite order, and two normalized feedback banks. Integer integrality and rational clearing are established by the preceding proofs, not merely inferred from the finite sample.

E.2.1 The uncontracted boundary is entire of infinite order

Boundary theorem. For $0 < q < 1$, the normalized formal solution of

$$T'(z) = 1 + T(qz)T(z), \qquad T(0) = 0$$

extends to an entire function of infinite order. The swapped boundary has the same property.

Proof of entire extension. The tangent-coefficient majorant gives an initial holomorphic germ. Suppose T is known on $|z| < R$. The function $T(qz)$ is known on $|z| < R/q$. On this larger disk solve the linear ODE $U' = 1 + T(qz)U$, $U(0) = 0$. Explicitly,

$$U(z) = e^{B(z)} \int_0^z e^{-B(w)}\, dw, \qquad B(z) = \int_0^z T(qw)\, dw.$$

The integrals are path independent on the disk. Linear-ODE uniqueness shows $U = T$ on the previous disk, and there $T(qz)$ equals the newly extended function at qz. Thus the same nonlinear equation holds on the enlarged disk. Iterating $R \mapsto R/q$ exhausts the plane.

Proof of infinite order. Positive coefficients imply $T(x) \geq x$ for $x > 0$ and $M(x) = T(x)$. The logarithmic derivative obeys

$$\frac{d}{dx} \log T(x) = \frac{1}{T(x)} + T(qx) \geq qx.$$

Integrating from one, with $T(1) \geq 1$, gives $T(x) \geq \exp(q(x^2 - 1)/2)$ for $x \geq 1$. For $R \geq 2/q$, integrate the same logarithmic derivative over $[R/2, R]$. Since $T(R/2) \geq 1$,

$$\boxed{\log M(R) \geq \frac{R}{2} \exp\left(\frac{q^3 R^2}{8} - \frac{q}{2}\right).}$$

Therefore $\log \log M(R) / \log R \to \infty$, which proves infinite order. □

For nonnegative parameters this gives a complete analytic/formal phase chart:

Parameter region	Normalized solution
$0 < q, r < 1$	Entire, finite order defined by $q^\rho + r^\rho = 1$
One parameter equals one, the other lies in $(0, 1)$	Entire, infinite order
$q = r = 1$	Tangent, meromorphic with its usual poles
$q > 0, r > 0, \max(q, r) > 1$	Formal solution with radius zero
One parameter equals zero	Linear solution z, regardless of the other scale

The finite-order formula applies in the open contraction square. It does not assign a finite order to the edge, where its defining scale equation has no positive root.

E.3 Exact root-filter sections

For an EGF $G(z) = \sum_{m\ge 0} a_m z^m/m!$, an integer base $b \ge 1$, a residue $0 \le j < b$, and $\omega = e^{2\pi i/b}$, define

$$\boxed{\mathcal{P}_{b,j}G(z) = \frac{1}{b}\sum_{k=0}^{b-1}\omega^{-jk}G(\omega^k z) = \sum_{m\equiv j\,(b)} a_m\frac{z^m}{m!}.}$$

This holds as a formal series and wherever the original series converges. Indeed the coefficient multiplier is the geometric sum $b^{-1}\sum_{k=0}^{b-1}\omega^{k(m-j)}$, equal to one or zero according to the residue. It proves all the projector identities

$$\sum_{j=0}^{b-1}\mathcal{P}_{b,j} = I, \qquad \mathcal{P}_{b,j}\mathcal{P}_{b,l} = \delta_{jl}\mathcal{P}_{b,j}.$$

The full-position section and the decimated lane are distinct arrays. A section keeps the original positions, inserting zeros outside the residue. A lane $x_j[n] = a_{bn+j}$ changes the index to n.

For an **ordinary** generating function $X(z) = \sum_m a_m z^m$, define $X_j(w) = \sum_n a_{bn+j}w^n$. Then

$$X(z) = \sum_{j=0}^{b-1} z^j X_j(z^b).$$

For an EGF the corresponding exact reconstruction is

$$G(z) = \sum_{j=0}^{b-1} z^j \sum_{n\ge 0}\frac{a_{bn+j}}{(bn+j)!}(z^b)^n.$$

One must retain $(bn+j)!$. Replacing it by $n!$ gives a different function. The root-filter section identity has no such factorial ambiguity.

E.4 Ordinary taps, EGF multiplication and differentiation

Let $h_0, \dots, h_{L-1}$ be a finite tap vector and let $a_m = 0$ for $m < 0$. Ordinary taps form

$$b_m = \sum_{t=0}^{L-1} h_t a_{m-t}.$$

For OGFs this is multiplication by $H(z) = \sum_t h_t z^t$: $B(z) = H(z)X(z)$. For EGFs it is a sum of repeated zero-constant antiderivatives:

$$\boxed{B_{\mathrm{EGF}}(z) = \sum_{t=0}^{L-1} h_t I^t G(z), \qquad IG(z) = \int_0^z G(w)\,dw.}$$

Proof. The EGF of the delayed sequence is $\sum_{m\geq t} a_{m-t}z^m/m! = I^t G(z)$. Summing taps gives the formula. Conversely, $G^{(t)}$ has coefficient sequence a_{m+t}, so derivatives sample future coefficients and do not implement these past delays. □

For two EGFs G_a, G_h, ordinary function multiplication instead gives the **Hurwitz product**

$$G_a(z)G_h(z) = \sum_m \left[\sum_{t=0}^{m} \binom{m}{t} h_t a_{m-t}\right] \frac{z^m}{m!}.$$

This is a binomial convolution. For example, with $a_m = 1$ and taps $h = (1,1)$, ordinary taps give $b_2 = 2$, while the Hurwitz product gives $b_2 = 3$. This explicit negative control catches a common normalization error.

Intrinsic nonlinear feedback taps are the parameters (h_t, q_t, r_t) inside $F' = 1 + \sum_t h_t F(q_t z)F(r_t z)$. They change the function's defining equation and its derivative recurrence. Ordinary FIR taps are a linear transformation of an already defined coefficient sequence. Both are useful, but they operate on different objects. The intrinsic-bank growth theorem is proved in Appendix A.

E.5 The exact finite polyphase tap matrix

For an OGF sequence a_m, define lanes $x_l[n] = a_{bn+l}$ and $X_l(w) = \sum_n x_l[n]w^n$. Apply finite ordinary taps and obtain $y_j[n] = b_{bn+j}$. Then the exact matrix identity is

$$\boxed{Y_j(w) = \sum_{l=0}^{b-1} H_{jl}(w)X_l(w), \qquad H_{jl}(w) = \sum_{\substack{0\leq t<L \\ t+l\equiv j\,(b)}} h_t w^{(t+l-j)/b}.}$$

Every exponent is a nonnegative integer. It records the carry across phase boundaries, rather than erasing it.

Proof. A term $h_t a_{bn+j-t}$ is in phase l exactly when $t + l \equiv j \pmod b$. Write $d = (t + l - j)/b$. That term is $h_t x_l[n - d]$, whose OGF is $h_t w^d X_l(w)$ by zero extension. Summing over taps and phases gives the matrix. □

For two phases and two taps,

$$\begin{pmatrix} Y_0 \\ Y_1 \end{pmatrix} = \begin{pmatrix} h_0 & h_1 w \\ h_1 & h_0 \end{pmatrix} \begin{pmatrix} X_0 \\ X_1 \end{pmatrix}.$$

The upper-right factor w is necessary: a delay from odd phase to even phase crosses one block. A diagonal-only phase operation cannot implement this filter. The code constructs the sparse matrix for any finite base and tap vector and checks that recombination gives the full direct convolution.

E.6 Reuse and evidence

From the package's `research/` directory, standard Python is enough:

```
python family_lab.py coefficients --q 1/4 --r 3/4 --n 8
python family_lab.py catalog --n 12 --output-dir examples
python checks/family_lab_checks.py
```

The reusable functions include `asymmetric_odd_derivatives`, `feedback_odd_derivatives`, `asymmetric_polynomials`, `section`, `phase_lanes`, `merge_lanes`, `ordinary_taps`, `hurwitz_product`, `derivative_shift`, `integral_shift`, `polyphase_tap_matrix`, and `apply_polyphase_matrix`. All core arithmetic is `fractions.Fraction` or integer arithmetic. The phase and tap API applies to any finite rational sequence, not just the special-function catalog.

The final completed run passed **8,038 exact assertions** and is recorded in `evidence/family_lab_checks.json`. Its scope includes:

- 18 catalog rows through A_{12}, independently compared with dense formal Picard iteration through degree 25.
- Bivariate polynomials through A_8, with 540 nonzero monomials checked for integer positivity, symmetry, parity and the degree bound.
- Tangent coefficients independently obtained by division of sine and cosine, plus hyperbolic tangent, scaled hyperbolic sine and linear anchors.
- Root-filter multipliers reduced exactly in cyclotomic fields for bases one through seven and indices zero through 31.
- Direct FIR convolution compared with phase-matrix convolution for 26 input lengths, seven bases and four tap vectors, including signed rational taps.
- The antiderivative interpretation of EGF taps and the factorial conversion of Hurwitz products, independently compared with ordinary Taylor products.
- Negative controls for omitted phase carries, aliasing lanes by concatenation, silent truncation, derivative/delay confusion and Hurwitz/FIR confusion.

The bounded checks validate the implemented paths in the recorded ranges. The universal polynomial, degree, clearing, root-filter and phase-matrix statements follow from the proofs above. Entire continuation and growth order require the analytic proofs, not these finite checks. Historical identification of a catalog row requires a separate literature comparison.

`evidence/family_lab_checks.json` records software version, code hashes, exact arithmetic, bounds, category counts and run time. It reports no failed assertion in this run. Independent audit identified two API input-validation defects: a fractional residue was accepted by the section operator, and an empty phase matrix accepted base zero. Both are now rejected and have passing regression checks. These defects affected invalid inputs, not the displayed identities. A draft prose example initially transcribed $A_3(1,2)$ and $A_4(1,2)$ incorrectly; the exact catalog comparison exposed the mismatch and corrected them to 35200 and 38041600. The code result did not change. Larger numerical evidence is unnecessary for these algebraic identities; an independent mathematical audit should examine the reductions.

APPENDIX F

Coupled contraction functions and their Perron growth law

F.1 Definition and exact coefficient construction

Fix real parameters

$$0 < q, r, a, b < 1.$$

Consider the normalized pair

$$\boxed{\begin{aligned} U'(z) &= 1 + U(qz)V(rz), \\ V'(z) &= 1 + U(az)V(bz), \\ U(0) &= V(0) = 0. \end{aligned}}$$

Theorem F.1. There is a unique pair of entire solutions. Both functions are odd and have strictly positive coefficients at every odd degree. Write

$$U(z) = \sum_{n\geq 0} u_n z^{2n+1}, \qquad V(z) = \sum_{n\geq 0} v_n z^{2n+1}.$$

Then $u_0 = v_0 = 1$, and, for $n \geq 1$,

$$u_n = \frac{1}{2n+1} \sum_{i=0}^{n-1} q^{2i+1} r^{2(n-1-i)+1} u_i v_{n-1-i},$$
$$v_n = \frac{1}{2n+1} \sum_{i=0}^{n-1} a^{2i+1} b^{2(n-1-i)+1} u_i v_{n-1-i}.$$

Proof. Comparing successive coefficients in the differential equations determines the coefficient of degree $k+1$ from coefficients of degrees at most k. Thus the formal pair is unique. The displayed

recurrence constructs an odd formal pair satisfying both equations. Formal uniqueness excludes any additional even coefficients. Strict positivity follows by induction.

The elementary bounds

$$0 < u_n \le 2^{-n}, \qquad 0 < v_n \le 2^{-n}$$

hold by simultaneous induction. If they hold below n, each product in either recurrence is at most $2^{-(n-1)}$, and there are n products. The resulting bound is $n2^{-(n-1)}/(2n+1) < 2^{-n}$. Hence the two series converge on $|z| < \sqrt{2}$, and define a holomorphic solution there.

Put $Q = \max(q, r, a, b) < 1$. If the pair is already defined on $|z| < R$, then

$$\int_0^z [1 + U(qw)V(rw)]\,dw, \qquad \int_0^z [1 + U(aw)V(bw)]\,dw$$

define holomorphic extensions on $|z| < R/Q$. The integrands are holomorphic on that disk. On the old disk the new functions agree with the old pair because their derivatives and values at zero agree. On the larger disk, every contracted argument still lies in the old disk, so the extensions satisfy the same equations. Iterating exhausts the complex plane. Any other entire solution agrees with the unique germ and therefore everywhere. □

In particular,

$$U(z) = z + \frac{qr}{3}z^3 + \frac{qr(qr\,q^2 + ab\,r^2)}{15}z^5 + O(z^7),$$
$$V(z) = z + \frac{ab}{3}z^3 + \frac{ab(qr\,a^2 + ab\,b^2)}{15}z^5 + O(z^7).$$

The factorial coefficients $A_n = (2n+1)!u_n$ and $B_n = (2n+1)!v_n$ satisfy

$$A_n = \sum_{i=0}^{n-1} \binom{2n}{2i+1} q^{2i+1} r^{2(n-1-i)+1} A_i B_{n-1-i},$$
$$B_n = \sum_{i=0}^{n-1} \binom{2n}{2i+1} a^{2i+1} b^{2(n-1-i)+1} A_i B_{n-1-i}.$$

Thus A_n, B_n are polynomials with nonnegative integer coefficients in the four scales. These formulas are exact algebraic constructions. Finite checks of them do not replace the analytic proof.

F.2 The characteristic exponent and its positive vector

For $s > 0$, let

$$P(s) = \begin{pmatrix} q^s & r^s \\ a^s & b^s \end{pmatrix}.$$

There is a unique $\rho > 0$ with

$$\boxed{(1-q^\rho)(1-b^\rho) = (ar)^\rho.}$$

Indeed, the left side strictly increases continuously from zero to one, while the right side strictly decreases continuously from one to zero. This equation is precisely $\det(I - P(\rho)) = 0$. Define

$$\widetilde{w} = (r^\rho, 1-q^\rho)^T, \qquad w = \frac{\widetilde{w}}{\max(r^\rho, 1-q^\rho)}.$$

Both coordinates of w are positive, $\max(w_1, w_2) = 1$, and direct multiplication gives

$$P(\rho)w = w.$$

The other eigenvalue is $q^\rho + b^\rho - 1$, whose absolute value is strictly less than one. Consequently

$$\boxed{\operatorname{spr} P(\rho) = 1.}$$

Conversely, a positive matrix of this form having spectral radius one has eigenvalue one and satisfies the determinant equation. This proves the proposed spectral characterization without requiring a numerical eigensolver. A positive left eigenvector is

$$\ell = (a^\rho, 1-q^\rho)^T, \qquad \ell^T P(\rho) = \ell^T.$$

The notation w for the growth vector is deliberately different from v_n, the coefficients of V.

F.3 Exact order and explicit positive type bounds

For $R > 0$, positivity gives

$$M_U(R) = \max_{|z|=R} |U(z)| = U(R), \qquad M_V(R) = V(R).$$

Set $F_1 = U$, $F_2 = V$, and $H_i(R) = \log F_i(R)$. Since $F_i(R) \geq R$, these logarithms are positive for $R > 1$. The type convention used here is

$$\underline{\tau}_i = \liminf_{R\to\infty} \frac{\log M_{F_i}(R)}{R^\rho}, \qquad \overline{\tau}_i = \limsup_{R\to\infty} \frac{\log M_{F_i}(R)}{R^\rho}.$$

Theorem F.2. Both functions have order ρ, positive lower type and finite upper type. More precisely, the explicit constants below satisfy

$$0 < c_- w_i \leq \underline{\tau}_i \leq \overline{\tau}_i \leq c_+ w_i < \infty, \qquad i = 1, 2.$$

Moreover,

$$\lim_{R\to\infty} \frac{\log\log M_{F_i}(R)}{\log R} = \rho.$$

This radial exponent limit is stronger than the limsup used to define order. It does not assert that either type has a limit or that growth is uniform in the angular variable.

F.3.1 Explicit lower comparison

Let

$$m = \min(q, r, a, b), \qquad Q = \max(q, r, a, b),$$

$$C = \frac{Q}{1-Q}, \qquad B = 1 + \frac{2}{m}, \qquad c_- = \frac{\log 2}{(B+C)^\rho}.$$

We prove the stronger statement

$$\boxed{H_i(R) \geq c_- w_i (R+C)^\rho \quad (R \geq 2,\ i = 1, 2).}$$

On $2 \leq R \leq B$, its right side is at most $\log 2$, because $w_i \leq 1$, whereas $H_i(R) \geq \log R \geq \log 2$.

For the first equation, integrate only over the final unit interval to obtain, when $R \geq B$,

$$U(R) \geq \int_{R-1}^{R} U(qt)V(rt)\,dt \geq U(q(R-1))V(r(R-1)).$$

The second equation gives the same inequality with (q, r) replaced by (a, b) and $U(R)$ replaced by $V(R)$. All four child radii are at least two. Every scale $p \in \{q, r, a, b\}$ satisfies

$$p(R-1) + C \geq p(R+C),$$

because $(1-p)C \geq p$. If the comparison already holds at the child radii, then

$$\begin{aligned} H_1(R) &\geq c_-\{w_1[q(R-1)+C]^\rho + w_2[r(R-1)+C]^\rho\} \\ &\geq c_-(q^\rho w_1 + r^\rho w_2)(R+C)^\rho = c_- w_1 (R+C)^\rho. \end{aligned}$$

The second row of $P(\rho)w = w$ proves the second component in exactly the same way.

For a formal propagation, put

$$d = (1-Q)B + Q > 0.$$

Every child of $R \geq B$ is at most $Q(R-1) \leq R - d$. Simultaneous induction over the intervals $[B + kd, B + (k+1)d]$, starting with the established seed interval, therefore proves both comparisons for

every $R \geq 2$. Continuity handles shared endpoints. The argument uses only monotonicity of positive powers and works unchanged when $0 < \rho < 1$.

F.3.2 Explicit upper comparison

Set

$$\Delta = \log(1/m), \qquad D = \max\left(\log\frac{1}{qr}, \log\frac{1}{ab}\right) + \log 2.$$

Choose any integer $N \geq 0$ satisfying $Q^{-N} \geq 3/m$, and define

$$W_N = (2^{N+1} - 1)\log 2 + (2^{N+1} - N - 2)\log(1/Q),$$

$$S = W_N + 1 + \Delta + D, \qquad c_+ = \frac{e^{-\rho}S}{\min(w_1, w_2)}.$$

These constants require only the parameters and the uniquely defined root ρ. They require no evaluation of an unknown solution.

To bound a seed interval, the coefficient majorant from Theorem F.1 gives $F_i(1) \leq 2$. Put $R_k = Q^{-k}$, $Z_0 = 2$, and

$$Z_k = Q^{-k}(1 + Z_{k-1}^2).$$

Monotonicity of the positive functions and the integral equations give $F_i(R_k) \leq Z_k$ simultaneously. As $Z_k \geq 1$,

$$\log Z_k \leq k\log(1/Q) + \log 2 + 2\log Z_{k-1}.$$

Summing this elementary recurrence gives $\log Z_N \leq W_N$. Therefore $H_i(e^t) \leq W_N$ throughout $1 \leq t \leq 1 + \Delta$, since $e^t \leq e/m < 3/m \leq R_N$.

Now let

$$G_i(t) = H_i(e^t) + t + D.$$

For $t \geq 1 + \Delta$, all child radii are at least e, so their function values are at least one. The full integral gives

$$H_1(e^t) \leq t + \log 2 + H_1(e^{t-\log(1/q)}) + H_2(e^{t-\log(1/r)}).$$

The definition of D converts this into

$$G_1(t) \leq G_1(t - \log(1/q)) + G_2(t - \log(1/r)).$$

Similarly,

$$G_2(t) \le G_1(t - \log(1/a)) + G_2(t - \log(1/b)).$$

On the seed interval, $G_i(t) \le S \le c_+ w_i e^{\rho t}$. The Perron equation propagates this comparison: substituting the bounds at the children in the first inequality gives $c_+ e^{\rho t}(q^\rho w_1 + r^\rho w_2) = c_+ w_1 e^{\rho t}$, and the second row works likewise. All logarithmic delays belong to $[\log(1/Q), \Delta]$. Induction in intervals of length $\log(1/Q) > 0$, after the seed interval, therefore proves

$$\boxed{H_i(R) \le c_+ w_i R^\rho - \log R - D \quad (R \ge e).}$$

The lower and upper comparisons imply the asserted positive, finite types. Taking logarithms of these bounds for sufficiently large R gives the claimed radial exponent limits and hence exact orders. □

F.4 The two type vectors have exactly the Perron proportions

The explicit constants above are conservative. There is nevertheless an exact statement about the relative types of the two components.

Theorem F.3. There exist positive finite constants $\underline{\tau} \le \overline{\tau}$ such that

$$\boxed{\begin{aligned}(\underline{\tau}_1, \underline{\tau}_2)^T &= \underline{\tau}\, w,\\ (\overline{\tau}_1, \overline{\tau}_2)^T &= \overline{\tau}\, w.\end{aligned}}$$

In particular,

$$\frac{\underline{\tau}_1}{\underline{\tau}_2} = \frac{\overline{\tau}_1}{\overline{\tau}_2} = \frac{r^\rho}{1 - q^\rho} = \frac{1 - b^\rho}{a^\rho}.$$

Either both ordinary type limits exist or neither does. When they exist, their vector is a positive multiple of w.

Proof. Use the final-unit integral inequality from the lower proof and divide by R^ρ. Taking the liminf gives

$$\underline{t} \ge P(\rho)\underline{t}, \qquad \underline{t} = (\underline{\tau}_1, \underline{\tau}_2)^T.$$

Here $p(R-1)$ tends to infinity continuously and $[p(R-1)]^\rho / R^\rho \to p^\rho$, which justifies each scaled liminf. The liminf of a sum is at least the sum of the liminfs. All quantities are positive and finite by Theorem F.2.

The full-integral inequality

$$H_1(R) \le \log R + \log 2 + H_1(qR) + H_2(rR)$$

and its second-row counterpart imply, on taking the limsup,

$$\bar{t} \le P(\rho)\bar{t}.$$

The terms $(\log R + \log 2)/R^\rho$ vanish. Dotting either componentwise inequality with the strictly positive left eigenvector ℓ from Section F.2 shows that its nonnegative difference vector has zero positive weighted sum. Every coordinate of that difference is therefore zero. Thus both type vectors are fixed by $P(\rho)$. Its eigenvalue-one space is one dimensional, so each is a positive multiple of w.

If one component has an ordinary type limit, its lower and upper types are equal. Because that coordinate of w is positive, this forces $\underline{\tau} = \overline{\tau}$, and the other component also has a type limit. □

This theorem does not assert a limit for $\log U(R)/\log V(R)$ when type oscillations persist. It also does not identify the scalar values of either type or prove their equality.

F.5 Reductions, a worked unequal pair, and parameter structure

Exact scalar reduction. The components coincide if and only if the unordered pairs of scales coincide:

$$U = V \quad \Longleftrightarrow \quad \{q, r\} = \{a, b\}.$$

For sufficiency, the scalar solution $T_{q,r}$ from `routes/asymmetric_dilation.md` makes $(T_{q,r}, T_{q,r})$ solve the coupled equations. Theorem F.1 gives uniqueness. For necessity, equality at degree three gives $qr = ab = p > 0$. Equality at degree five then gives $q^2 + r^2 = a^2 + b^2$. The two positive unordered pairs have the same product and the same sum $\sqrt{q^2 + r^2 + 2p}$, so they coincide. This characterizes equality of the normalized components. A stronger assertion about all possible changes of variables requires its own nonreduction theorem.

On either scalar reduction locus, the characteristic equation is equivalent to $q^\rho + r^\rho = 1$, recovering the scalar order theorem. At $q = r = a = b = 1/2$,

$$U(z) = V(z) = \sqrt{2}\sinh(z/\sqrt{2}), \qquad \rho = 1.$$

A genuinely unequal order-one pair. Set

$$(q, r, a, b) = \left(\frac{1}{5}, \frac{2}{5}, \frac{3}{5}, \frac{7}{10}\right).$$

The determinant identity at $\rho = 1$ is $(1 - 1/5)(1 - 7/10) = (3/5)(2/5) = 6/25$. Thus the exact order is one, and

$$w = (1/2, 1)^T.$$

The first terms are

$$U(z) = z + \frac{2}{75}z^3 + \frac{88}{234375}z^5 + \frac{18814}{8544921875}z^7 + O(z^9),$$
$$V(z) = z + \frac{7}{50}z^3 + \frac{8211}{1250000}z^5 + \frac{85664601}{625000000000}z^7 + O(z^9).$$

Both lower and upper exponential types of V are exactly twice the corresponding types of U. The row sums of $P(1)$ are $3/5$ and $13/10$. Consequently neither an unweighted average row condition nor the maximum of the two scalar row orders yields this example's coupled order. The positive eigenvector accounts for the exchange of growth between the components.

For this example the elementary lower constants are $m = 1/5$, $Q = 7/10$, $C = 7/3$, $B = 11$, and $c_- = 3\log 2/40$. Hence, for every $R \geq 2$,

$$\log U(R) \geq \frac{3\log 2}{80}\left(R + \frac{7}{3}\right), \qquad \log V(R) \geq \frac{3\log 2}{40}\left(R + \frac{7}{3}\right).$$

Dependence of the order on the scales. The determinant equation shows that the order depends on the self scales q, b and the product ar of the two cross scales. Changing a and r while keeping their product fixed leaves the order fixed, provided both remain in $(0, 1)$. The Perron vector and the normalized functions generally change.

For any prescribed $s > 0$ and any $q, r \in (0, 1)$, choices satisfying

$$a^s r^s = (1 - q^s)(1 - b^s), \qquad 0 < a, b < 1,$$

lie on the order-s surface. For instance, one may select q, r, b with $(1 - q^s)(1 - b^s) < r^s$, then define

$$a = \frac{[(1 - q^s)(1 - b^s)]^{1/s}}{r}.$$

This constructs exact order surfaces without fitting growth from truncated series.

APPENDIX G

When the pair reduces, and when its parameters are intrinsic

Throughout, $q, r, a, b \in (0, 1)$. Let the normalized coupled solution be

$$U' = 1 + U(qz)V(rz), \qquad V' = 1 + U(az)V(bz), \qquad U(0) = V(0) = 0.$$

Write $U(z) = z + u_1 z^3 + u_2 z^5 + u_3 z^7 + \cdots$ and $V(z) = z + v_1 z^3 + v_2 z^5 + v_3 z^7 + \cdots$. Put $p = qr, k = ab$. Coefficient matching gives

$$\begin{aligned} u_1 &= \frac{p}{3}, & v_1 &= \frac{k}{3}, \\ u_2 &= \frac{p}{15}(pq^2 + kr^2), & v_2 &= \frac{k}{15}(pa^2 + kb^2), \\ u_3 &= \frac{p}{7}(q^4 u_2 + p^2 u_1 v_1 + r^4 v_2), & v_3 &= \frac{k}{7}(a^4 u_2 + k^2 u_1 v_1 + b^4 v_2). \end{aligned}$$

Define the fifth-order separation quantity

$$\boxed{D = k^2 u_2 - p^2 v_2 = \frac{pkar}{15}(q^2 - b^2)(qb - ar).}$$

This factorization will distinguish equality of normalized functions up to amplitude and argument rescaling from a change of coordinates in their defining functional differential operator. These are different equivalence relations.

G.1 Exact classification of component rescaling

Theorem G.1. The following statements are equivalent:

1. There are nonzero complex constants A, B such that $V(z) = AU(Bz)$ for every complex z.
2. $D = 0$.
3. $q = b$ or $qb = ar$.

If these conditions hold, put $s = \sqrt{k/p} > 0$, and let $T_{x,y}$ denote the normalized scalar solution $T' = 1 + T(xz)T(yz)$, $T(0) = 0$. Then

$$\boxed{U(z) = \sqrt{s}\, T_{q,sr}(z/\sqrt{s}), \qquad V(z) = s^{-1/2} T_{q,sr}(\sqrt{s}\, z).}$$

The effective scales belong to $(0, 1)$: if $q = b$, then $sr = \sqrt{ar}$, and if $qb = ar$, then $s = b/r$ and $sr = b$.

Proof. Normalization gives $AB = 1$. Comparing cubic coefficients gives $B^2 = k/p$, and comparing fifth coefficients gives $v_2 = (k/p)^2 u_2$. Thus component rescaling implies $D = 0$, even when complex rescalings are allowed. The displayed factorization, strict positivity, and $q, b > 0$ show that $D = 0$ is equivalent to $q = b$ or $qb = ar$.

For the converse define the displayed pair using $T = T_{q,sr}$. Direct differentiation gives

$$U'(z) = 1 + T(qz/\sqrt{s})T(r\sqrt{s}\, z) = 1 + U(qz)V(rz).$$

The second equation reduces to equality of the unordered pairs of arguments

$$\{q\sqrt{s},\ s^{3/2}r\} = \{a/\sqrt{s},\ b\sqrt{s}\}.$$

When $qb = ar$, one has $a = sq$ and $b = sr$, giving equality in the displayed order. When $q = b$, one has $a = s^2 r$, giving equality after interchanging the factors. The pair also has the required initial values and derivatives. Uniqueness of the formal coefficient recursion identifies it with the coupled solution. Finally, $V(z) = s^{-1}U(sz)$, proving rescaling.

The positive parameter domain therefore contains two explicit reduction surfaces. Outside them the two component functions cannot be obtained from one another by amplitude and argument rescaling. This statement does not exclude every representation using previously known functions.

G.2 Derivatives through order seven recover the scales

Theorem G.2. If $D \neq 0$, the six coefficients $(u_1, v_1, u_2, v_2, u_3, v_3)$ uniquely determine the ordered tuple (q, r, a, b) within $(0, 1)^4$. Consequently, equality of the two labeled normalized germs implies equality of these parameters in this regime.

Proof. First recover $p = 3u_1$, $k = 3v_1$. If $x = q^2$, then $r^2 = p^2/x$, and the equation for u_2 gives

$$px^2 - \frac{15u_2}{p}x + kp^2 = 0.$$

This leaves at most two positive candidates. If there are two distinct positive roots x, x', their product is $xx' = kp$. The corresponding seventh-coefficient values differ by

$$u_3(x) - u_3(x') = \frac{p}{7}(x^2 - x'^2)\left(u_2 - \frac{p^2}{k^2}v_2\right) = \frac{pD}{7k^2}(x^2 - x'^2).$$

The difference is nonzero because $D \neq 0$ and the distinct positive roots have distinct squares. Thus u_3 selects the unique root q^2, giving $q = \sqrt{x} > 0$ and $r = p/q$. A repeated quadratic root already gives a unique value and requires no selection.

Likewise $y = a^2$ obeys

$$py^2 - \frac{15v_2}{k}y + k^3 = 0,$$

with root product $yy' = k^3/p$. The two candidate seventh coefficients have difference

$$v_3(y) - v_3(y') = \frac{k}{7}(y^2 - y'^2)\left(u_2 - \frac{p^2}{k^2}v_2\right) = \frac{D}{7k}(y^2 - y'^2),$$

which is again nonzero for distinct positive candidates. Recover $a = \sqrt{y}$ and $b = k/a$. All selections must also respect the contraction domain. Since the supplied coefficients arise from an admissible pair, at least one admissible selection exists. The preceding differences give uniqueness.

This is an exact-data inverse theorem. The displayed differences become small as $D \to 0$, so the argument does not supply a uniform stable inverse near the reduction surfaces. It also does not identify unlabeled components without the additional component-permutation equivalence.

G.3 A worked pair with exact order one

Take

$$(q, r, a, b) = \left(\frac{1}{5}, \frac{2}{5}, \frac{3}{5}, \frac{7}{10}\right), \qquad p = \frac{2}{25}, \quad k = \frac{21}{50}.$$

At $\rho = 1$, the characteristic matrix has positive eigenvector $(1/2, 1)^T$ with eigenvalue one. Its other eigenvalue is $-1/10$. The growth theorem therefore gives exact order one for both components. Here $q \neq b$ and $qb \neq ar$, so $D \neq 0$. The pair is outside both reduction surfaces and its four labeled parameters are recoverable from the coefficients through degree seven.

APPENDIX H

Constant linear coordinates and coupled dilation

H.1 Exact meaning of decoupling

Let $q, r, a, b > 0$, with contraction < 1 imposed when discussing the normalized entire solution. For an arbitrary analytic vector input $X = (u, v)$ with $u(0) = v(0) = 0$, define the functional vector field

$$\mathcal{F}[X](z) = \begin{pmatrix} 1 + u(qz)v(rz) \\ 1 + u(az)v(bz) \end{pmatrix}. \tag{S1}$$

A nonzero constant row $c = (c_1, c_2) \in \mathbb{C}^2$ is an **autonomous scalar projection** if some scalar functional $\mathcal{H}$ satisfies

$$c\mathcal{F}[X] = \mathcal{H}[cX] \quad \text{for every such analytic input } X. \tag{S2}$$

The functional $\mathcal{H}$ may use the whole scalar input. Thus this definition allows any scalar dilation equation, not only a prescribed quadratic ansatz. Equality (S2) means that two vector inputs with the same scalar projection have the same projected vector field. It is an identity of functional differential operators. It does not assert an identity only along the distinguished normalized solution.

A constant invertible change $W = PX$ completely decouples the operator if both rows of P are autonomous scalar projections. No assumption about the form of their scalar functionals is needed.

H.2 Classification of autonomous linear projections

Theorem H.1. For positive nonzero scales, a nonzero row c satisfies (S2) if and only if

$$q = a, \qquad r = b, \qquad c = \gamma(1, -1), \qquad \gamma \neq 0. \tag{S3}$$

In that exceptional case the projected vector field is identically zero. Consequently, no invertible constant linear change completely decouples (S1), including when some or all scales coincide. If $(q, r) \neq (a, b)$, there is not even one nonzero autonomous scalar projection. Four pairwise distinct contraction scales are a special case of this stronger result.

Proof. Subtract the constant forcing. Define

$$Q_c[u, v](z) = c_1 u(qz)v(rz) + c_2 u(az)v(bz).$$

If (S2) holds, Q_c is constant on every fiber of $(u, v) \mapsto c_1 u + c_2 v$. Fix $z_0 \neq 0$. Polynomial interpolation gives a scalar polynomial f with $f(0) = 0$ and $f(sz_0) = 1$ at every distinct scale $s \in \{q, r, a, b\}$. For inputs $u = xf, v = yf$, where $x, y \in \mathbb{C}$,

$$Q_c[xf, yf](z_0) = (c_1 + c_2)xy. \tag{S4}$$

It must depend only on $c_1 x + c_2 y$. If $c_1 + c_2 \neq 0$, differentiating the polynomial xy along the fiber direction $(c_2, -c_1)$ would give

$$c_2 y - c_1 x = 0 \quad \text{for every } x, y,$$

which forces $c = 0$, a contradiction. Therefore $c_2 = -c_1$, and scaling the row reduces the question to $c = (1, -1)$.

For this row, put $u = w + g, v = g$. This input and $(w, 0)$ have the same projection w. The second input has $Q_c[w, 0] = 0$, so autonomy forces

$$w(qz)g(rz) - w(az)g(bz) + g(qz)g(rz) - g(az)g(bz) = 0 \tag{S5}$$

for all zero-constant analytic w, g. Setting $w = 0$ and subtracting that instance of (S5) leaves

$$w(qz)g(rz) = w(az)g(bz). \tag{S6}$$

Taking successively $(w, g) = (z, z), (z^2, z), (z, z^2)$ yields $qr = ab$, $q^2 r = a^2 b$, and $qr^2 = ab^2$. Nonzero scales then give $q = a$ and $r = b$. Conversely these equalities make the two components of (S1) identical on every input, so $(1, -1)\mathcal{F}[X] = 0$. The only possible autonomous rows therefore span a one-dimensional space, which cannot be the two rows of an invertible matrix. □

The same proof works on odd analytic inputs for positive scales: choose $f(z) = zp(z^2)$ by interpolation at the distinct positive scale squares, and use $(z, z), (z^3, z), (z, z^3)$ in (S6). Positivity then resolves the equalities of squares. The theorem does not depend on allowing even inputs.

H.3 Tensor explanation for four distinct scales

The preceding proof also makes a coordinate invariant obstruction explicit. Under an invertible state change, write the original coordinates as $u = \ell_1(W), v = \ell_2(W)$, where ℓ_1, ℓ_2 are independent linear forms. At the pair of distinct nodes (qz, rz), the first quadratic term has bilinear coefficient

$$B = \ell_1 \otimes \ell_2.$$

It has rank one, but is not symmetric: $B - B^{\mathsf{T}} = \ell_1 \wedge \ell_2 \neq 0$. At four distinct nonzero nodes, polynomial interpolation lets their vector values vary independently, so terms supported at (az, bz) cannot cancel this coefficient. A scalar autonomous channel at the same node pair would require $B = \kappa\ell \otimes \ell$, a symmetric rank-one tensor, after projecting the output onto that channel. For any output row with a nonzero coefficient on this term, the alternating part remains nonzero. The other node pair gives the same obstruction if the first output coefficient vanishes.

This is not a rank-only argument: the tensor $\ell_1 \otimes \ell_2$ already has rank one. Its nonzero alternating part is the decisive invariant at distinct nodes. When the nodes of a product coincide, the symmetric quadratic form uv has matrix

$$\begin{pmatrix} 0 & 1/2 \\ 1/2 & 0 \end{pmatrix},$$

of rank two, whereas a square of one linear coordinate has rank one. Rank is then the appropriate obstruction. The fiber proof in Theorem H.1 handles node coincidences and cancellations without mixing these two cases.

H.4 Particular solutions and degenerate parameters

Theorem H.1 is an operator statement. It does not exclude coincident components for particular initial data, algebraic relations along a solution, elimination into a scalar equation of higher order, nonlinear coordinate changes, or identities with other named special functions.

For contraction scales, the normalized analytic germ is unique. If $(a, b) = (q, r)$, its components coincide because their derivatives are identical and their initial values agree. The common component is the scalar family $T' = 1 + T(qz)T(rz), T(0) = 0$. The same coincidence holds if $(a, b) = (r, q)$: (T, T) solves both equations because multiplication is commutative, and uniqueness identifies the normalized solution. For $q \neq r$, this reversed-pair case has no autonomous scalar operator projection by Theorem H.1, despite having $U = V$ along its normalized solution. This is a concrete reason the two notions must remain distinct.

In fact, equality of normalized components occurs exactly when the unordered scale pairs agree:

$$U = V \quad \Longleftrightarrow \quad \{q, r\} = \{a, b\}. \tag{S7}$$

To prove necessity, write $U = V = T = z + c_1 z^3 + \cdots$. Then $3c_1 = qr = ab > 0$. Comparing the z^4 coefficients of $T(qz)T(rz) = T(az)T(bz)$ gives $c_1 qr(q^2 + r^2) = c_1 ab(a^2 + b^2)$, so both products and sums of squares agree. Positive scales then have equal sums and are the roots of the same quadratic. Sufficiency is the uniqueness argument above. For example, $(q, r, a, b) = (1/2, 1/3, 1/3, 1/2)$ has coincident normalized components and no nonzero autonomous operator projection.

At $q = r = a = b = s > 0$, the variables $w = u + v, d = u - v$ give

$$w' = 2 + \tfrac{1}{2}\big(w(sz)^2 - d(sz)^2\big), \qquad d' = 0.$$

This triangular system is not a completely decoupled operator. The normalized solution lies in the invariant subspace $d = 0$.

Zero scales lie outside Theorem H.1. On zero-constant inputs, a product vanishes identically if either of its scales is zero. If both products vanish, both equations are already $u' = v' = 1$. If only the first product vanishes, the projection u is autonomous, regardless of whether the second pair agrees with the first. Thus extending Theorem H.1 to zero scales would be false. Scale one and positive scales greater than one do not affect the algebraic operator theorem, although the contraction-domain entire growth theorems do not automatically extend to them. Negative or complex scales and odd-input coincidences caused by signs are not classified here.

H.5 Claim status

Theorem H.1 and (S7) are proved above. The proof is elementary and independent of the coupled growth theorem. Historical priority for these precise operator statements is not asserted. The theorem provides a specified nondecoupling result, not a universal assertion that the normalized functions cannot reduce to any previously studied function class.

APPENDIX I

A visual atlas of finite resolution

A structural change need not produce a large change in the measurements we can make. A tiny feedback tap can change the order of an entire function. An excluded prime can change the exact arithmetic inverse. A negative atom can destroy positivity of a measure. Each change becomes visible at a different resolution.

This atlas makes those statements quantitative. Its three controls are observation radius, absolute precision and polynomial degree. Each example includes a bound that can be evaluated without trusting the appearance of a curve. The large radii below are sufficient guarantees from conservative estimates. The degree bounds bracket a detection problem. Neither is presented as an optimal threshold.

Family	Structural difference	Finite observation	Certificate that resolves it
Positive feedback	A nonzero fast tap changes entire order	Values on a fixed complex disk	A sufficient radius for a factor of two separation
Arithmetic depth	The excluded prime set changes	Values or finitely many derivatives on a disk	A bracket for the negative depth needed to reach an absolute tolerance
Signed sieve	One prime shelf has negative mass	All polynomial quadratic forms up to a given degree	An explicit rational polynomial with negative quadratic form

I.1 A weak tap that changes global growth

Let the normalized positive feedback function satisfy

$$F_\varepsilon'(z) = 1 + (1-\varepsilon)F_\varepsilon(z/4)^2 + \varepsilon F_\varepsilon(3z/4)^2, \qquad F_\varepsilon(0) = 0, \qquad 0 \le \varepsilon \le 1.$$

The base theorem gives a unique entire function with nonnegative odd coefficients. At zero weight, the order is $1/2$. At every positive weight it is

$$\rho = \frac{\log 2}{\log(4/3)} \approx 2.40942084.$$

Thus the order jumps at a parameter value where the entire functions themselves converge uniformly on every compact set.

I.1.1 The disk has a numerical error budget

Write $f = f_{3/4}$ for the normalized diagonal function, and $f(z) = \sum_{n\ge 0} d_n z^{2n+1}$. The inherited tap continuity theorem gives

$$\sup_{|z|\le R} |F_\varepsilon(z) - F_0(z)| \le \varepsilon L(R), \qquad L(R) = \sum_{n\ge 1} n d_n R^{2n+1} = \frac{Rf'(R) - f(R)}{2}. \tag{RA-1}$$

The following elementary certificate makes the unit disk example fully computable. Positive coefficient domination by tangent, followed by $\sin x \le x$ and $\cos x \ge 1 - x^2/2$, gives

$$f(4/3) \le \tan(4/3) \le 12.$$

For $N \ge 1$ and $0 \le R \le 1$, put $t = 3R/4$. If $(N+2)t^2 \le N+1$, then nt^{2n+1} is nonincreasing for $n \ge N+1$, and hence

$$0 \le L(R) - \sum_{n=1}^{N} n d_n R^{2n+1} \le 12(N+1)t^{2N+3}. \tag{RA-2}$$

Indeed the left side is a sum of $d_n(4/3)^{2n+1}$ multiplied by nt^{2n+1}. Bound the multiplier by its first value, then use the positive total mass $f(4/3) \le 12$. The coefficients d_n are rational. With $N = 40$, the exact rational upper bound is less than

$$L(1) < 0.241890267.$$

The decimal shown here is rounded upward from the rational certificate. Consequently

$$\boxed{\sup_{|z|\le 1} |F_{10^{-12}}(z) - F_0(z)| < 2.41890267 \times 10^{-13},}$$

although their entire orders are different. If observations have an absolute error allowance at least half this bound, midpoint data can be consistent with both functions throughout the disk. This is an ambiguity under a stated noise allowance, not equality of their exact values.

See Figure 7.1 in Chapter 7.

How to read the figure. The left curves divide the difference by the tap weight, so the relevant small quantity is the plotted height multiplied by ε. The right panel records the proved order, which is determined by arbitrarily large radii. The curve computation uses powers through z^{201}, with a normalized analytic omitted-tail bound below 5.26×10^{-23} on the unit interval. Ordinary floating rounding is separate from that analytic tail bound.

I.1.2 A radius at which a difference is guaranteed

The base lower-type theorem supplies, for every $0 < \varepsilon \le 1$,

$$\log F_\varepsilon(R) \ge c_\varepsilon (R + 3/\varepsilon)^\rho \ge c_\varepsilon R^\rho \qquad (R \ge 2),$$
$$c_\varepsilon = \frac{\log 2}{(4/\varepsilon + 8/3)^\rho}.$$

For the slow function, the base upper-type construction with $q = r = 1/4$, $N = 2$, yields

$$\log F_0(R) \le C_0 \sqrt{R} \qquad (R \ge e), \qquad C_0 = e^{-1/2}(1 + 22 \log 2) \approx 9.85566103.$$

The value of C_0 comes directly from the earlier explicit constants: $V_2 = 15 \log 2$, $\Delta = 2 \log 2$, and $B_+ = 5 \log 2$. Thus $V_2 + 1 + \Delta + B_+ = 1 + 22 \log 2$.

Define

$$R_2(\varepsilon) = \max \left\{ e, \left(\frac{2C_0}{c_\varepsilon} \right)^{1/(\rho - 1/2)}, \left(\frac{2 \log 2}{c_\varepsilon} \right)^{1/\rho} \right\}. \tag{RA-3}$$

Then, for every $R \ge R_2(\varepsilon)$,

$$\boxed{F_\varepsilon(R) \ge 2F_0(R).}$$

To prove this, the last two constraints imply that $c_\varepsilon R^\rho$ is at least both $2C_0\sqrt{R}$ and $2 \log 2$. It is therefore at least their half-sum $C_0\sqrt{R} + \log 2$. Exponentiating proves the claim.

Tap weight	Difference on the unit disk is at most	Sufficient radius R_2, rounded
10^{-3}	2.419×10^{-4}	2.029×10^{5}
10^{-6}	2.419×10^{-7}	1.237×10^{9}
10^{-9}	2.419×10^{-10}	7.549×10^{12}

Tap weight	Difference on the unit disk is at most	Sufficient radius R_2, rounded
10^{-12}	2.419×10^{-13}	4.608×10^{16}

The radius column displays the analytic formula approximately. For a certificate use the formula itself or a rigorously rounded upper value. These large numbers reflect the conservatism of the global comparison. They do not mean that observations at all smaller radii fail. The formula grows proportionally to $\varepsilon^{-\rho/(\rho-1/2)}$ as the tap vanishes.

See Figure 7.2 in Chapter 7.

I.2 An excluded prime and the precision needed to see it

Fix $a = \beta = 2$, and use the arithmetic depth family

$$A_Q(s) = \sum_{\substack{n \geq 2 \\ \mu(n)^2 = 1 \\ (n,Q)=1}} n^{-4}(1 - n^{-2})^{2s}.$$

For a prime p, let $D_p = A_1 - A_p$. This positive difference consists exactly of the squarefree atoms divisible by p. Its largest frequency is

$$\lambda_p = -2\log(1 - p^{-2}),$$

and its total mass is $D(4)/(p^4 + 1)$, where $D(4) = \zeta(4)/\zeta(8) = 105/\pi^4$.

I.2.1 Exact disk bounds include derivative measurements

For every integer $k \geq 0$ and $R \geq 0$,

$$\sup_{|s| \leq R} |D_p^{(k)}(s)| \leq \lambda_p^k e^{R\lambda_p} \frac{D(4)}{p^4 + 1}. \tag{RA-4}$$

This is the inherited arithmetic inverse theorem, now read as a precision requirement. For fixed R, the envelope is of order p^{-4-2k}. Each additional derivative suppresses the large-prime difference even further in absolute units. This does not rule out methods that rescale derivatives and account for their corresponding noise amplification.

At integer radius $R = 5$, an especially simple rational certificate follows from $D(4) < \zeta(4) < 4/3$:

$$\boxed{\sup_{|s| \leq 5} |D_p(s)| < \frac{4}{3(p^4 + 1)}(1 - p^{-2})^{-10}.} \tag{RA-5}$$

For derivatives, multiply this rational bound by $[2/(p^2-1)]^k$, using $-\log(1-u) \le u/(1-u)$. Thus this part of the certificate needs no transcendental evaluation at all.

Excluded prime	Rational upper bound on $\lvert s\rvert \le 5$, rounded upward
101	1.283×10^{-8}
1009	1.287×10^{-12}
10007	1.330×10^{-16}

See Figure 7.3 in Chapter 7.

I.2.2 Increasing negative depth gives a two-sided threshold bracket

There is also an elementary lower bound, because the removed prime atom is present:

$$\boxed{p^{-4}e^{\lambda_p T} \le D_p(-T) \le \frac{D(4)}{p^4+1}e^{\lambda_p T} \qquad (T \ge 0).} \tag{RA-6}$$

Choose an absolute tolerance $\eta > D(4)/(p^4+1)$. The strict inequality makes the initial difference smaller than the tolerance. Define

$$T_- = \frac{\log\big(\eta(p^4+1)/D(4)\big)}{\lambda_p}, \qquad T_+ = \frac{\log(\eta p^4)}{\lambda_p}. \tag{RA-7}$$

Then $D_p(-T) \le \eta$ for $0 \le T \le T_-$, while $D_p(-T) \ge \eta$ for $T \ge T_+$. The true crossing exists and is unique because $D_p(-T)$ is continuous and strictly increasing. Therefore it belongs to $[T_-, T_+]$. If the tolerance hypothesis fails, the interval starting at zero is not certified by this formula. The executable record represents an absent lower interval by `null`.

The bracket width and its large-prime scale are explicit:

$$T_+ - T_- = \frac{\log\big(D(4)p^4/(p^4+1)\big)}{\lambda_p}, \qquad T_+ = \frac{p^2}{2}\big(4\log p + \log\eta\big)(1+O(p^{-2})).$$

For $\eta = 10^{-6}$, rounded values are:

Prime	No larger than tolerance through T_-	At least tolerance by T_+
101	23,307.789	23,690.516
1009	7,012,695.633	7,050,894.424
10007	1,149,287,766.447	1,153,045,061.461

These are approximate evaluations of exact analytic endpoints, not directed-rounding intervals.

I.2.3 The direct difference and subtraction of full functions have different conditioning

The positive series for D_p can be evaluated directly if the excluded prime is already specified. Recovering it by subtracting independently evaluated full functions can be much harder. The atom $n = 2$ in A_1 gives

$$\boxed{\frac{A_1(-T)}{D_p(-T)} \geq \frac{p^4+1}{16D(4)} e^{(\lambda_2-\lambda_p)T}.} \tag{RA-8}$$

At the sufficient endpoint T_+, the base-ten logarithm of this lower bound is about 5,924 for $p = 101$, 1,761,864 for $p = 1009$, and 288,119,991 for $p = 10007$. These are conditioning scales for subtracting full signals. They are not running times, required precision for every possible algorithm, or claimed numerical evaluations of the full functions at those enormous depths. The logarithmic bound is computed directly without forming those functions.

See Figure 7.4 in Chapter 7.

I.3 A negative atom that every low-degree test misses

Consider the one-prime signed sieve at $p = 2$, with $\lambda_2 = -1 - \delta$, $\delta > 0$. Its nodes are $x_n = (1 - n^{-2})^2$, and its quadratic form is

$$Q_\delta(f) = \sum_{\substack{n\geq 1 \\ \mu(n)^2=1 \\ n \text{ odd}}} n^{-4} f(x_n)^2 - \delta \sum_{\substack{n\geq 1 \\ \mu(n)^2=1 \\ n \text{ even}}} n^{-4} f(x_n)^2.$$

Every even squarefree atom has negative mass. We will certify that all nonzero real polynomials through degree four nevertheless have positive quadratic form for $\delta = 10^{-12}$, and then construct a degree-seven polynomial of negative quadratic form. This is an assertion about every polynomial in a finite-dimensional space, not a plot of a few test vectors.

I.3.1 A rational certificate for every polynomial through a chosen degree

Choose $d + 1$ distinct odd squarefree labels $n_0, \ldots, n_d$, including 1, and set $y_i = x_{n_i}$. Their Lagrange polynomials are

$$\ell_i(x) = \prod_{j\neq i} \frac{x - y_j}{y_i - y_j}, \quad b_i = \prod_{j\neq i} \frac{\max(y_j, 1 - y_j)}{|y_i - y_j|}, \quad K_d = \sum_{i=0}^{d} n_i^4 b_i^2.$$

For $x \in [0, 1]$, we have $|\ell_i(x)| \leq b_i$. Interpolation and weighted Cauchy–Schwarz give, for every real polynomial of degree at most d,

$$|f(x)|^2 \le \left(\sum_{i=0}^{d} n_i^{-4} f(y_i)^2\right)\left(\sum_{i=0}^{d} n_i^4 \ell_i(x)^2\right) \le K_d \sum_{i=0}^{d} n_i^{-4} f(y_i)^2.$$

The total even mass satisfies $\sum_{n \text{ even}} \mu(n)^2 n^{-4} < \frac{1}{16}(1+\frac{1}{3}) = 1/12$. Keeping the selected nodes in the positive part yields the explicit bound

$$\boxed{Q_\delta(f) \ge \left(1 - \frac{\delta K_d}{12}\right) \sum_{i=0}^{d} n_i^{-4} f(y_i)^2.} \tag{RA-9}$$

A nonzero polynomial of degree at most d cannot vanish at all $d+1$ nodes. Thus $\delta < 12/K_d$ proves strict positive definiteness of the Hankel matrix of order $d+1$.

For $d = 4$, use labels $1, 3, 5, 7, 11$. Exact rational arithmetic gives

$$K_4 \approx 1.50393441996 \times 10^{11}, \qquad 12/K_4 \approx 7.9790713217 \times 10^{-11} > 10^{-12}.$$

The inequality is checked as an exact rational comparison. Therefore every nonzero polynomial of degree at most four has positive quadratic form in the chosen signed measure.

I.3.2 A shorter detector by killing the first positive shelves

Let S be exactly the set of all odd squarefree labels $n \le K$, where K is an odd squarefree integer, and let n_+ be the next such label. Assume $n_+ > 2$, and define

$$P_{S,m}(x) = \prod_{n \in S} \frac{x - x_n}{x_2 - x_n} \left(\frac{1-x}{1-x_2}\right)^m,$$

$$C_S = \prod_{n \in S} \frac{1 - x_n}{|x_2 - x_n|}, \qquad r_S = \frac{1 - x_{n_+}}{1 - x_2} < 1.$$

This polynomial has degree $|S| + m$, equals one at x_2, and kills every positive atom through the cutoff. At each remaining positive node, the product of the absolute root factors is at most C_S, and the last factor is at most r_S^m. Dropping all other negative atoms and bounding the positive tail by the integral $\sum_{n>K} n^{-4} \le 1/(3K^3)$ gives

$$\boxed{Q_\delta(P_{S,m}) \le -\frac{\delta}{16} + \frac{C_S^2}{3K^3} r_S^{2m}.} \tag{RA-10}$$

For any chosen S, a computable sufficient exponent is the first nonnegative integer m for which

$$r_S^{2m} < \frac{3K^3\delta}{16C_S^2}.$$

It can be found by multiplying rational numbers, without logarithms or eigenvalues. Searching finitely many choices of S improves the sufficient degree but does not prove its optimality.

For the worked defect $\delta = 10^{-12}$, take

$$S = \{1,3,5,7\}, \quad K = 7, \quad n_+ = 11, \quad m = 3.$$

Then

$$C_S = \frac{756482048}{20777538825}, \qquad r_S = \frac{3856}{102487},$$

and $P_{S,3}$ has degree seven. The exact rational right side of (RA-10) is strictly negative and is approximately

$$\boxed{Q_{10^{-12}}(P_{S,3}) \leq -5.8845708899 \times 10^{-14}.}$$

The negative atom contributes -6.25×10^{-14}. The full positive tail contributes at most $3.6542911008 \times 10^{-15}$, a bound that covers every omitted atom. The exact certificate is stored as numerator and denominator. The original generic isolating detector needed degree 21 for this defect. Using the known sign pattern and killing later positive shelves reduces the exhibited degree to seven.

See Figure 7.5 in Chapter 7.

The fifth-order Hankel matrix is therefore positive definite, while the eighth-order matrix is not positive semidefinite. The two intervening polynomial degrees, five and six, are not decided by these certificates. A numerical eigenvalue could suggest a sharper boundary, but it would be a different calculation requiring its own conditioning and error analysis.

I.4 What the three examples establish together

The three resolution controls act on different mathematical objects. Radius controls what part of an entire function is sampled. Precision controls whether two different arithmetic parameters are distinguishable within an observation model. Degree controls the richness of a positivity test. The common lesson has a precise form: a property determined by an unbounded collection of tests need not have a uniform margin on each bounded subcollection.

Here the positive tap changes a proved global order. The excluded prime changes an exactly recoverable radical. The signed sieve lies outside the exact positivity domain even while a whole low-degree polynomial space passes. Each conclusion follows from explicit formulas and local proofs. There is no claim that the three mechanisms are identical, and no historical novelty claim for interpolation, spectral peeling, or the use of isolating polynomials.

I.5 Reproduction and evidence

Run from the package's `research/` directory:

```
python checks/resolution_v11.py
python build_resolution_figures.py
```

The first command uses only the Python standard library. It records **985 exact rational assertions** and **16 floating algebra checks**, with source hashes and exact certificate numerators and denominators. It tests interpolation identities in the monomial basis, all selected root values, sample envelope inequalities, exact negative quadratic forms for finite sums, coefficient continuity bounds and each displayed certificate. The universal analytic conclusions rely on the proofs above, rather than on the finite count.

The figure command uses NumPy, Matplotlib and mpmath. Six figures are saved in PDF and PNG form. The weak-tap curves use 100 decimal digits and an explicit positive-coefficient tail bound. Every other curve displays a closed analytic bound or rational certificate, so it has no omitted arithmetic series. Displayed floating values and polynomial curves are not interval arithmetic. The script never evaluates the huge full arithmetic functions in the cancellation example.

One preliminary presentation issue was corrected during development: a negative formula for T_- was initially clamped to zero. That would misleadingly label an already visible difference as invisible at zero. The finished formula requires its stated tolerance hypothesis, and the executable record marks an absent interval by `null`. The exact assertion run passed. This correction did not affect any of the three listed prime examples.

APPENDIX J

Exact laboratory and certified evaluation

The reusable module `coupled_lab.py` uses Python's standard library and imports the existing exact coefficient, phase and tap operations from `family_lab.py`. The figure builder additionally uses NumPy and Matplotlib. Neither script contacts an external service. The generic integer and signed catalog rows are formal power series, with no claim of analytic convergence.

J.1 Normalization and recurrence

Write

$$U(z) = \sum_{n\geq 0} A_n \frac{z^{2n+1}}{(2n+1)!}, \qquad V(z) = \sum_{n\geq 0} B_n \frac{z^{2n+1}}{(2n+1)!}.$$

The exact recurrence is

$$A_n = \sum_{i+j=n-1} \binom{2n}{2i+1} q^{2i+1} r^{2j+1} A_i B_j, \qquad B_n = \sum_{i+j=n-1} \binom{2n}{2i+1} a^{2i+1} b^{2j+1} A_i B_j,$$

with $A_0 = B_0 = 1$. Coefficients with even derivative index vanish. Swapping the components sends the parameter tuple (q, r, a, b) to (b, a, r, q). Identical rows $(a, b) = (q, r)$, or exchanged rows $(a, b) = (r, q)$, yield the scalar reduction $U = V = T_{q,r}$.

Both derivative arrays are polynomials in four scale variables with nonnegative integer coefficients. Their total degree is at most $n(n+1)$. Indeed, a recurrence term with $i + j = n - 1$ has degree at most $2n + i(i+1) + j(j+1) \leq n(n+1)$. If all four denominators divide D, then $D^{n(n+1)} A_n$ and $D^{n(n+1)} B_n$ are integers. The clearing factor is a convenient uniform choice and need not be minimal.

J.2 An elementary exact evaluation certificate

This argument uses $0 < q, r, a, b < 1$ and does not require the order theorem. Let $Q = \max(q, r, a, b)$. All ordinary odd Taylor coefficients are positive and at most one: induction in the ordinary recurrence bounds the coefficient of z^{2n+1} by $n/(2n+1)$ for $n \geq 1$. Thus both series converge on the unit disk and, for $0 \leq x < 1$,

$$\max(U(x), V(x)) \leq \frac{x}{1-x^2}.$$

Analytic continuation by the integral equations expands each known disk by the factor $1/Q$, so both solutions are entire. Positive coefficients give $\max_{|z|\leq x} |F(z)| = F(x)$ for either component. The integral equations therefore imply

$$M(x) := \max(U(x), V(x)) \leq x\big(1 + M(Qx)^2\big).$$

Start at the first member $Q^k x < 1$ of this finite contraction ladder, use $x/(1-x^2)$ there, and repeatedly apply $B(x) = x(1 + B(Qx)^2)$ backward. This defines the rational `disk_majorant` bound for rational parameters and radius. The implementation has explicit recursion and integer size guards, which raise errors rather than returning a weakened result.

If F_N retains odd indices $0, \ldots, N$, then for $S > R \geq 0$,

$$\max_{|z|\leq R} |F(z) - F_N(z)| \leq B(S) \left(\frac{R}{S}\right)^{2N+3}.$$

For every omitted exponent $m \geq 2N+3$, use $R^m \leq (R/S)^{2N+3} S^m$, sum positive terms, and bound their sum by $F(S) \leq B(S)$. No extra geometric denominator is needed. For rational $x \geq 0$, `certified_evaluation` returns the exact interval $[F_N(x), F_N(x) + B(S)(x/S)^{2N+3}]$ for each component.

J.3 Worked calls

```
from fractions import Fraction as Q
import coupled_lab as lab

p = (Q(1,5), Q(2,5), Q(3,5), Q(7,10))
A, B = lab.coupled_odd_derivatives(*p, last=12)
certificate = lab.certified_evaluation(*p, Q(1), last=30, outer_radius=2)
root = lab.pf_order(*p)  # floating approximation, not interval arithmetic

derivatives = lab.full_egf_coefficients(B)
phases = lab.phase_lanes(derivatives, 3)
matrix = lab.polyphase_tap_matrix([1, -2, 1], 3)
length = len(derivatives) + 2
output_phases = lab.apply_polyphase_matrix(phases, matrix, length)
output = lab.merge_lanes(output_phases, length)
```

At $x = 1$, with $N = 30$ and $S = 2$, the common tail bound is below 1.600×10^{-13}. The partial values are approximately $U(1) = 1.027044341827337$ and $V(1) = 1.1467074957737624$. These displayed decimals are rounded illustrations. The returned fractions are the actual certificate.

Run the independent checks and regenerate figures from the package's `research/` directory:

```
python3 checks/coupled_v11.py
python3 build_coupled_figures.py
```

The first command passes 1,559 exact assertions, 10 numerical comparisons, and 13 separate input/resource guards. Independent constructions include dense ordinary Taylor Picard iteration, sine/cosine division for tangent, the exact sinh formula, component symmetry, and direct convolution versus phase carry. The test counts describe bounded implementation checks, not universal proofs.

Evidence and limitations

The main chapters develop entire existence, nonrescaling, arithmetic non-D-finiteness, one-prime transport and base orbit convergence. Appendices A–J supply the extended arguments. The preserved foundational review records cover Appendices A–E and their exact API. The coupled-family records cover the proofs, resolution certificates and exact APIs underlying Appendices F–J. These are project review records, not claims of external peer review or kernel certification.

Classical external leaves are named explicitly. In particular, ordinary orthogonal-polynomial theory, Hadamard factorization, Laplace uniqueness, and spectral Mellin regularization are established machinery. The local proofs verify their application and do not presume historical novelty.

Checks accompanying the proofread edition

The complete manuscript was reviewed for prose, definitions, hypotheses, notation, cross-references and agreement between chapter summaries and proof appendices. Corrections include the Hankel order convention, zero-orbit notation, the real-polynomial domain of signed quadratic forms and several missing definitions. The chapter text now includes both finite-test nonconvexity examples proved in Appendix C.

Fresh execution covered all ten foundational check scripts and the three coupled and resolution scripts. The foundational scripts passed **19,871 exact and 5,576 numerical assertion statements**. The coupled scripts passed **5,272 exact and 26 numerical assertion statements**, with 13 separate operational guards. All 14 coupled and resolution figure pairs were regenerated. Counts describe executed finite assertions, not independent theorems or exhaustive parameter coverage.

The first foundational orchestration attempt reached the execution time limit after nine scripts had recorded passing results. The final script was then run separately against the same isolated input snapshot and passed. The retained logs distinguish this recovered execution failure from a mathematical or numerical assertion failure.

The editorial change log, exact source diff and fresh execution records are included in the package. No Lean build was performed. Analytic conclusions continue to rest on the written proofs and their stated hypotheses.

What the coupled extension establishes

Result	Scope
Coupled entire construction	Unique normalized pair for four positive strict contractions, with positive odd coefficients
Common growth law	Exact order from the characteristic matrix, positive lower type, finite upper type, and exact Perron proportions for both type vectors
Component reduction	Rescaling occurs exactly on $q = b$ or $qb = ar$
Generic exact inverse	Coefficients through degree seven identify all four ordered scales when $D \neq 0$
Operator obstruction	No invertible constant linear change decouples the defining operator on all analytic inputs
Resolution certificates	Explicit compact, radius, prime-depth and polynomial-degree bounds for the three worked examples

Verification and reproducibility

The archived coupled-system run records **5,272 exact assertions and 26 numerical assertions**. Thirteen input and resource guards are recorded separately. The exact inverse is checked on 256 rational parameter tuples. The coupled API is compared with an independent dense Picard construction and classical anchors. The resolution checks verify the exact rational certificates. These counts are separate from the earlier four-family evidence of 19,871 exact and 5,576 numerical assertions.

The preserved coupled-family review reconstructs the proof implications and the source files. It corrected an initial-segment quantifier in the detector theorem. The worked certificate already used that initial segment. The source package records the correction, the repair of a figure label, and the successful checks.

Questions that remain open

The coupled theorem does not determine an ordinary type limit, uniform angular growth, or the complex zero geometry. Stable finite-precision recovery near the reduction surfaces remains open. The resolution bounds are constructive and can be conservative. The sieve example leaves degrees five and six undecided. The literature comparison does not settle historical priority.

The exact API and its checks run with the Python standard library. NumPy, Matplotlib, and mpmath generate the figures. The full manuscript supplies the proof appendices and the source archive contains the code and inputs needed for the computations.

Established results and open questions

The foundational families close selected structural questions and admit a reproducible visual treatment. Historical priority is a distinct question that the bounded literature review does not settle.

Established results	Remaining questions
Positive lower and finite upper dilation type	Existence of an optimal type limit and logarithmic modulation
Joint analytic parameter dependence and compact tap bounds	General minimal-bank identifiability
Exact arithmetic parameter recovery up to modulus radical	Stable recovery within bounded prime classes
All-prime signed-atom detectors and positivity domain	Sharp sieve-root asymptotics and multiplicities
Global orbit-zeta continuation and shifted determinants	Functional equations and derivative-weighted zero sums
Integer coefficient and exact polyphase/tap machinery	Historical priority of the candidate extensions

Structural distinctions among the families

The asymmetric dilation family has intrinsic parameters, and its off-diagonal members cannot be obtained by rescaling the diagonal family. Its nonnegative real scale regimes are classified in Appendix E. The arithmetic inverse and signed-resolution results address different questions about parameter recovery and finite detection. The orbit continuation applies established spectral methods to a specified seed, with the branch conventions and hypotheses checked locally.

A common finite-resolution lesson

A weak tap can change asymptotic order while preserving compact convergence. A large excluded prime can change an exact arithmetic parameter while hiding within a small bounded-window error. A negative atom can evade low-degree positivity and become detectable at a calculable larger degree. These are three different proved mechanisms. Their shared resolution theme does not make them identical constructions.

Evidence with declared ranges

The archived foundational review reconstructed five proof chapters and examined their mathematical statements. The recorded release run executed ten scripts, with 25 pinned inputs and byte-identical isolated snapshots. All inputs remained unchanged, every declared result was present, and the schema validator passed.

19,871 exact assertion statements + 5,576 numerical assertion statements passed.

The exact total comprises 19,331 principal checks and 540 separately recorded helper checks in the inverse reconstruction. Operational path and process guards are excluded. Counts are assertion statements, not counts of theorems or every scalar operation inside a grouped assertion.

In that recorded run, the API contributes 8,038 exact assertions and 18 catalog rows through index 12. Dilation type and continuity add 6,091 exact checks. Arithmetic inverse examples include rank 10,000, negative depth 500, and large excluded primes. The multiple-prime run tests 102 positive parameter/depth cases, 1,395 orthogonality conditions, 381 recurrence cases, and 40 conditional pencils. Spectral continuation tests classical unshifted and shifted anchors.

Recovered failures are retained

The preserved audit documents early environment and plotting issues, an unsuitable absolute determinant residual, and the previously known one-dilation case. Two API validation defects were reproduced and fixed. A draft sequence example had two miscopied integers and was corrected against the exact catalog. Initial figure footer and label overlaps were repaired. A direct publisher-source retrieval failed; an authenticated publisher preview supplied the classical Laplace-uniqueness comparison instead.

Exact analytic tail envelopes are distinguished from floating-point rounding. All decimal arithmetic and root approximations are ordinary high precision, not interval certificates. No analytic Lean certificate is claimed. The universal conclusions rely on the proofs, not on the number of checks.

A reproducible research package

The package preserves the research manuscripts, code, catalogs, review records and bounded execution evidence. The typeset monograph uses 32 vector figures: 18 for the foundational families and 14 for coupled systems and finite resolution. The corresponding generators and preview images remain in the research archive. Input and output hashes identify the retained evidence.

The source files preserve the earlier claim ledger and open questions as provenance. Later proof chapters supersede the earlier statements where a new argument supplies a closed result. The distinction is recorded in the verification documents rather than folded into the mathematical theorem count.

Reproduce the work

Build the book with `python monograph/build.py` from the package root. The script requires XeLaTeX and resolves contents, citations and cross-references through successive passes. Research commands are run from the `research/` directory, whose `requirements.txt` records the scientific dependencies. The package README supplies complete commands for the isolated foundational and coupled verification suites. Figure generators rebuild the atlas from formulas and recorded numerical examples.

The standard-library API is portable. Numerical checks additionally require mpmath. No network access, external submission, or dependency installation is part of the verification run. PDF byte identity can change with timestamps and font environments; mathematical outputs retain their own provenance.

The remaining questions admit concrete starting points: type-limit analysis for dilation, precision-controlled arithmetic inversion within bounded parameter classes, sharper sieve-root asymptotics, and spectral weighted sums. They remain research questions rather than hidden dependencies of the proved statements in this volume.

Dilation: computation and proof scope

`checks/dilation_type.py` uses exact `fractions.Fraction` arithmetic for its finite assertions. It checks the algebraic fixed-width and interval-propagation conditions for rational scales and weights, the positive homogeneous weight-polynomial majorant, derivative bounds on a normalized simplex, the improved total-variation coefficient bound, and a distinct ordered-tree evaluation against the recurrence. Scalar examples and the explicit real type constants are displayed at high precision separately from exact assertions.

The finite checks do not establish universal analytic conclusions. The growth and convergence results depend on the proofs in Appendix A. Historical priority is a separate literature question. No numerical fit is presented as evidence that a type limit exists.

The earlier moving-width lower argument used a fixed $\alpha < 1$; it proved orders below ρ and then recovered the order by $\alpha \uparrow 1$, but did not establish positive lower type at ρ. This is a limitation of that argument, not a counterexample. The fixed-width comparison closes precisely that missing implication. The evidence archive retains execution failures, their causes and the subsequent corrected runs.

Coupled growth: scope and open questions

The decisive extension is from a scalar positive comparison to a comparison weighted by a positive eigenvector. The fixed-width integral controls the lower type at the exact exponent. A fixed proportional interval $[\alpha R, R]$, with $\alpha < 1$, would only give a smaller exponent through $\alpha^s P(s)$. Letting α tend to one recovers exact order but does not, by itself, yield positive lower type. This is a limitation of that alternative route, not a failure of the theorem.

The complete proofs in Appendix F close the target on the strictly positive contraction domain. No computed example is used as a universal analytic premise. The displayed rational Taylor coefficients were evaluated directly from the exact recurrence with Python `fractions.Fraction` as a transcription check. Their independent algebraic residual checks belong to the archived exact computation record.

Remaining questions include the existence and value of ordinary type limits, possible oscillations, zeros, angular growth, connection formulas, and regimes with zero, negative, complex, or noncontracting scales. Positivity and strict contraction are hypotheses of the results here. This route makes no historical priority claim and no claim of a Lean formalization.

The preserved self-review checked coefficient and eigenvector notation, logarithm and power domains, seed and child interval endpoints, and both vector orientations. Its recorded conclusion was that no unresolved gap had been identified in that argument. This is a statement about the scope and outcome of that review, not a substitute for independent verification.

Coupled inverse: verification scope

The identities above are algebraic and the proofs use exact positive parameters. The companion check script compares the first coefficients against the full independent recursion, verifies the factorization over a rational grid, checks the candidate-selection formulas, and tests both reduction surfaces by comparing many exact Taylor coefficients. Finite checks test the implementation and the worked examples. The equivalence and recovery theorems follow from the proofs.

Historical priority of these specific statements remains a separate literature question.

Notation and glossary

Notation is defined locally when each family is introduced. The same letter can serve different roles in separate chapters. In particular, a is an arithmetic weight parameter in Chapter 2, a contraction in Chapter 6, and a spectral shift in Appendix D.

Contracted feedback $T_{q,r}$.
The normalized odd entire solution of $T'_{q,r}(z) = 1 + T_{q,r}(qz)T_{q,r}(rz)$, $T_{q,r}(0) = 0$, for $0 < q, r < 1$. The diagonal notation is $f_q = T_{q,q}$.

Feedback bank F_Θ.
A finite collection of channels with $h_j \geq 0$, $\sum_j h_j = 1$ and $0 < q_j, r_j < 1$, entering $F'_\Theta = 1 + \sum_j h_j F_\Theta(q_j z)F_\Theta(r_j z)$. Zero-weight channels are removed before taking an active-channel maximum.

Maximum modulus and entire order.
$M_f(R) = \max_{|z|=R} |f(z)|$. For a nonpolynomial entire function,

$$\rho(f) = \limsup_{R\to\infty} \frac{\log\log M_f(R)}{\log R}.$$

At positive finite order ρ, the lower and upper types used here are the liminf and limsup of $\log M_f(R)/R^\rho$. Their equality is not assumed.

Coupled pair (U, V).
The normalized entire solution of $U' = 1 + U(qz)V(rz)$, $V' = 1 + U(az)V(bz)$ and $U(0) = V(0) = 0$, with $q, r, a, b \in (0, 1)$.

Perron balance.

spr P denotes the spectral radius of a matrix. The characteristic exponent satisfies $\operatorname{spr}\begin{pmatrix} q^\rho & r^\rho \\ a^\rho & b^\rho \end{pmatrix} = 1$.

A positive right eigenvector gives the proportions of the two type vectors.

Arithmetic depth $A_{a,\beta,Q}$.
The entire sum $\sum_{n\geq 2,\ (n,Q)=1} \mu(n)^2 n^{-2a}(1 - n^{-\beta})^{2s}$, with $a > 1/2$, $\beta > 0$, $Q \geq 1$ integer and the real logarithm in the complex power. The atom $n = 1$ is excluded at every depth.

Möbius function and modulus radical.
$\mu(1) = 1$. For a product of k distinct primes, $\mu(n) = (-1)^k$. If a prime square divides n, then $\mu(n) = 0$. The radical $\mathrm{rad}(Q) = \prod_{p|Q} p$ records the excluded prime set, with $\mathrm{rad}(1) = 1$.

Squarefree Dirichlet sum.
For $v > 1$, $Z_Q(v) = \zeta(v)\zeta(2v)^{-1}\prod_{p|Q}(1 + p^{-v})^{-1}$. The unrestricted notation is $D(v) = Z_1(v)$. Thus $A_{a,\beta,Q}(0) = Z_Q(2a) - 1$.

Prime-sieve measure.
$\nu_{F,\lambda}$ is the arithmetic atomic measure obtained by multiplying the mass at $x_n = (1 - n^{-2})^2$ by $\prod_{p\in F}(1 + \lambda_p \mathbf{1}_{p|n})$. It is positive exactly when every real strength satisfies $\lambda_p \geq -1$.

Hankel order and polynomial degree.
For moments $M_j = \int x^j \, d\nu$, the order-m matrix is $H_m = [M_{i+j}]_{0\leq i,j<m}$. It tests quadratic forms of real polynomials of degree at most $m - 1$. At depth k, the matrix is $[M_{k+i+j}]_{0\leq i,j<m}$. An order-five test therefore covers degree four, not degree five.

Signed quadratic form.
For real polynomials, $Q_\nu(f) = \int f(x)^2 \, d\nu(x)$. On a positive measure it is a squared norm. On a signed measure it may be negative and is not a norm.

Orbit spectral zeta $\mathcal{Z}_N$.
Let $d_N(w) = \sum_{n\geq 0}(-1)^n w^n/(Nn)!$ and $D_N(z) = d_N(z^N)$, $N \geq 2$. The series $\mathcal{Z}_N(s) = \sum_j w_j^{-s}$ initially runs over the zeros w_j of d_N, counted with multiplicity, for $\Re s > 1/N$. Each w_j represents one N-fold rotation orbit of zeros of D_N. Powers use $\operatorname{Arg} w \in (-\pi, \pi]$.

Rising factorial.
$(s)_k = s(s + 1)\cdots(s + k - 1)$ for $k \geq 1$, and $(s)_0 = 1$. It occurs in the shifted spectral residues.

Coefficient conventions.
An ordinary generating function uses $\sum_n a_n z^n$. An exponential generating function uses $\sum_n a_n z^n/n!$. Their product and shift rules differ.

Polyphase section and finite taps.
Polyphase splits a coefficient sequence by residue class. Finite impulse response (FIR) taps act by finite ordinary convolution. A phase matrix must retain the carry delay when a tap crosses a residue-class boundary. This is not the Hurwitz product of exponential generating functions.

Resolution certificate.
An explicit bound or rational witness for a structural distinction at a specified radius, precision or polynomial degree. A sufficient threshold need not be optimal.

The word *packet* describes several analytic, arithmetic and spectral representations. Its meaning is fixed by the objects and maps in each construction, not by an assumed equivalence among the families.

References

The references below identify classical definitions, proof inputs and adjacent constructions. They do not constitute an exhaustive priority review. The arithmetic seed and the Gamma–Laguerre comparisons inherited from the project are documented in the preserved research archive.

[1] Miguel A. Méndez. *Combinatorial differential operators in: Faà di Bruno formula, enumeration of ballot paths, enriched rooted trees and increasing rooted trees*. Australasian Journal of Combinatorics 89(3) (2024), 350–384. Example 2.4 contains the diagonal feedback equation. https://ajc.maths.uq.edu.au/pdf/89/ajc_v89_p350.pdf

[2] Radu Dascaliuc, Tuan N. Pham, Enrique Thomann and Edward C. Waymire. *Transformation of Stochastic Recursions and Critical Phenomena in the Analysis of the Aldous-Shields-Athreya Cascade and Related Mean Flow Equations*. arXiv:2411.00629v2 (2025). The nonlinear equation $u' = -u + u(\alpha t)^2$ is an adjacent model, not the equation studied here. https://arxiv.org/abs/2411.00629v2

[3] Mark W. Coffey. *On the coefficients of the Baez-Duarte criterion for the Riemann hypothesis and their extensions*. arXiv:math-ph/0608050 (2006). Its signed Möbius weights differ from the positive squarefree weights used here. https://arxiv.org/abs/math-ph/0608050

[4] NIST Digital Library of Mathematical Functions. Sections 5.5 and 5.12 give the gamma reflection and beta identities. Section 10.46 defines the Mittag–Leffler function. Sections 16.8 and 16.21 give the generalized hypergeometric and Meijer G differential equations. Section 18.2 develops general orthogonal-polynomial theory. https://dlmf.nist.gov/

[5] V. B. Uvarov. *The connection between systems of polynomials that are orthogonal with respect to different distribution functions*. USSR Computational Mathematics and Mathematical Physics 9(6) (1969), 25–36. https://doi.org/10.1016/0041-5553(69)90124-4

[6] Noam D. Elkies. *Functions of finite order: product formula and logarithmic derivative*. Harvard Math 259 course notes. The finite-order Hadamard theorem supplies the classical factorization input. https://people.math.harvard.edu/~elkies/M259.02/prod.pdf

[7] Alyssa Byrnes, Lin Jiu, Victor H. Moll and Christophe Vignat. *Recursion Rules for the Hypergeometric Zeta Functions*. arXiv:1305.1892 (2013). Hypergeometric zero spectra and coefficient recursions provide related constructions. https://arxiv.org/abs/1305.1892

[8] André Voros. *Zeta functions for the Riemann zeros*. Annales de l'Institut Fourier 53(3) (2003), 665–699. Sections 2.1–2.2 develop related canonical-product and Mellin methods. https://doi.org/10.5802/aif.1955

[9] André Voros. *Erratum: Zeta functions for the Riemann zeros*. Annales de l'Institut Fourier 54(4) (2004), 1139. https://doi.org/10.5802/aif.2046

[10] The OEIS Foundation Inc. *The On-Line Encyclopedia of Integer Sequences*, sequence A000182. This is the tangent-number anchor. No unmatched-prefix novelty claim or submission to OEIS is asserted. https://oeis.org/A000182

[11] Hussam Alrabaiah, Israr Ahmad, Kamal Shah and Ghaus Ur Rahman. *Qualitative analysis of nonlinear coupled pantograph differential equations of fractional order with integral boundary conditions*. Boundary Value Problems 2020, article 138. This is a coupled fractional boundary-value system with different hypotheses. https://doi.org/10.1186/s13661-020-01432-2

[12] Pawel Blasiak and Philippe Flajolet. *Combinatorial Models of Creation–Annihilation*. Séminaire Lotharingien de Combinatoire 65 (2011), B65c. Proposition 24 and Note 25 discuss multitype increasing trees and differential systems. https://arxiv.org/abs/1010.0354v3

[13] R. Daniel Mauldin and S. C. Williams. *Hausdorff Dimension in Graph Directed Constructions*. Transactions of the American Mathematical Society 309(2) (1988), 811–829. Its spectral-radius balance describes a geometric dimension. The analytic order law here requires its own proof. https://sites.math.unt.edu/~mauldin/papers/no67.pdf

[14] Charles Knessl and Wojciech Szpankowski. *Binary Trees, Left and Right Paths, WKB Expansions, and Painlevé Transcendents*. Proceedings of ANALCO (2006), 198–204. The ordinary generating-function identity has different normalization and coefficient rules from the differential system here. https://www.cs.purdue.edu/homes/spa/papers/analco06.pdf

[15] René L. Schilling, Renming Song and Zoran Vondraček. *Bernstein Functions: Theory and Applications*. First edition. De Gruyter, 2010. ISBN 978-3-11-021530-4. Proposition 1.2 and Theorem 1.4 give the classical Laplace uniqueness and Bernstein representation results. https://doi.org/10.1515/9783110215311